NASA Contractor Report 4046
DOT/FAA/PM-86/50, I

The Terminal Area Simulation System

Volume I: Theoretical Formulation

F. H. Proctor

CONTRACT NAS1-17409
APRIL 1987

NASA

NASA Contractor Report 4046
DOT/FAA/PM-86/50, I

The Terminal Area Simulation System

Volume I: Theoretical Formulation

F. H. Proctor
MESO, Inc.
Hampton, Virginia

Prepared by MESO, Inc., under subcontract
to ST Systems Corporation (STX)
for NASA Langley Research Center and
the U.S. Department of Transportation,
Federal Aviation Administration
under Contract NAS1-17409

National Aeronautics
and Space Administration

Scientific and Technical
Information Branch

1987

TABLE OF CONTENTS

TABLE OF CONTENTS (Continued)

TABLE OF CONTENTS (Continued)

TABLE OF CONTENTS (Continued)

TABLE OF CONTENTS (Continued)

LIST OF TABLES

LIST OF FIGURES

ABSTRACT

A new three-dimensional numerical cloud model has been developed for the general purpose of studying convective phenomena. The model utilizes a time splitting integration procedure in the numerical solution of the compressible nonhydrostatic primitive equations. Turbulence closure is achieved by a conventional first-order diagnostic approximation. Open lateral boundaries are incorporated which minimize wave reflection and which do not induce domain-wide mass trends. Microphysical processes are governed by prognostic equations for potential temperature water vapor, cloud droplets, ice crystals, rain, snow, and hail. Microphysical interactions are computed by numerous Orville-type parameterizations. A diagnostic surface boundary layer is parameterized assuming Monin-Obukhov similarity theory. The governing equation set is approximated on a staggered three-dimensional grid with quadratic-conservative central space differencing. Time differencing is approximated by the second-order Adams-Bashforth method. The vertical grid spacing may be either linear or stretched. The model domain may translate along with a convective cell, even at variable speeds. In storm splitting cases, the domain translates with the convective cell having cyclonic rotation and allows the other cell(s) to pass through the lateral boundary without detrimental consequences.

Potential applications of the model range from the simulation of shallow cumulus to supercell cumulonimbus, including such convective phenomena as downbursts, tornadoes, gust fronts, and hailstorms.

FOREWORD

The work reported herein was primarily supported by the National Aeronautics and Space Administration under contract NAS1-17409. The work was performed at the Langley Research Center in Hampton, Virginia under the direction of Dr. Roland Bowles of the Flight Management Branch. Additional support was provided by the Defense Nuclear Agency through an interagency agreement with NASA under contract NAS1-17661.

I would like to express special appreciation to Ms. Mary Bousquet for producing most of the computer plots, Ms. Sylvia Caldwell of ST Systems Corp. (STX), for typing the report, and Dr. Sue-li Chuang formerly of ST Systems Corp. (STX), for his assistance. Also I would like to acknowledge my colleagues Dr. David Bacon of Science Applications International Corporation, Ms. Pamela Price and Dr. Mike Kaplan of MESO, Inc. for reviewing this manuscript. Computations were carried out on the NASA Langley CYBER VPS 32.

1. INTRODUCTION

Three-dimensional, convective cloud models have now advanced to a stage where they can be directly compared to observed data fields. This has been made possible by the current evolution of high-speed and large in-core memory vector computers. The earliest three-dimensional cloud models were developed by Steiner (1973), Miller and Pearce (1974), Pastushkov (1975), Schlesinger (1975, 1978), Lipps (1977), Klemp and Wilhelmson (1978a), Cotton and Tripoli (1978), and Clark (1979). These pioneering models were limited by computer restraints, and were run with relatively crude grids and simple microphysics. Nevertheless, they were able to produce much information on the dynamics of buoyant convection within vertically-sheared environments. Refinements in these models have continued to progress (e.g., Yau, 1980; Cho and Clark, 1981; Wilhelmson and Chen, 1982; Tripoli and Cotton, 1982; Yau and Michaud, 1982; Schlesinger, 1984a, 1984b; Smolarkiewicz and Clark, 1985); but only a few, so far, have attempted to verify their model simulations with detailed observed data sets. Of the 3-D models, only Cotton et al. (1982) have included parameterizations of ice-phase microphysics. They found that its inclusion moderately affected the dynamics of the simulated clouds. The significance of including the ice phase has also been shown in other studies with one- and two-dimensional models. For example, Ogura and Takahashi (1971) have found that the exclusion of the ice-phase resulted in a considerable change in the evolution of the downdraft. Willoughby et al. (1984) and Lord et al. (1984) using a 2-D axisymmetric model, have found that inclusion of ice-phase microphysics resulted in dramatic differences in a hurricane simulation; one important finding was that the locations of mesoscale downdrafts were controlled by falling ice particles. Ice-phase microphysics

cannot be casually neglected from model developments. It may have an important impact, especially with regard to simulations of downburst phenomena and deep tropospheric convection.

The purpose of this report is to present the development of a new three-dimensional numerical model. The model, the Terminal Area Simulation System (TASS), has a meteorological framework and is formulated for the general purpose of studying the physical-dynamical character of convective clouds and storms. The TASS model is capable of realistic simulations of convective clouds ranging from nonprecipitating cumulus to intense, long-lasting, supercell hailstorms. Its application, however, is not limited to convective clouds; the model may be applied to many other microscale and meso-gamma scale phenomena. In fact, considerable care has been taken in the formulation, so that the model is capable of valid simulations of tornadic and severe downburst phenomena. One major use of the model, so far, has been in the study of downburst-related wind shear and its impact on aviation safety (e.g., Chuang et al., 1984; Proctor, 1985a, 1985b). The model is currently being used to examine the three-dimensional structure of downbursts and to provide realistic data for real-time flight simulations.

A brief description of the TASS model is as follows. The model utilizes a nonhydrostatic, compressible and unsteady set of governing equations which are solved on a three-dimensional staggered grid. The model divides water into six bulk categories each governed by a prognostic equation. The six categories are: 1) water vapor, 2) ice crystals, 3) cloud droplets, 4) rain, 5) snow, and 6) hail/graupel. The former three categories represent nonprecipitating forms of water, while the latter three represent precipitating forms of water. The hail/graupel category may consist of either hail or graupel. Note that all three phases of water (i.e., vapor, liquid,

and solid) are included. Parameterization of the numerous microphysical interactions (that result in exchanges of water between the six categories) are similar to those given in Lin et al. (1983), and Rutledge and Hobbs (1983). As for treating turbulence mixing, the TASS model adopts the subgrid closure approach (e.g., Deardorff, 1970; 1972; 1973). That is, scales of turbulence larger than the assumed grid size are simulated explicitly within the flow field; while scales of turbulence less than the grid size are parameterized from a closure approximation. The subgrid closure model currently in use is a conventional, first-order, diagnostic approximation. TASS also incorporates surface stresses which are dependent upon stratification, ground roughness, and local winds. Numerical stability and conservation in the solution of the governing equations relies on an appropriate choice of numerics and boundary conditions. The TASS model uses quadratic-conservative space differencing and incorporates a modified Orlanski radiation boundary scheme. Application of the radiation boundary condition to the open lateral boundaries allows the outward propagation of waves with minimal reflection. Also, the procedure for applying the radiation boundary conditions is free of domain-wide mass trends. Other features of TASS are 1) the option of a vertical grid-size stretching, 2) movable mesh with time varying translation speed, 3) a numerical filter and sponge applied below the top boundary, and 4) specification of an initial environment from a sounding that is either observed or predicted from a regional model simulation. Output from TASS includes three-dimensional fields of wind velocity, rain, snow, hail, cloud water (cloud droplets and ice crystals), radar reflectivity, temperature, and pressure (see Fig. 1).

Details of the model formulation are found in Chapters 2-6. In Chapter 2 the basic model assumptions are listed. In Chapter 3 the model framework,

governing equations, boundary conditions, and turbulence closure are discussed. The cloud microphysics, including the development of the microphysical parameterizations, are described in detail in Chapter 4. The initial and reference conditions are discussed in Chapter 5. This section includes the formulation for the initial perturbation fields which are necessary in order to trigger convective development. In Chapter 6 the numerical procedure is described. This section includes the formulation for the variable-speed, grid-translation algorithm, as well as the details of the finite-difference equations, grid, and numerical stability criteria. Also included in Chapter 6 are some important numerical details in the computation of the cloud microphysics and a brief discussion of the model code.

Several test simulations with the TASS model are described in Chapter 7. These test cases assume simplified atmospheric conditions, and are useful in demonstrating the validity of the model coding and formulation. A more severe test of the model performance is discussed in a second report, in which TASS simulated results are compared and evaluated against observed data sets.

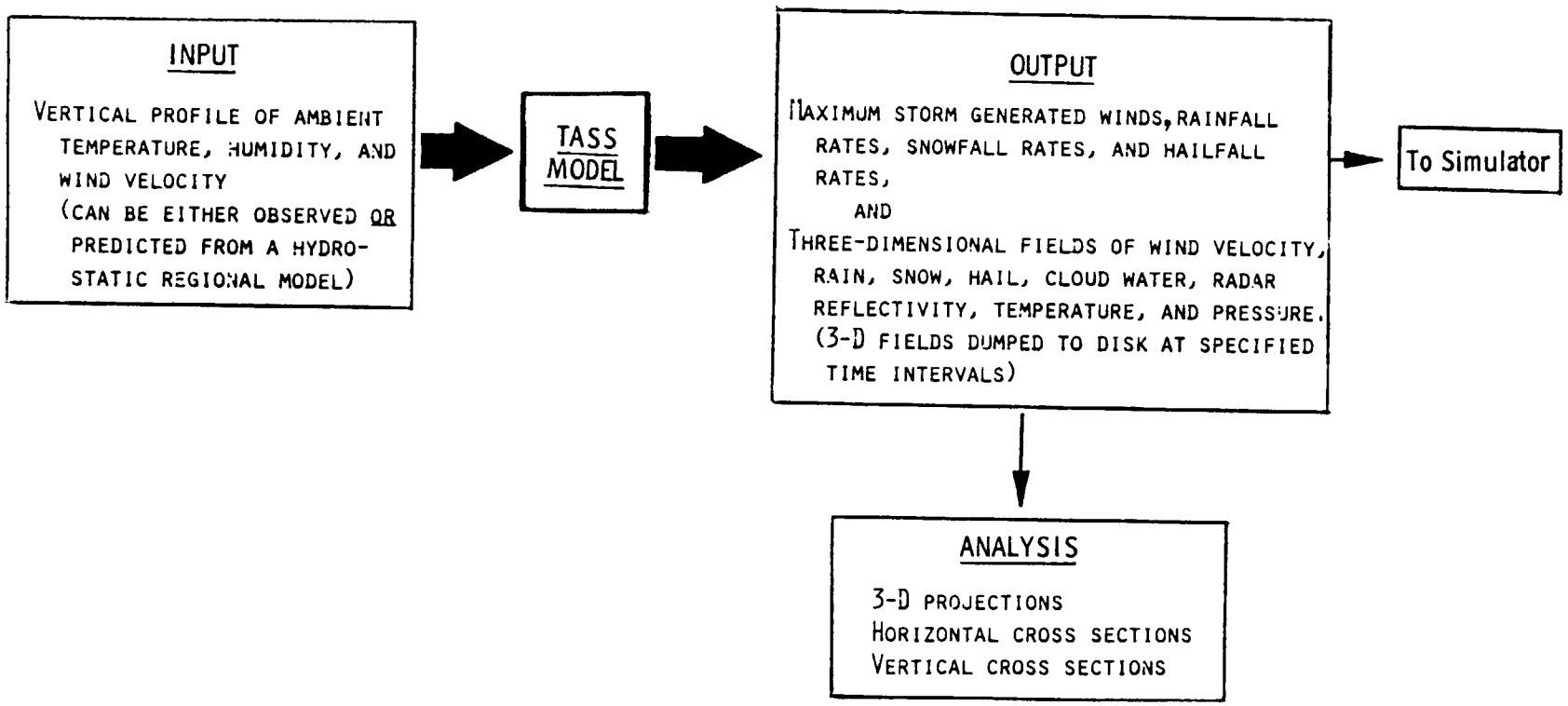

Fig. 1. Schematic of Data Flow

2. BASIC MODEL ASSUMPTIONS

The TASS model has been developed for the general purpose of studying convective phenomena with time scales of several hours or less. The primary model assumptions are:

1) an equation set which is valid for subsonic and high-Reynold's number turbulent flow;

2) Reynolds' averaging of equation set is roughly equal to grid size;

3) thermal radiation is neglected;

4) the first grid point above the ground lies within the surface stress layer;

5) the ground is flat with a homogeneous surface roughness;

6) only a passive interaction with the large-scale environment -- disturbances can propagate out of the limited model domain, but not into the domain;

7) the initial environment is horizontally homogeneous and in steady balance -- convection is initiated by adding a velocity and/or temperature perturbation;

8) supersaturation with respect to liquid water is not allowed --

condensation occurs at a rate which maintains saturation;

9) subgrid-scale condensation is neglected;

10) hydrometeors are classified into five bulk categories and microphysical interactions are parameterized;

11) rain, snow, and hail/graupel assume inverse-exponential size distributions;

12) cloud ice crystals have a monodispersive size distribution;

13) falling hydrometeors instantaneously achieve their terminal velocity and have no horizontal slip relative to air motion; and

14) electrical effects (e.g., drop charging) are ignored.

3. DYNAMIC MODEL

Model Framework

The model framework assigns a reference environment which is a function of only the height coordinate and is in hydrostatic balance. The dependent variables may be expanded in terms of the reference environment as (symbols are listed in the Appendix A)

$$u(x,y,z,t) = U_o(z) + u'(x,y,z,t),$$

$$v(x,y,z,t) = V_o(z) + v'(x,y,z,t),$$

$$P(x,y,z,t) = P_o(z) + p(x,y,z,t),$$

$$\theta(x,y,z,t) = \theta_o(z) + \theta'(x,y,z,t),$$

$$\rho(x,y,z,t) = \rho_o(z) + \rho'(x,y,z,t),$$

$$Q_v(x,y,z,t) = Q_{vo}(z) + Q_v'(x,y,z,t),$$

where x, y, and z are respectively the Cartesian coordinate in the west to east, south to north, and vertical direction; t is the time coordinate; u and v are respectively the west to east and south to north velocity component; P is pressure, θ is potential temperature; ρ is the air density, Q_v is the mixing ratio for vapor; U_o, V_o, P_o, ρ_o, θ_o, Q_{vo} are the reference components, and u', v', p, ρ', θ' and Q_v' are the deviations from their respective

reference quantities. The values of the reference environment may be taken from an actual hydrostatically-balanced environmental sounding.

The reference environment also represents the initial model environment. Details of the initial and reference environment formulations are discussed in section 5.

Governing Equations

The model incorporates the unsteady primitive equations in nonhydrostatic and compressible form. As in Cotton and Tripoli (1978), dimensional pressure and potential temperature (along with moisture substances) are chosen as the prognostic thermodynamic variables. Closure of the equation set is obtained by diagnosing density and temperature.

In deriving the following equations the hydrometeors are assumed to instantaneously achieve their respective terminal velocities; and thus, the total mass per unit volume of atmosphere is equal to the sum of the masses (per unit volume of atmosphere) of dry air, water vapor, cloud droplets, cloud ice crystals, rain, snow, and hail (see Appendix B). This assumption leads to an equation of state having the form

$$\rho = \frac{P}{RT} (1 - 0.61\ Q_v + Q_T), \qquad (1)$$

where $Q_T = Q_{CD} + Q_{IC} + Q_R + Q_{SN} + Q_H$. Here, R is the gas constant for dry air; T is the air temperature; and Q_T is the total of the water substance which is a sum of the mixing ratios of cloud droplets, Q_{CD}, ice crystals, Q_{IC}, rain, Q_R, snow, Q_{SN}, and hail, Q_H.

The governing equations consist of eleven prognostic equations. They are

expressed in a form that is consistent with the fully-elastic mass-continuity equation (i.e., $d\rho/dt = -\rho \nabla \cdot V$) as follows.

Three equations for momentum

The equations for momentum are expressed in Cartesian tensor notation as

$$\frac{\partial u_i}{\partial t} + \frac{H}{\rho_o}\frac{\partial p}{\partial x_i} = -\frac{\partial u_i u_j}{\partial x_j} + u_i \frac{\partial u_j}{\partial x_j} + g(H-1)\,\delta_{i3} - 2\,\Omega_j\, u'_k\, \varepsilon_{ijk} + \frac{1}{\rho_o}\frac{\partial \tau_{ij}}{\partial x_j} + \left(\frac{\partial u_i}{\partial t}\right)^* . \qquad (2)$$

The Einstein summation convention is used for vector quantities; u_i is the ith velocity component (i,j,k index from 1 to 3, $u_1 = u$, $u_2 = v$, $u_3 = w$, $x_1 = x$, $x_2 = y$, and $x_3 = z$), ε_{ijk} is the alternating unit tensor, Ω_j is the jth component of the Earth's angular velocity, g is the gravitational acceleration, and δ is the Kronecker delta. Eq. (2) is in nonBoussinesq form as derived in Proctor (1982). The advection terms, represented by the first two terms on the right-hand-side of Eq. (2), are expressed in this expanded form in order that quadratic-conservative numerical formulations can be applied[1].

Coriolis effects are retained even though Klemp and Wilhelmson (1978b) found that their inclusion produced only minor changes in cumulonimbus simulations. An approximate formulation of the coriolis effect follows that of Tripoli and Cotton (1982). They assume that the initial fields are in geostrophic balance, and they neglect the horizontal variations of the initial

[1]The advection term can also be expressed as $[\partial u_i u_j \rho_o/\partial x_j + u_j \partial u_i \rho_o/\partial x_j]/\rho_o$ (e.g. Tripoli and Cotton, 1980). This form, as well as the form expressed in Eq. (2) were tested in an axisymmetric simulation of a firestorm; even under these severe conditions results from both of the formulations were nearly identical.

pressure and temperature fields that are due to coriolis effects. These assumptions lead to the formulation in Eq. (2) in which the coriolis acceleration only affects the perturbation velocity.

The next-to-last term in Eq. (2) is due to Reynolds' averaging. The Reynolds' stresses, τ_{ij}, are a result of subgrid-scale fluctuations of velocity. Details of the subgrid formulation are discussed later in this section.

The last term in Eq. (2) is an external forcing term which is added in order to maintain a steady initial state. Details of this procedure will be discussed in section 5.

The density ratio term H represents the ratio of the reference density of the environment to the local density. It may be diagnosed (see Proctor, 1982) as

$$H \equiv \rho_o/\rho = (\theta/\theta_o)\ (P_o/P)^{1/\eta}\ [1 + 0.61\ (Q_v - Q_{vo}) - Q_T], \qquad (3a)$$

where $\eta \equiv C_p/C_v$ -- the ratio of specific heats of air at constant pressure and constant volume. The exponentiated term in Eq. (3a) can be expanded, resulting in an expression which is more computationally efficient, yet still valid for most atmospheric problems (where $p << P_o$). This alternate expression, which is used in almost all of the model experiments, is

$$H = [\theta/\theta_o - p/\eta P_o]\ [1.0 + 0.61\ (Q_v - Q_{vo}) - Q_T]. \qquad (3b)$$

Prognostic equation for pressure deviation

The prognostic equation for pressure deviation is

$$\frac{\partial p}{\partial t} + \eta P \frac{\partial u_j}{\partial x_j} = - \frac{\partial u_j p}{\partial x_j} + p \frac{\partial u_j}{\partial x_j} + \rho_o g u_j \delta_{j3}$$

$$+ \frac{\eta P}{\theta} \frac{d\theta}{dt} - \eta P \left[\frac{dQ_T}{dt} - .61 \frac{dQ_v}{dt}\right] (1 - .61Q_v + Q_T)$$

$$+ \frac{1}{\rho_o} \frac{\partial S(P)}{\partial x_j} \qquad (4)$$

where S(P) is due to subgrid-scale fluctuations. The derivation of this equation can be found in Appendix B.

Thermodynamic equation

The thermodynamic energy equation is written for potential temperature which is conserved in dry-adiabatic processes. The prognostic equation for potential temperature is

$$\frac{\partial \theta}{\partial t} = - \frac{\partial u_j \theta}{\partial x_j} + \theta \frac{\partial u_j}{\partial x_j} + \frac{1}{\rho_o} \frac{\partial S(\theta)}{\partial x_j}$$

$$+ \frac{\theta}{C_p T} [L_v S_v + L_f S_f + L_s S_s] + \left(\frac{\partial \theta}{\partial t}\right)^* \qquad (5)$$

where L_v, L_f, and L_s are respectively the latent heats of vaporization, fusion, and sublimation; S_v, S_f and S_s represent the rate of phase conversions of water in units of mass of water per unit of time per unit mass of dry air. This basic formulation of the thermodynamic equation was derived by Das (1969) and has been found to have reasonable accuracy (e.g., Wilhelmson, 1977).

Six equations for water substance

A coupled set of six prognostic continuity equations govern the distribution of water vapor, and liquid phase and solid phase water substances. Each variable for water substance is expressed in terms of a mixing ratio (mass of water substance per mass of dry air) which is conserved in the absence of turbulence mixing, phase changes, and microphysical interactions.

The prognostic equations for water vapor, nonprecipitating cloud droplets, nonprecipitating cloud ice crystals, rain, snow, and hail are, respectively,

$$\frac{\partial Q_v}{\partial t} = -\frac{\partial u_j Q_v}{\partial x_j} + Q_v \frac{\partial u_j}{\partial x_j} + \frac{1}{\rho_o}\frac{\partial S(Q_v)}{\partial x_j} + S_{vap} + \left(\frac{\partial Q_v}{\partial t}\right)^*, \tag{6}$$

$$\frac{\partial Q_{CD}}{\partial t} = -\frac{\partial u_j Q_{CD}}{\partial x_j} + Q_{CD}\frac{\partial u_j}{\partial x_j} + \frac{1}{\rho_o}\frac{\partial S(Q_{CD})}{\partial x_j} + S_{CD}, \tag{7}$$

$$\frac{\partial Q_{IC}}{\partial t} = -\frac{\partial u_j Q_{IC}}{\partial x_j} + Q_{IC}\frac{\partial u_j}{\partial x_j} + \frac{1}{\rho_o}\frac{\partial S(Q_{IC})}{\partial x_j} + S_{IC}, \tag{8}$$

$$\frac{\partial Q_R}{\partial t} = -\frac{\partial u_j Q_R}{\partial x_j} + Q_R\frac{\partial u_j}{\partial x_j} + \frac{1}{\rho_o}\frac{\partial Q_R \overline{W}_R \rho_o}{\partial x_j}\delta_{3j} + \frac{1}{\rho_o}\frac{\partial S(Q_R)}{\partial x_j} + S_R, \tag{9}$$

$$\frac{\partial Q_{SN}}{\partial t} = -\frac{\partial u_j Q_{SN}}{\partial x_j} + Q_{SN}\frac{\partial u_j}{\partial x_j} + \frac{1}{\rho_o}\frac{\partial Q_{SN} W_S \rho_o}{\partial x_j}\delta_{3j} + \frac{\partial S(Q_{SN})}{\partial x_j} + S_{SN}, \tag{10}$$

$$\frac{\partial Q_H}{\partial t} = -\frac{\partial u_j Q_H}{\partial x_j} + Q_H\frac{\partial u_j}{\partial x_j} + \frac{1}{\rho_o}\frac{\partial Q_H \overline{W}_H \rho_o}{\partial x_j}\delta_{3j} + \frac{\partial S(Q_H)}{\partial x_j} + S_H. \tag{11}$$

The last term in Eqs. (6) - (11) is a source term resulting from microphysical interactions between each of the bulk categories. In the absence of evaporation from the ground, continuity of water substances requires:

$$S_{vap} + S_{CD} + S_{IC} + S_R + S_{SN} + S_H = 0.$$

Since Eqs. (9) - (11) govern precipitating categories of water substance, a fall-out or slip term is included. In these terms the bulk terminal velocities for rain, snow and hail are represented by $\overline{W}_R$, W_S , and $\overline{W}_H$, respectively. The terminal velocities are by definition positive and are directed vertically downward. Details of their formulation and the modeled microphysics will be discussed in section 4.

Treatment of Subgrid Processes

If the dependent variables in the governing equations are treated as averages over the grid volumes, the equations themselves should be treated as similarly averaged, giving rise to residual terms. In the presence of turbulence motion these terms represent subgrid Reynolds stresses in the momentum equation and subgrid eddy transport in the remaining prognostic equations. This approach to turbulence closure allows the resolvable eddies to be modeled explicitly, while the influence of the subgrid eddies (the effects of eddies approximately equal to or less than the grid size) are "parameterized" (e.g., Deardorff, 1970; 1972; 1973; Sommaria, 1976). An overview of subgrid scale modeling can be found in Herring (1979).

Subgrid Reynolds stresses

The subgrid Reynolds stress tensor according to 1st-order closure theory (e.g., Clark, 1979) is

$$\tau_{ij} = \rho_o K_M D_{ij},$$

in which the deformation tensor D_{ij} is defined

$$D_{ij} = \frac{\partial u_i}{\partial x_j} + \frac{\partial u_j}{\partial x_i} - \frac{2}{3}\frac{\partial u_k}{\partial x_k}\delta_{ij}.$$

The subgrid eddy-viscosity for momentum is

$$K_M = (\alpha \Delta)^2 \, |DEF| \, (1-R_f)^{0.5}, \tag{12}$$

where α is an empirical constant, Δ is the subgrid-turbulence length scale, $|DEF|$ is the absolute magnitude of the local rate of deformation, and R_f is the Richardson flux number. The averaging length scale is related to the grid size as

$$\Delta = (2\Delta x \cdot 2\Delta y \cdot 2\Delta z)^{1/3}. \tag{13}$$

Studies by Clark et al. (1977,1979) and Love and Leslie (1977) suggest that the averaging length should be related to twice the grid length rather than the grid length as in Deardorff (1978). The magnitude of the local rate of deformation is

$$|DEF| = \tfrac{1}{2} D_{ij} \cdot D_{ij} = \left[-\tfrac{2}{3}\Phi^2 + \sum_{ij} \frac{\partial u_i}{\partial x_j}\left(\frac{\partial u_i}{\partial x_j} + \frac{\partial u_j}{\partial x_i}\right)\right]^{0.5},$$

where the divergence is defined as

$$\Phi = \sum_k \frac{\partial u_k}{\partial x_k}. \tag{14}$$

The local Richardson flux number is related to the local Richardson number

as

$$R_f = (K_T/K_M)R_i \qquad \text{for} \qquad -100 \leq R_f \leq 0.99,$$

and the local Richardson number is defined (e.g., Duran and Klemp, 1983) as

$$R_i = \frac{g}{|DEF|^2} \begin{cases} \frac{1}{T}\frac{\partial\theta}{\partial z} + 0.61\frac{\partial}{\partial z}(Q_v - Q_{vo}) \\ \qquad -\frac{\partial}{\partial z}(Q_R + Q_{SN} + Q_H) & \text{for } Q_{CD} + Q_{IC} \leq 0, \\ \frac{1}{T}\frac{\partial\theta_e}{\partial z} + 0.61\frac{\partial}{\partial z}(Q_v + Q_{CD} + Q_{IC} - Q_{vo}) \\ \qquad -\frac{\partial}{\partial z}(Q_{CD} + Q_{IC} + Q_v) \\ \qquad -\frac{\partial}{\partial z}(Q_R + Q_{SN} + Q_H) & \text{for } Q_{CD} + Q_{IC} > 0; \end{cases}$$

where the equivalent potential temperature is defined

$$\theta_e = \theta \exp\left[(L_s Q_v + L_f Q_{IC})/C_p T\right].$$

An arbitrary upper bound of 0.99 is enforced on R_f in order to guarantee a minimal amount of diffusion. An arbitrarily lower bound of -100 is also assumed.

In the above formulation, the subgrid eddy mixing is affected by the local shears through the deformation term, and is modified by the stratification through the Richardson flux number. When the stratification is neutral ($R_f = 0$), Eq. (12) reduces to the Smagorinsky turbulence model which has been applied with great practical success in planetary boundary layer studies (e.g., Deardorff, 1970; 1972). Clark et al. (1977, 1979) has

examined several closure assumptions in simulations of homogeneous isotropic turbulence and has found that the Smagorinsky model adequately accounted for the transfer turbulence energy to the subgrid scales. They also have found that the optimal dissipation of grid-scale turbulence energy occurred when $\alpha = 0.186$. This value falls within the range of other experimental and theoretical values, and should remain invariant of grid size (at least as long as Δ is within the inertial subrange). The impact of unequal grid sizes on this turbulence closure scheme is unknown.

Subgrid eddy transport

Also from lst-order closure theory, the subgrid covariances in Eqs. (5) - (11) are approximated as

$$S(q) = \rho_o K_T \, \partial q/\partial x_j \qquad (15)$$

where $q = \theta$, Q_v, Q_{CD}, Q_{IC}, Q_R, Q_{SN}, or Q_H. The subgrid eddy-mixing coefficient for heat, K_T, is assumed for all scalar variables (except pressure). Its value is taken from theoretical considerations by Deardorff (1973) to be

$$K_T = 2.5 \, K_M \qquad \text{for } z > \Delta z.$$

Similar to Eq. (15) the subgrid transport for pressure deviation is assumed as

$$S(p) = \rho_o K_M \, \partial p/\partial x_j.$$

Surface boundary

The choice of surface boundary conditions can have an important influence in convective cloud simulations. For instance, Schlesinger (1982) found that a significant impact on simulated storm development resulted, when he changed his model surface winds from the customary free-slip to semi-slip. The change to the semi-slip boundary condition was made so as to take into effect the retarding effect of the earth's surface. Schlesinger found that the orientation of the flanking line and the dominance of the right moving convective cell (after storm splitting) were strongly affected by the choice of surface boundary conditions. The ground boundary layer also was found to play a crucial role in the axisymmetric simulations of a tornado by Proctor (1982). His model simulations demonstrated that surface convergence induced by a parent vortex, and the subsequent release of latent heat of condensation, may lead to the formation of a tornado. His simulations also demonstrated that frictional convergence was responsible for the extreme upward velocities in a tornado at a few tens of meters above the ground. These studies and others have demonstrated that friction at the earth's surface can exert some influence on convective systems. Friction at the earth's surface may alter the depth, speed, and orientation of storm-produced surface outflows, and may also influence the propagation and intensity of convective storms.

In the absence of detailed surface-layer data below convective storms, it is difficult to formulate and test surface boundary conditions for cloud models. In this model as in Sommeria (1976), a constant flux or stress layer is assumed to extend from the ground to the first grid point above the surface (at height $h \equiv \Delta z/2$). Conditions within this layer are parameterized using the

nondimensional shear and temperature gradient functions, as deduced from field observations by Businger et al. (1971). The model surface formulation described below is completely diagnostic; it does not include a moisture or temperature budget for the ground.

At $z = h$:

$$K_M = (kh)^2 \, |DEF| \, (1 - \frac{\phi_M}{\phi_H} R_i)^{0.5},$$

and

$$K_T = K_M \, \phi_M/\phi_H,$$

where k is von Karman's constant (0.4), and ϕ_M and ϕ_H are respectively the nondimensional wind shear and temperature gradient. Within the surface layer ($0 < z < h$), relationships for u, v, θ, and K_M are based on Monin-Obukhov similarity theory and are derived in Appendix C. The mean velocity gradients in the surface layer are

$$\langle\frac{\partial u}{\partial z}\rangle = u(h)/h, \quad \text{and} \quad \langle\frac{\partial v}{\partial z}\rangle = v(h)/h.$$

The mean temperature gradient in the surface layer is

$$\langle\frac{\partial \theta}{\partial z}\rangle = \frac{T_o(1 + .61\, Q_{vo})\, [u(h)^2 + v(h)^2]}{g\, h^2} \frac{G_H}{G_M^2} (\frac{h}{L}),$$

where G_H and G_M are universal functions that can be deduced from field observations and L is the Monin-Obukhov length. The mean eddy-viscosity for

momentum within the surface layer is

$$\langle K_M \rangle = K_M(h)\ \phi_M/G_M.$$

The values for ϕ_M and ϕ_H are determined from measurements of Businger et al. (1971), i.e.,

unstable $(h/L) < 0$	stable $(h/L) > 0$
$\phi_M = [1 - 15\ (h/L)]^{-0.25}$	$\phi_M = 1 + 4.7\ (h/L)$
$\phi_H = 0.74\ [1 - 9\ (h/L)]^{-0.5}$	$\phi_H = 0.74 + 4.7\ (h/L).$

Likewise, the universal functions are

$$G_M = \ln\ (h/z_o) - \psi_M,$$
$$G_H = 0.74\ [\ln\ (h/z_o) - \psi_H],$$

where

$$\psi_M = \begin{cases} -4.7\ (h/L) & \text{for } (h/L) \geq 0, \\ -0.352\ (h/L)^3 - 1.43\ (h/L)^2 - 2.22\ (h/L) & \text{for } -2 < (h/L) < 0; \\ -6.35\ (h/L) & \text{for } (h/L) \geq 0, \end{cases}$$

$$\psi_H = \begin{cases} 0.74/\phi_H - 1 & \text{for } -0.08 \leq (h/L) \leq 0, \\ 0.1326 - 2.341\ (h/L) - 1.278\ (h/L)^2 - 0.2879\ (h/L)^3 & \text{for } -2 < (h/L) < -0.08 \end{cases}$$

In the formulas for ψ_M and ψ_H, approximate curve fits have been substituted

for the unstable cases ($h/L < 0$). [The third-order approximations for ψ_m was devised by Schultz (1979).]

The Monin-Obukhov length is determined from the local Richardson number (at $z = h$) as

$$\frac{z}{L} = \begin{cases} R_i/0.95 & \text{for} \quad R_i < 0, \\ R_i/(1 - 5\,R_i) & \text{for} \quad 0 < R_i < 0.1674, \\ 38.227 - 463.71\,R_i + 1442.2\,R_i^2 & \text{for} \quad 0.1674 \leq R_i < 0.1875, \\ 308.49 - 3323.9\,R_i + 9010.6\,R_i^2 & \text{for} \quad 0.1875 \leq R_i \leq 0.2. \end{cases}$$

The first two approximations are from Haltiner and Williams (1980), the latter two are curve fits determined from the relationship

$$R_i = (z/L)\,\phi_H/\phi_M{}^2.$$

The eddy diffusion for temperature and moisture substance, K_T, is set equal to zero at the surface. Hence, the subgrid fluxes of vapor, temperature, etc., are not allowed through the ground surface. The effect of evaporation from a rain-soaked ground is parameterized by adding a source term (at the lowest grid level above the ground) in each the prognostic vapor and thermodynamic equations. The formulation for ground evaporation is presented in section 4.

Other boundary conditions at the ground surface are:

$$w = 0, \qquad \frac{\partial Q_v}{\partial z} = 0,$$

$$\frac{\partial Q_{CD}}{\partial z} = 0, \quad \text{and} \quad \frac{\partial Q_{IC}}{\partial z} = 0.$$

The surface boundary condition for pressure is consistent with the vertical equation of momentum at z = o; i.e.,

$$\frac{\partial p}{\partial z} = (\rho_o/H)\ [(H - 1)\ g + \frac{\partial \tau_{j3}}{\partial x_j}].$$

Values at the ground for precipitating moisture substance (rain, snow, and hail) are determined by applying upstream time-differencing to the following equations:

$$\frac{\partial Q_{RN}}{\partial t} = \overline{W}_R \frac{\partial Q_{RN}}{\partial z}\ ,$$

$$\frac{\partial Q_{SN}}{\partial t} = W_S \frac{\partial Q_{SN}}{\partial z}\ ,$$

$$\frac{\partial Q_H}{\partial t} = \overline{W}_H \frac{\partial Q_H}{\partial z}\ ;$$

hence, precipitating hydrometeors fall through the surface boundary at a rate determined by their mean terminal velocity.

Open lateral boundaries

Computational constraints dictate a requirement for lateral boundaries even though no physical counterpart exist. Open lateral boundaries should allow the mean flow and superimposed wave modes to pass freely and unobstructed. They should also be formulated such that they guarantee conservation; i.e., they should not artifically create mass, water vapor, etc. The proper formulation of the lateral boundaries is essential for accurate simulations.

An increasingly popular boundary condition for nonperiodic but open flow

boundary conditions is the Sommerfeld radiation condition:

$$\frac{\partial \phi}{\partial t} + C \frac{\partial \phi}{\partial r} = 0, \tag{16}$$

where ϕ is any prognostic variable, r is the space coordinate perpendicular to the boundary, and C is phase velocity normal to the boundary. Orlanski (1976) determined C locally from (16) at an interior grid point then applied it to the radiation boundary condition at the following time step; hence he assumed

$$C_b^N = C_{b-1}^{N-1},$$

where N represents the time level and b-1 represents first interior point adjacent to the boundary point. Thus, he assumed that the phase speed at the boundary is equal to phase speed at the adjacent interior point from the previous time step. Orlanski applied this procedure in several cases of two-dimensional flow which was governed by a prognostic vorticity equation. He found this formulation to work quite well; allowing disturbances to propagate through the boundary with minimal reflection and distortion of the interior solution.

In nonhydrostatic primitive equation models the procedure used by Klemp and Wilhelmson (1978a), Clark (1979), and Tripoli and Cotton (1980) is to apply the radiation boundary condition to the velocity component normal to the boundary, and to apply one or more of the following conditions to the remaining dependent variables along the boundary: 1) use upwind differencing if the normal velocity is directed outward, 2) set the variable equal to a fixed reference value, and/or 3) specify the normal gradient equal to zero.

The phase velocity in (1) is either specified as in Klemp and Wilhelmson, or determined locally as in Orlanski (1976). However, these formulations often led to runaway circulations and unrealistic trends in the domain-wide mass fields (Clark, 1979; Tripoli and Cotton, 1980, 1982). A new procedure for applying the radiation boundary condition in primitive equation models has been formulated by Proctor (1985a). This procedure includes the "Orlanski radiation boundary condition"; that is Eq. (16) with the phase speed extrapolated from the interior as in Orlanski (1976); however, it is in a form consistent with the Adams-Bashforth time differencing scheme. The procedure, as outlined below, differs from the conventional approach and is essentially free of mass trends and run-away circulations. In fact, a periodic adjustment to the domain-wide pressure field [as in Klemp and Wilhelmson (1978a)] is never needed throughout any of the simulations.

At each of the four lateral boundaries, the boundary conditions are as follows:

(1) The radiation boundary condition is applied to the pressure deviation and the components of velocity that are tangent to the boundary [e.g., Eq. (16) is applied to u and w at the north and south boundaries];

(2) The vertical velocity is set equal to zero at its boundary point whenever the flow normal to the boundary is directed into the domain;

(3) The horizontal velocity and pressure can relax to their reference values at boundary points where the radiation boundary condition is applied; i.e.,

$$\frac{\partial u}{\partial t} = \varepsilon(U_o - u)$$

is applied to u at the north and south boundaries;

$$\frac{\partial v}{\partial t} = \varepsilon(V_o - v)$$

is applied to v at the east and west boundaries; and

$$\frac{\partial p}{\partial t} = - \varepsilon\ p$$

is applied to p at all four boundaries when the phase speed determined by Eq. (16) is directed into the domain. [The value for ε is $10^{-2}\ s^{-1}$.]

(4) The component of velocity normal to the boundary is determined from continuity by assuming that the normal gradient of three-dimensional divergence vanishes; thus at the north and south boundaries

$$\left(\frac{\partial v}{\partial y}\right)_b = - \left(\frac{\partial u}{\partial x} + \frac{\partial w}{\partial z}\right)_b + \Phi_{b-1},$$

likewise, on the east-west boundaries

$$\left(\frac{\partial u}{\partial x}\right)_b = - \left(\frac{\partial v}{\partial y} + \frac{\partial w}{\partial z}\right)_b + \Phi_{b-1},$$

where Φ_{b-1} is the divergence evaluated at the first interior point;

(5) The boundary values for the remaining variables are determined from upstream time differencing if the flow normal to the boundary is directed outward; otherwise if the flow is inward, they are set to their reference values; i.e., $\theta = \theta_o$, $Q_v = Q_{vo}$, $Q_{CD} = 0$, $Q_{IC} = 0$, $Q_R = 0$, $Q_{SN} = 0$, $Q_H = 0$.

In addition to the boundary conditions, a second-order filter is applied to the u, v, w, θ, and Q_v fields along the three columns of grid points adjacent to each lateral boundary. Application of the filter is necessary in order to eliminate $2\Delta x$ and $4\Delta x$ waves. The Orlanski radiation boundary condition is suspected of not being able to handle the fast changing phase speeds of the numerically-generated high frequency waves; thus making filtering next to the boundaries necessary.

The above formulation for the lateral boundaries allows the outward propagation of disturbances with minimal reflection. But, of course, it cannot account for the influence and inward propagation of disturbances, that (in the real world) may lie outside of the model domain.

Top boundary

At the top boundary the vertical velocity is set equal to zero and the potential temperature is held fixed to its reference value. These conditions are not unappropriate if the top boundary is chosen at a reasonably high altitude. However, an artifact of this choice is the reflection of upward propagating gravity waves. To reduce wave reflection, a "filter and sponge" (Perkey and Kreitzberg, 1976) are applied within the four rows below the top boundary.

In the application of the sponge the local rate terms for u, v, w, p, and θ are multiplied by a weighting coefficient W_B, which is a function of the level beneath the top boundary. The weighting coefficients for w and θ are:

$$W_B(I) = \begin{cases} 0.0 & \text{for} \quad I = b \\ 0.4 & \text{for} \quad I = b-1 \\ 0.7 & \text{for} \quad I = b-2 \\ 0.9 & \text{for} \quad I = b-3 \end{cases}$$

where b refers to the grid points for w or θ at the top boundary level;

b-1, the first level beneath the boundary; etc. For u, v, and p a porous sponge condition is assumed and the coefficients are given as:

$$W_B(I) = \begin{cases} 0.7 & \text{for} \quad I = b-1 \\ 0.9 & \text{for} \quad I = b-2 \end{cases} .$$

The values of u, v, and p at the top boundary are assigned derivative boundary conditions as follows: for horizontal velocity a free slip boundary condition is assumed; that is,

$$\frac{\partial u}{\partial z} = \frac{\partial v}{\partial z} = 0;$$

for the pressure deviation, its vertical gradient is assumed to vanish at the top boundary, i.e.,

$$\frac{\partial p}{\partial z} = 0.$$

Similarly at the top boundary, the subgrid eddy viscosity and water substance variables are

$$\frac{\partial K_M}{\partial z} = \frac{\partial K_T}{\partial z} = 0,$$

and

$$\frac{\partial Q_{CD}}{\partial z} = \frac{\partial Q_{IC}}{\partial z} = \frac{\partial Q_R}{\partial z} = \frac{\partial Q_{SN}}{\partial z} = \frac{\partial Q_H}{\partial z} = 0.$$

The mixing ratio for water vapor, on the other hand, is specified to its reference value as $Q_v = Q_{vo}$.

4. CLOUD MICROPHYSICS

The cloud hydrometeors are subdivided into five bulk categories: 1) cloud droplets, 2) ice crystals, 3) rain, 4) snow, and 5) hail. The hydrometeors comprising the cloud droplets and ice crystal categories are assumed to be small and nonprecipitating. The ice crystals are assumed to have a monodispersive size distribution. The remaining categories represent precipitating hydrometeors and are assumed to have a continuous inverse exponential size distribution. All hydrometeors except ice crystals are assumed spherical. The parameterization of the cloud microphysics is similar to those described by Orville and Kopp (1977), Lin et al. (1983) and Rutledge and Hobbs (1983).

The size distribution for rain is taken as (Marshall and Palmer, 1948)

$$N(D_R) = N_{OR} \exp (- D_R/\Lambda_R), \tag{17}$$

where $N(D_R)$ is the number of raindrops per unit diameter per unit volume, D_R is the raindrop diameter, Λ_R is the inverse of the slope of the rain distribution, and N_{OR} is the intercept. Similarly the size distribution for snow is assumed as (Gunn and Marshall, 1958)

$$N(D_S) = N_{OS} \exp (- D_S/\Lambda_S); \tag{18}$$

and the distribution for hail or graupel is taken as (Federer and Waldvogel, 1975)

$$N(D_H) = N_{OH} \exp (- D_H/\Lambda_H). \tag{19}$$

The slope factors can be determined from the above distributions as (e.g., Lin et al., 1983)

$$\Lambda_R = (\rho_o Q_R / \pi N_{OR}\ \delta_w)^{0.25}, \tag{20}$$

$$\Lambda_S = (\rho_o Q_{SN} / \pi N_{OS}\ \delta_S)^{0.25}, \tag{21}$$

$$\Lambda_H = (\rho_o Q_H / \pi N_{OH}\ \delta_H)^{0.25}, \tag{22}$$

where δ_w, δ_S, and δ_H are respectively the densities of water, snow, and hail.

In the microphysical parameterizations the intercept for rain is assumed constant and the intercepts for snow and hail are functions of height only. The values for the intercepts are derived from measured size distributions. For rain, observations during a thunderstorm by Sekhon and Srivastava (1971) lead to a value of $N_{OR} = 2.5 \times 10^7\ m^{-4}$. This value is larger than that found by Marshall and Palmer (1948) for widespread rain; but, is nearly identical to the N_{OR} for hurricane rainfall reported by Lord et al. (1984). The intercept for snow is determined from data reported in Houze et al. (1979) as

$$N_{OS} = 5.5 \times 10^6 \exp\ [-\ 0.088\ (T_o - T_M)]\ \ m^{-4},$$

where T_o is the temperature of the reference environment (degrees Kelvin) and T_M is the melting-point temperature (273.16 K). The intercept for hail is taken as

$$N_{OH} = \begin{cases} 4 \times 10^4\ m^{-4} & \text{for } T_o \leq T_M, \\ 4 \times 10^4 \exp[-\ 0.088\ (T_o - T_M)] & \text{for } T_o > T_M. \end{cases}$$

The hail intercept at altitudes above the melting level is assumed constant; the value of 4×10^4 m^{-4} was deduced by Orville and Kopp (1977) from data reported in Federer and Waldvogel (1975). The decrease in N_{OH} with temperature at altitudes below the melting level is an attempt to crudely approximate the decrease in N_{OH} that is due to the more favorable melting of the smaller hail sizes. For example, in a two-dimensional simulation of a hailstorm by Kopp et al. (1983), the hail intercept was found to be about an order of magnitude lower at the ground than above the melting level.

The hail category is represented by two different types of spherical ice particles: moderate density graupel and hail. As in Cotton et al. (1982), only one type is allowed at a given grid point and time. Hail is assumed present only when the computed mean graupel diameter exceeds 5 mm. The two types of particles differ in that the assumed density for graupel particles is lower. Only hail particles are allowed wet growth; otherwise, the parameterization of the two types of particles are identical. In the following text both types of particles will be referred to as hail.

The density of hail[2] is

$$\delta_H = \begin{cases} 900 \text{ kg m}^{-3} & \text{if } \overline{D}_G > 5 \times 10^{-3} \text{ m} \\ 450 \text{ kg m}^{-3} & \text{if } \overline{D}_G \leq 5 \times 10^{-3} \text{ m}, \end{cases}$$

where the mass weighted mean diameter of the graupel particle is

$$\overline{D}_G = 4 \left[\rho_o Q_H / 450 \pi N_{OH}\right]^{0.25} \quad [\text{m}].$$

[2]The value for the density of the hail particles is taken from Vittori and di Caporiacco (1959); the assumed value for moderate density graupel is derived from data in Pruppacher and Klett (1978).

The values of the other densities are assumed as 1000 kg m^{-3} for liquid water and 100 kg m^{-3} for snow (e.g., Rutledge and Hobbs, 1983).

Terminal Velocities

Rain

The mass-weighted mean terminal velocity for rain can be determined as (Rutledge and Hobbs, 1983)

$$\overline{W}_R = \frac{\int_o^\infty N(D_R)\, M\,(D_R)\, W_R\,(D_R)\, dD_R}{\int_o^\infty N(D_R)\, M\,(D_R)\, dD_R}, \tag{23}$$

where $W_R(D_R)$ is the terminal velocity of a raindrop having diameter D_R and mass $M(D_R) = \pi\, \delta_w\, D_R^3/6$. Rutledge and Hobbs' (1983) polynomial fit to the experiment data of Gunn and Kunzer (1949) yields (all units MKS)

$$W_R(D_R) = -0.267 + 5150\, D_R - 1.0225 \times 10^6\, D_R^2 + 7.55 \times 10^7\, D_R^3. \tag{24a}$$

Also from the data of Gunn and Kinzer, an alternative approximation for terminal velocity is (Liu and Orville, 1969)

$$W_R(D_R) = 843\, D_R^{0.8}. \tag{24b}$$

Eq. (24b) is less exact than (24a) but leads to a more simple integration of the microphysical equations. Substitution of Eqs. (24a) and (17) into (23) yields a mass-weighted mean terminal velocity for rain as

$$\overline{W}_R = [- 0.267 + 2.06 \times 10^4 \Lambda_R - 2.045 \times 10^7 \Lambda_R^2 + 9.06 \times 10^9 \Lambda_R^3] \ (1.2 /\rho_o)^{0.4} \qquad (25a)$$

(for $\Lambda_R > 1.3132 \times 10^{-5}$ m). Substitution of Eqs. (24b) and (17) into (23) yields

$$\overline{W}_R = 843 \ \Gamma(4.8) \ \Lambda_R^{0.8}/6 \qquad (25b)$$

Values for the mean mass-weighted terminal velocity are computed from Eq. (25a) since it is more precise and computationally efficient. A correction factor is included in (25a) in order to account for the change in fallspeed with air density (Foote and Toit, 1969). Eqs. (24b) and (25b) are used only in the development of the microphysical parameterizations.

Snow

The terminal velocity of snow, in nature, varies slowly with increasing particle size; more significant variances in fallspeed are due to snow type (e.g., rimed dendrites; graupel like snow). The fallspeed assumed in the model is deduced from the data of Locatelli and Hobbs (1974) and Jiusto and Bosworth (1971). The terminal velocity for snow is assumed to vary only with air density, and is given by (where units are in the MKS system)

$$W_S = 1.1 \ (1.2/\rho_o)^{0.5}. \qquad (26)$$

Hail

From McDonald (1960), the terminal velocity of a hailstone having diameter D_H is

$$W_H(D_H) = [4\ g\ \delta_H\ D_H/3\ \rho_o\ C_D]^{0.5}. \qquad (27)$$

The drag coefficient for hailstones is assumed constant with a value of $C_D = 0.45$ (Macklin and Ludlam, 1961). The mean mass-weighted terminal velocity for hail is determined by substituting Eqs. (19) and (27) into an expression similar to (23) and integrating over all particle sizes; giving,

$$\overline{W}_H = 1.09375\ [4\pi\ g\ \delta_H/3\ \rho_o C_D]^{0.5}\ \Lambda_H^{0.5}. \qquad (28)$$

Parameterization of Microphysical Production Terms

For most of the microphysical interactions, the production terms are parameterized by integrating over the assumed size spectrum. For example, if the mass growth of a single raindrop due to a particular interaction is dM/dt, then the rate of production of Q_R is given by

$$\text{PRODUCTION RATE} = \frac{dQ_R}{dt} = \frac{1}{\rho_o} \int_o^\infty \frac{dM}{dt}\ N(D_R)\ dD_R.$$

A description of the microphysical production terms which appear in Eqs. (5) - (11) follows below. The production terms have units of per second; unless otherwise stated all units are expressed in the MKS system.

Condensation and evaporation of cloud droplets

Condensation of water vapor into cloud drops is assumed to occur at rate which maintains saturation with respect to water vapor. Likewise, evaporation of cloud droplets is assumed to occur at a rate such that either saturation is maintained or all available cloud droplets are depleted. From Proctor (1982),

$$PCDWV1 = \frac{1}{\Delta t}\begin{cases}\lambda_v & \text{if} \quad \lambda_v + Q_{CD} \geq 0, \\ -Q_{CD} & \text{if} \quad \lambda_v + Q_{CD} < 0\end{cases}$$

where Δt is the time step and λ_v is defined:

$$\lambda_v = (Q_v - Q_{sv})/[1 + Q_{sv}\, L_v^2/C_p\, R_v\, T^2].$$

[A derivation of the above equation is in Appendix D.] The saturation mixing ratio for vapor[3] is determined from

$$Q_{sv} = e_{sv}\,[Q_v + \varepsilon]/P, \tag{30}$$

where, ε is the ratio of gas constants ($\varepsilon \equiv R_v/R = 0.622$), and e_{sv} is the saturation vapor pressure with respect to water.

Mean cloud droplet radius

A mean radius for cloud droplets is needed in several microphysical parameterizations. It is determined by assuming that the number of cloud droplets per unit volume (n_{CD}) remains constant; thus, the average mass of a cloud droplet is

$$\overline{M}_{CD} = Q_{CD}\,\rho_o/n_{CD}, \tag{31}$$

and the mean radius of a cloud droplet is

[3]The customary definition for saturation mixing ratio is $Q_{sv} = e_{sv}\,\varepsilon/[p-e_{sv}]$ (e.g., Berry et al., 1945). However a reexamination shows that $Q_{sv} \equiv \rho_{sv}/\rho_d = e_{sv}\,\varepsilon/(p-e_v) = e_{sv}\,[Q_v + \varepsilon]/p$. In firestorm simulations the customary definition was found to give negative saturation mixing ratios in areas of high temperature, where e_{sv} exceeded p.

$$\bar{r}_{CD} = [3\, Q_{CD}\, \rho_o / 4\, \pi\, \delta_w\, n_{CD}]^{1/3}. \qquad (32)$$

The value assumed for n_{CD} can be estimated from the condensation nuclei spectra, or if not available, climatology of the area being modeled. For example, typical values in extreme continental areas are $\sim 10^9\ m^{-3}$; while in contrast, values in maritime regions can be as low as $\sim 10^7\ m^{-3}$. Note that for a given concentration of cloud droplet water, Eq. (32) implies that the mean cloud droplet radii are larger in maritime clouds than in continental clouds.

Cloud ice crystals

The treatment of ice crystals follows that of Rutledge and Hobbs (1983). The ice crystals are assumed to be hexagonal plates and to have a monodispersive size distribution. The number concentration of ice crystals is assumed to be given by the concentration of ice nuclei active at temperature T (e.g., Fletcher, 1962):

$$n_{IC} = \begin{cases} 10^9 & T < 230.95, \\ \beta_{IC} \exp[0.6\ (T_M - T)] & \text{for} \quad T_M \geq T \geq 230.95, \\ 0 & T > T_M, \end{cases} \qquad (33)$$

where n_{IC} is the number of ice crystals m^{-3}, and β_{IC} is a constant usually taken as $10^{-2}\ m^{-3}$. An arbitrary upper limit of 10^9 crystals m^{-3} is assumed. No ice crystal processes occur (except for instantaneous melting) at temperatures above 273.16 K.

Ice crystal initiation

Following Rutledge and Hobbs (1983), the ice crystal process is initiated by assuming the immediate presence of small ice crystals having an initial diameter of 12.9 μm, whenever the air is saturated with respect to ice. The rate of production of ice crystals is computed at temperatures less than 268.16 K and is given by

$$\text{PICWV1} = \frac{1}{\Delta t} \text{MIN}\ [10^{-12}\ n_{IC}/\rho_o,\ \lambda_s] \tag{34}$$

where

$$\lambda_s \equiv (Q_v - Q_{si})[1 + Q_{si}\ L_s^2/C_p\ R_v\ T^2]^{-1}.$$

The saturation mixing ratio with respect to ice is

$$Q_{si} = e_{si}\ (Q_v + \varepsilon)/P, \tag{35}$$

where e_{si} is the vapor pressure with respect to ice.

The lesser of the two rates in Eq. (34) is chosen so as to guarantee that the computed growth of the ice crystals will not exceed the vapor available for growth. The latter rate has been replaced by a more exact formulation than that assumed by Rutledge and Hobbs. The new formulation accounts for the implicit adjustment of the saturation mixing ratio (see Appendix D).

Deposition and sublimation of ice crystals

The mass rate of change due to the depositional growth of an ice particle (e.g., Pruppacher and Klett, 1978) is (where A_1^* and B_1^* are expressed in terms

of the reference environment)

$$dM/dt = C[Q_v - Q_{si}]F_I/[Q_{si}A_1^* + B_1^*]; \qquad (36)$$

where,

$$A_1^* \equiv \frac{L_v}{k_T T_o}\left(\frac{L_s}{R_v T_o} - 1\right); \quad \text{and} \quad B_1^* \equiv (\rho_o D_w)^{-1},$$

where k_T is the thermal conductivity of air and D_w is the diffusivity of water vapor in air.

For a small hexagonal plate-like ice crystal the capacitance coefficient C is $4\,\overline{D}_{IC}$; the ventilation factor is assumed unity ($F_I = 1$); and the mean ice crystal mass is $Q_{IC}\,\rho_o/n_{IC}$ (e.g., Rutledge and Hobbs, 1983). Substitution into Eq. (36) yields

$$P1 = 4\,n_{IC}\,\overline{D}_{IC}\,[Q_v - Q_{si}]/\rho_o[Q_{si}\,A_1^* + B_1^*],$$

where the mean diameter of the hexagonal plate-like ice crystals is given by Rutledge and Hobbs as

$$\overline{D}_{IC} = 16.3\,[Q_{IC}\,\rho_o/n_{IC}]^{0.5}. \qquad (37)$$

If supersaturation with respect to ice exists (i.e., $Q_v > Q_{si}$) then

$$PICWV2 = MIN\,[P1;\ \lambda_s/\Delta t], \qquad (38a)$$

or if subsaturation exists (i.e., $Q_v < Q_{si}$) then

$$PICWV2 = MAX\ [P1, -Q_{IC}/\Delta t, \lambda_s/\Delta t]; \tag{38b}$$

The smaller of the two arguments are taken as the rate in (38a) so as to guarantee that the computed growth of ice crystals by deposition does not exceed the vapor available for growth. Similarly in (38b), the greater of the three arguments are taken so as to guarantee the computed sublimation rate does not exceed the vapor deficit, nor exceed the amount of ice crystal water available.

Growth of ice crystals due to riming

The fall velocities of ice crystals and cloud droplets are very small and can be ignored in many cloud processes. However, the difference in the fall speeds between cloud droplets and ice crystals is important when ice crystal growth due to the accretion of supercooled cloud droplets is considered (i.e., riming). The growth equation due to riming for an ice crystal (Orville and Kopp, 1977) is

$$\frac{dM}{dt} = \rho\ Q_{CD}\ \frac{\pi D_{IC}^2}{6}\ (\Delta V)\ E_{ICCD}, \tag{38}$$

where ΔV is the difference in terminal velocity of the ice crystals and cloud droplets, and E_{ICCD} is the collection efficiency of ice crystals collecting supercooled cloud droplets. From the above equation, the rate of production due to riming is

$$PICCD1 = \frac{\pi}{6}\ \bar{D}_{IC}^2\ Q_{CD}\ n_{IC}\ (\Delta V)\ E_{ICCD} \tag{39}$$

The collection efficiency is assumed zero if the cloud droplet radius, $\overline{r}_{CD}$, is less than 6×10^{-6} m, or if the ice crystal diameter $\overline{D}_{IC}$ is less than 150×10^{-6} m; otherwise, a collection efficiency of 0.5 is assumed. These values assumed for E_{ICCD} were derived from the data presented in Pitter (1977). His theoretical results showed that collection between cloud droplets and ice crystal plates would not occur if the radius of the droplets are less than 6 μm, or if the plate diameters are less than 150 μm.

Melting of ice crystals

In regions where $T > 273.16$ K ice crystals are instantaneously melted into cloud droplet water, hence the rate of production of ice crystals due to melting is

$$PICCD2 = - Q_{IC}/\Delta t.$$

Spontaneous freezing of cloud droplets

Spontaneous freezing of cloud drops occur if $T < 233.16$ K ; that is

$$PICCD3 = Q_{CD}/\Delta t.$$

Autoconversion of cloud droplets into rain

In nature, slowly falling cloud droplets often collect other cloud droplets; and by this process, may eventually grow into raindrops. The parameterization of this process, which results in the conversion of cloud droplet water into rainwater, is called the autoconversion of rainwater processes. Kessler (1969) hypothesized an autoconversion rate which was initiated when the cloud droplet water exceeded a certain threshold value.

Other formulations developed by Berry (1968), Simpson and Wiggert (1969), and Berry and Reinhardt (1974b) are more elaborate than the Kessler formulation, since they are based on data obtained from detailed stochastic growth models. The Berry-Reinhardt formulation should be superior to the Berry formulation since the former is based on more recent experiments which utilize an improved numerical treatment.

The Berry-Reinhardt formulation is assumed here; it is determined from the expression for the average autoconversion rate as (Pruppacher and Klett, 1978)

$$PRCD1 = L_2/T_2 \qquad \text{if} \qquad L_2 > 0, \text{ and } T_2 > 0; \tag{40}$$

where from Berry and Reinhardt (1974a, 1974b), L_2 and T_2 are

$$L_2 = 0.027\ [100\ r'^3\ \bar{r}_{CD} - 0.4]\ Q_{CD}, \tag{41}$$

$$T_2 = 3.72\ [r' - 7.5]^{-1}\ (\rho_o Q_{CD})^{-1}, \tag{42}$$

and

$$r' = 10^6(\sigma/0.38)^{1/3}\ \bar{r}_{CD}. \tag{43}$$

These parameters are based on the evolution of a bimodal droplet spectrum from an initially unimodal (gamma) droplet size distribution; specifically, r' is a droplet radius parameter, T_2 represents the time required (in seconds) for the predominant radius of the larger mode[4] to reach 50 μm, and L_2 is the liquid

[4]The mode which has the larger sized droplets.

water content (g g^{-1}) at time T_2 associated with the larger mode. Autoconversion is not computed unless both L_2 and T_2 exceed their threshold values.

Threshold values of cloud droplet water needed before autoconversion can take place, as based on Eqs. (40) - (43), are given in Table 1. According to this formulation autoconversion is unlikely in extreme continental conditions; rain, if it does occur, must be initiated by the Bergeron process. This is supported by observations in continental areas such as the High Plains, which typically find that rain is initiated by the melting of snow, graupel, and hail (e.g., Dye et al., 1974; Cannon et al., 1974; Knight et al., 1974; Heymsfield, 1982). On the other hand, in maritime clouds, the autoconversion of rain from cloud droplet water is important, if not essential, for rain formation. For example, "warm" rain clouds (convective rain clouds whose tops never penetrate above the melting level) are often found within maritime regions. Autoconversion of rain from cloud droplet water is the only process by which rain can be initiated in "warm" clouds. Note from Table 1 that the threshold for autoconversion is very small in maritime conditions. Also from Table 1, it is interesting to note that the value assumed by Kessler (1969) for the threshold of autoconversion (0.5 g m^{-3}) corresponds to typical values of n_{CD} and σ.

Collection of cloud droplets by rain

The growth rate of a single raindrop due to the collection of small cloud droplets along its path is determined from the continuous collection equation (e.g., Liu and Orville, 1969); i.e.,

$$\frac{dM}{dt} = \rho_o \, Q_{CD} \, W_R(D_R) \, \frac{\pi D_R^2}{4} \, E_{RCD}.$$

TABLE 1. THRESHOLD CLOUD DROPLET WATER CONTENT NEEDED FOR AUTOCONVERSION TO RAIN

Threshold Cloud Droplet Water ($g\ m^{-3}$) [Derived from Eqs. (40) - (43)]	n_{CD} [$\#/cm^3$]	σ [Dispersion Coefficient]	Location & Reference
0.1	50	0.366	Maritime - Simpson & Wiggert (1969)
0.5	200	0.30	
1.5 - 2.1	689 - 927	0.35 - 0.38	Upwind of St. Louis - Fitzgerald & Spyers-Duran (1973)
2.8 - 3.7	1157 - 1472	0.30 - 0.32	Downwind of St. Louis - Fitzgerald & Spyers-Duran (1973)
9.2	2000	0.146	Extreme Continental - Simpson & Wiggert (1969)
1.8 - 17.7	760 - 3166	0.12 - 0.32	Colorado High Plains - Knight et al. (1982)

Following Liu and Orville the integration of the above equation over all drop sizes with $N(D_R)$ drops as defined in Eq. (17) and $W_R(D_R)$ as defined in Eq. (24b); gives

$$PRCD2 = \frac{30\pi}{76} \Lambda_R^3 Q_{CD} \overline{W}_R N_{OR} \overline{E}_{RCD}. \tag{44}$$

The mean collection efficiency of raindrops accreting cloud droplets ($\overline{E}_{RCD}$) is determined from a least-square curve fit of experimental data that is tabulated in Mason (1971). The formulation, which is based on a constant raindrop radius of 1000 μm, is given as

$$\overline{E}_{RCD}(\overline{r}_{CD}) = - 0.27544 + 0.26249 \times 10^6 \overline{r}_{CD} - 1.8896 \times 10^{10} \overline{r}_{CD}^{\,2} + 4.4626 \times 10^{14} \overline{r}_{CD}^{\,3}. \tag{45}$$

which is computed for: $1.2 \times 10^{-6} \leq \overline{r}_{CD} \leq 20 \times 10^{-6}$. The collection efficiency is set equal to unity, if the mean cloud droplet radius as determined by Eq. (32) exceeds 20×10^{-6} m (20 μm); if, on the other hand, the cloud droplet radius is less than 1.2×10^{-6} m (1.2 μm), accretion of cloud droplets by raindrops is not allowed.

Evaporation of raindrops

Evaporation of raindrops is computed whenever the air is subsaturated and there is an insufficient amount of cloud droplet water to erase the subsaturation. From Mason (1971) the rate of evaporation of a raindrop having mass M is

$$-\frac{dM}{dt} = \frac{2\pi D_R (Q_v - Q_{sv}) F_R}{\frac{L_v Q_{sv}}{k_T T}\left(\frac{L_v}{R_v T} - 1\right) + \frac{1}{D_w \rho}} .$$

The ventilation factor for raindrops is given by Ranz and Marshall (1952) as

$$F_R = 1 + 0.3\, S_M^{1/3}\, R_e^{0.5},$$

where the Reynolds number is defined:

$$R_e = W_R(D_R)\, D_R/\nu_m,$$

where ν_m is the molecular viscosity of air.

With Eqs. (17), (24b) and (25b), integration over the drop size spectrum gives a production term for the raindrop evaporation as

$$PRWV1 = 2\pi N_{OR} \frac{T[Q_v - Q_{sv}]\, \Lambda_R^2\, [1 + 0.3179\, S_M^{1/3}\, (\Lambda_R \overline{W}_R/\nu_m)^{0.5}]}{Q_{sv}\, [A_2^*/T - A_3^*] + T/D_w}, \quad (46)$$

where

$$A_2^* \equiv \rho_o\, L_v^2/R_v k_T \text{ , and } \qquad A_3^* \equiv \rho_o\, L_v/k_T.$$

The evaporation rate may not exceed the amount of rain available; i.e.,

$$PRWV1 = MAX\, [PRWV1, -Q_R/\Delta t].$$

Conversion of ice crystals to snow

Following Rutledge and Hobbs (1983), the conversion of ice crystals to snow is computed whenever the ice crystal mass exceeds 9.4×10^{-10} kg. Hence from Eq. (37), the transfer of ice crystal water to snow occurs at a rate which maintains a maximum average ice crystal diameter of 500 μm; i.e.,

$$PSIC1 = (Q_{IC} - a)/\Delta t, \tag{47}$$

where the conversion threshold is: $a = 9.4 \times 10^{-10} \, n_{IC}/\rho_o$.

Collection of cloud droplets by snow

The production of snow due to the accretion of cloud droplets is parameterized in the same manner as the collection of cloud droplets by rain. The terminal velocity for snow [Eq. (26)] is assumed to be independent of diameter; this leads to an accretion rate given by

$$P_2 = 0.5 \, \pi \, N_{OS} \, Q_{CD} \, \Lambda_S^3 \, W_S E_{SCD}. \tag{48}$$

If the temperature is less than 273.16 K the accreted cloud water (P_2) is converted into snow:

$$PSCD1 = P_2. \tag{49}$$

If the temperature is greater than 273.16 K the collected cloud water is transferred to rain:

$$PRCD3 = P_2. \tag{50}$$

The collection efficiency of snow for cloud droplets E_{SCD}, is assumed unity (e.g., Lin et. al., 1983).

Collection of rain by snow

If the temperature is less than 273.16 K, snow grows by the accretion of rain. The rate at which snow accretes rainwater is

$$P3 = \int_0^\infty \int_0^\infty E_{RS} \frac{\pi}{4} (D_R+D_S)^2 W_R(D_R) \delta_w \frac{\pi}{6} D_R^3 N(D_R) N(D_S) dD_R dD_S,$$

where $W_R >> W_s$ is assumed. Integration after substituting Eqs. (17), (18) and (24b) yields:

$$P3 = 0.5 \pi N_{OS} Q_R \overline{W}_R \Lambda_S[13.92 \Lambda_R^2 + 4.8 \Lambda_R\Lambda_S + \Lambda_S^2]E_{RS}. \quad (51)$$

Snow is produced from the accretion of rain only if $T \leq 273.16$ K:

$$PSR1 = P3 \quad \text{if} \quad T \leq T_M.$$

The collection efficiency of snow for rain E_{RS}, is assumed unity (e.g., Lin et al., 1983; Rutledge and Hobbs, 1984).

Collection of ice crystals by snow

The production of snow due to the accretion of ice crystals is parameterized in the same manner as the collection of cloud droplets by snow. Ice crystals which only occur at temperatures less than 273.16 K are accreted at a rate given by

$$PSIC2 = 0.5\ \pi\ N_{OS}\ Q_{IC}\ \Lambda_S^3\ W_S\ E_{SIC}. \tag{52}$$

The collection efficiency of snow for ice crystals is assumed:

$$E_{SIC}(T) = \exp[0.38(T-T_M)]. \tag{53}$$

Eq. (53) is based on experimentally determined efficiencies that are presented in Pruppacher and Klett (1978). Note that ice crystals are less likely to stick to snow particles at lower temperatures.

Autoconversion of ice crystal water into snow

Ice crystals may grow into snow particles by processes of deposition of vapor and accretion of cloud droplets. The initiation of snow due to these processes are parameterized in Eq. (47). Snow may also form due to the collision and aggregation of ice crystals. Following Lin et al. (1983), this process is parameterized by an autoconversion formula as,

$$PSIC3 = 10^{-3}(Q_{IC} - 10^{-3}/\rho_o)\ E_{SIC}, \tag{54}$$

which is computed whenever $\rho_o Q_{IC}$ exceeds 10^{-3} kg m^{-3}.

Melting of snow

The formulation for melting of ice particles is discussed in Wisner et al. (1972). The formulation assumes that the heat required for melting is supplied by the following processes: (1) the conduction of heat from the air, (2) the transfer of latent heat due to condensation of water vapor on the surface of the ice particle, and (3) the heat supplied by the collection of

rain and cloud droplets. The parameterization for the melting of snow utilizes Eqs. (18), (26), (48), (51) and (55), and follows Lin et al. (1983). The melting of snow results in the production of rain, and is only computed when $T > T_M$. The rate of melting is

$$PSR2 = -\frac{2\pi N_{0S}}{\rho_o L_f}\left[k_T(T-T_M) + L_v D_w \rho_o (Q_v - Q_{ssv})\right] \Lambda_S^2$$

$$\times \left[0.86 + 0.28\, S_M^{1/3} (\pi W_S \Lambda_S / \nu_m)^{0.5}\right]$$

$$-\frac{C_w(T-T_M)}{L_f}\left[PSR1 + P2\right] - PSR1; \qquad (55)$$

where Q_{ssv} is the saturation vapor mixing ratio (with respect to liquid water) at the surface of the snow particle; i.e.,

$$Q_{ssv} = e_{sv}(T_M)\,[Q_v + \varepsilon]/P. \qquad (56)$$

The melting rate may not exceed the amount of snow available, i.e.,

$$PSR2 = MAX\,[PSR2, -Q_{SN}/\Delta t].$$

The last term in Eq. (55) is based on the requirement that raindrops be shed at the same rate that they are collected. The net effect of raindrop collection by melting snow particles is to further enhance the melting rate.

Growth of snow by deposition and sublimation

The depositional growth of a spherical snow particle is given by Eq. (36) where C is equal to $2\pi D_S$, and with the ventilation factor for snow is given

as (Hall and Pruppacher, 1976)

$$F_S = 0.86 + 0.28\ S_M^{1/3}\ Re^{0.5}, \tag{57}$$

where Re is now $W_S D_S/\nu_m$.

Multiplying Eq. (36) by (18) and integrating over all particle sizes with W_S defined in (26) yields

$$P4 = \frac{2\ \pi\ N_{OS}\Lambda_S^2[Q_v - Q_{si}][0.86 + 0.21\ S_M^{1/3}(\pi\ W_S\Lambda_S/\nu_m)^{0.5}]}{\rho_o[Q_{si}A_1^* + B_1^*]} \tag{58}$$

Similar to the formulation of Eqs. (38a) and (38b), the rate of production of snow by deposition is

$$PSWV1 = MIN\ [P4,\ \lambda_s/\Delta t] \qquad \text{if } Q_v \geq Q_{si};$$

the rate of production due to sublimation is

$$PSWV1 = MAX\ [P4,\ -Q_{SN}/\Delta t,\ \lambda_s/\Delta t] \qquad \text{if } Q_v \leq Q_{si}.$$

Deposition and sublimation of snow are not computed if melting is taking place; i.e.,

$$PSWV1 = 0 \qquad \text{if PSR2} < 0.$$

Condensation and evaporation of wet snow

Condensation or evaporation of snow is assumed to occur only during melting. Evaporation may take place whenever snow particles melt in air that

is below liquid water saturation. Formulation of the process assumes: (1) melting and accretion produces a liquid surface completely surrounding the particle; and (2) the temperature of the liquid surface is in equilibrium with the snow particle. Hence, evaporation occurs if the vapor pressure of the air is less than the saturation vapor pressure at 273.16 K; otherwise, water vapor is condensed onto the wet snow particle.

The growth rate of a wet particle where the liquid is in thermal equilibrium with ice is

$$\frac{dM}{dt} = 2 \pi D_w \rho_o (Q_v - Q_{ssv}) D_S F_S . \tag{59}$$

Multiplying by Eq. (18) and integrating over all sizes yields

$$P5 = 2 \pi N_{OS} D_w (Q_v - Q_{ssv}) \Lambda_S^2 \times [0.86 + 0.21 S_M^{1/3} (\pi W_S \Lambda_S / \nu_m)^{0.5}]. \tag{60}$$

The rate of condensation or evaporation is only computed when melting is occurring; i.e., PSR2 < 0.

If $Q_v < Q_{ssv}$, then evaporation from the wet snow results in the production of water vapor:

$$PRWV2 = MAX [P5, - P6];$$

where P6 = PRCD3 - PSR2 + P3.

The above formulation limits the rate of evaporation to the amount of liquid water available from melting and accretion. In other words, the rate of evaporation cannot exceed the rate which liquid water is produced on the

snow particle.

On the other hand, if condensation of vapor takes place on the snow particles, then the condensed water is converted (at the same rate) into rain water:

PRWV2 = P5.

Note that for a sufficiently moist atmosphere, rain due to melting snow may consist partly of water actually melted from a snow particle, and partly of water that was condensed onto the snow particle.

Spontaneous freezing of raindrops

The parameterization of the spontaneous freezing of supercooled raindrops follows Wisner et al. (1972). This process is included in the TASS formulation, even though Lin et al. (1983) has found this process to be secondary to drop freezing due to ice crystal collection. The formulation is based on the probability function developed by Bigg (1953) from laboratory experiments:

$$PF = 1 - \exp[-\alpha_1(\pi D_R^3/6)\ t\ G_F(T)]; \tag{61}$$

where

$$G_F(T) = \begin{cases} 0 & \text{if } T > 269.16, \\ \exp[\alpha_2(T_M - T)] - 1 & \text{if } T \leq 269.16. \end{cases}$$

The constants α_1 and α_2 are based on experimental data; the values assumed here are taken from Wisner et al. as

$$\alpha_1 = 100 \text{ m}^3\text{s}^{-1}, \quad \text{and} \quad \alpha_2 = 0.66 \text{ K}^{-1}.$$

From Eq. (61), Wisner et al. obtained an equation for the number of drops frozen per unit volume, $N(D_R)$, as

$$- \frac{dN(D_R)}{dt} = \pi\alpha_1 N(D_R) \, D_R^3 \, G_F(T)/6. \tag{62}$$

The formulation of Eq. (62) is based on the assumption that the number of drops frozen is small compared to the total number of drops within a unit volume.

The production rate at which raindrops freeze per unit volume can be obtained from eq. (62) as

$$P7 = \frac{1}{\rho_o} \int_o^\infty - \frac{dN(D_R)}{dt} \, M(D_R) \, dD_R.$$

Substitution of Eqs. (17) and integrating yields

$$P7 = 20\pi \, \alpha_1 \, Q_R \, \Lambda_R^3 \, G_F(T). \tag{63}$$

In the application of Eq. (63), a maximum of 25% of the available rainwater is allowed to freeze per time step. This arbitrary upper limit should be applied, since the development of Eq. (63) is based on the assumption that only a small portion of the number of drops per unit volume actually freeze.

If $Q_R \geq 10^{-4}$ g g^{-1}, then hail is produced from the freezing of raindrops:

$$PHR1 = MIN \, [P7, \, Q_R/4 \, \Delta t]. \tag{64a}$$

Raindrops associated with water contents less than 10^{-4} g g^{-1} are assumed to be too small to classify as hail when frozen, and instead are converted to snow. Hence, if $Q_R < 10^{-4}$ g g^{-1}, snow is produced by the freezing of rain:

$$PSR3 = MIN\ [P7,\ Q_R/4\ \Delta t]. \tag{64b}$$

Raindrop freezing due to collection of ice crystals

The collection of ice crystals by supercooled raindrops results in the production of either hail or snow. Raindrop freezing due to this process usually dominates over spontaneous drop freezing (Lin et al., 1983).

Following Lin et al., if Q_R exceeds 10^{-4} g g^{-1}, the collection of ice crystals by rain results in the production of hail. Since the collection of an ice crystal by a raindrop results in both particles changing to hail, two production terms are needed: the transfer of rainwater to hail due the collection of ice crystals, PHR2, and the transfer of ice crystal water to hail due to the collection of ice crystals by raindrops, PHIC1. If Q_R is less than 10^{-4} g g^{-1}, the collection of ice crystals by rain results in both the transfer of ice crystal water to snow and rainwater to snow.

Assuming the continuous collection equation, the rate of collection of ice crystal water by raindrops is

$$P8 = \frac{15\pi}{38}\ \Lambda_R^3\ Q_{IC}\ \overline{W}_R\ N_{OR}\ E_{RIC}. \tag{65}$$

The rate at which rainwater is transformed to hail or snow due to the collection of ice crystals is (assuming the hydrometeors are uniformly distributed throughout the grid volume)

$$P9 = \frac{1}{\rho_o} \int_o^\infty E_{RIC} \frac{\pi}{4} D_R^2 W_R(D_R) \delta_w \frac{\pi}{6} D_R^3 n_{IC} N(D_R) dD_R; \quad (66)$$

which becomes,

$$P9 = 6.96 \pi n_{IC} \Lambda_R^2 Q_R \overline{W}_R E_{RIC}. \quad (67)$$

Thus if $Q_R > 10^{-4}$ g g^{-1}, then PHIC1 = P8, and PHR2 = P9; if $Q_R \leq 10^{-4}$ g g^{-1}, then PSIC4 = P8, and PSR4 = P9.

As in Lin et al. (1983), the collection efficiency of supercooled rain for ice crystals E_{RIC}, is assumed unity.

Freezing of supercooled raindrops resulting from the collection of snow

If the temperature is less than 273.16 K and the rain water content exceeds 10^{-4} g g^{-1}, hail is produced by the raindrop collection of snow particles. Again the process requires two production terms.

The production rate of hail from rain collecting snow can be determined from the rate at which snow accretes rainwater. Hence from Eq. (51),

PHS1 = PSR1 if $T < T_M$ and $Q_R > 10^{-4}$.

The rate at which rainwater accretes snow is

$$PHS2 = \frac{1}{\rho_o} \int_o^\infty \int_o^\infty E_{RS} \frac{\pi}{4} (D_R+D_S)^2 W_R(D_R) \delta_S \frac{\pi}{6} D_S^3 N(D_R) N(D_S) dD_R dD_S.$$

Substituting Eqs. (17), (18) and (24B), and integrating yields:

$$PHS2 = \frac{15\pi}{38} N_{OR} Q_{SN} \overline{W}_R \Lambda_R [250 \Lambda_S^2/63 + 20 \Lambda_R \Lambda_S/7 + \Lambda_R^2] E_{RS}, \quad (68)$$

which is only computed when

$$T < 273.16 \text{ K, and } Q_R > 10^{-4} \text{ g g}^{-1}.$$

Production of hail from the riming of snow

The riming of large snow particles, especially in regions of large cloud-droplet concentrations, may lead to the initiation of hail.

Price (1985) and Price et al. (1986) assume that the conversion of hail from the riming of snow occurs when snow contents, exceeding 0.1 g kg^{-1}, are in coexistence with supercooled cloud-droplet concentrations of 1 g kg^{-1} or more. If these threshold conditions are met, they assume that the snow mass converted to hail, per time step, is equal to the mass of the snow particles greater than some diameter, D_o. The derivation of this formulation assumes a continuous size distribution of snow particles; thus with Eq. 18, the mass of snow (per mass of dry air) of snow particles greater than D_o is

$$M_S = N_{OS} \delta_S \int_{D_o}^{\infty} D_S^3 \exp(D_S/\Lambda_S) dD_S.$$

Price (1985) and Price et al. (1986) obtain a production rate by integrating the above equation and dividing by the time step and density of air:

$$PHS3 = \frac{Q_{SN}}{6\Lambda_S^3 \Delta t} \exp(-\frac{D_o}{\Lambda_S})[D_o^3 + 3 D_o^2 \Lambda_S + 6 D_o \Lambda_S^2 + 6 \Lambda_S^3]. \qquad (69a)$$

In order to increase computational efficiency, a least-square curve fit is formulated from Eq. (69a) as

$$\text{PHS3} = \frac{Q_{SN}}{\Delta t} \begin{cases} 0 & \text{if} \quad \Lambda_S < 3.5 \times 10^{-4}, \\ [-2.31 \times 10^{-3} + 114\ \Lambda_S - 6.05 \times 10^{5}\ \Lambda_S^2 + 8.59 \times 10^{8}\ \Lambda_S^3] & \\ \qquad \text{if} \quad 3.5 \times 10^{-4} \leq \Lambda_S < 7.5 \times 10^{-4}, & \\ [-0.35 + 445\ \Lambda_S + 2.95 \times 10^{5}\ \Lambda_S^2 - 1.21 \times 10^{8}\ \Lambda_S^3] & \\ \qquad \text{if} \quad 7.5 \times 10^{-4} \leq \Lambda_S \leq 2.0 \times 10^{-3}, & \\ 0.75 & \text{if} \quad \Lambda_S > 2 \times 10^{-3}, \end{cases} \tag{69b}$$

where D_o in (69a) is assumed to have a value of 5×10^{-3} m. PHS3 is only computed if $T < T_M$, $Q_{CD} \geq 10^{-3}$ g g^{-1}, and $Q_{SN} > 10^{-4}$ g g^{-1}.

Collection by hail of ice crystals

The production rate for hail due to ice crystal collection is determined from the continuous collection equation when T is less than 273.16 K. The parameterization follows Lin et. al. (1983) and is formulated in a similar manner as PRCD3 in Eq. (44). The production rate for hail collecting cloud ice is

$$\text{PHIC2} = \frac{3\pi}{7}\ N_{OH}\ Q_{IC}\ \Lambda_H^3\ \overline{W}_H\ E_{HIC}. \tag{70}$$

During hail dry growth the collection efficiency for hail collecting ice crystals is $E_{HIC} = 0.3$, which is based on the experimental data of Latham and Saunders (1970). In the case of hail wet growth, E_{HIC} is set to unity.

Collection by hail of cloud droplets

The production rate for hail due to cloud droplet collection is

determined from the continuous collection equation, and is formulated in a similar manner as PRCD2 in Eq. (44); the production rate is (Lin et. al., 1983),

$$PHCD1 = \frac{3\pi}{7} N_{OH} Q_{CD} \Lambda_H^3 \overline{W}_H \overline{E}_{HCD}. \quad (71)$$

The mean collection efficiency for hail collecting cloud drops, $\overline{E}_{HCD}$, is based on Langmuir's (1948) theoretical efficiency for potential flow; it is given by

$$\overline{E}_{HCD} = [\overline{K}_s/(\overline{K}_s + 0.5)]^2. \quad (72)$$

The Stokes number (e.g., Byers, 1965) is:

$$K_s = \delta_w 4 W_H r_{CD}^2/9 \mu_D D_H. \quad (73)$$

where μ_D is the dynamic viscosity of air. The mean Stokes number is defined from K_s by substituting the mean mass-weighted terminal velocity [Eq. (28)] and the mean mass-weighted hail diameter $[\overline{D}_H = 4\Lambda_H]$ into Eq. (73); the mean Stokes number is given as

$$\overline{K}_s = \delta_w \overline{W}_H \overline{r}_{CD}^2/9 \mu_D \Lambda_H.$$

Collection by hail of rain

The rate at which rainwater is collected by hail is (Wisner et al., 1972)

$$PHR3 = \frac{1}{\rho_o} \int_o^\infty \int_o^\infty \frac{\pi}{4} (D_R+D_H)^2 |W_H-W_R| \frac{\pi}{6} D_R^3 \delta_w N(D_R) N(D_H) dD_R dD_H E_{HR}. \quad (74)$$

Following Wisner et al., integration of Eq. (74) is possible if differences in terminal velocities are approximated by

$$|W_H - W_R| \simeq |\overline{W}_H - \overline{W}_R|,$$

where $\overline{W}_R$ and $\overline{W}_H$ are respectively given by Eqs. (25a) and (28). Substitution of Eqs. (17) and (19) into (74) and integrating gives

$$PHR3 = 0.5\ \pi N_{OH} |\overline{W}_H - \overline{W}_R|\ Q_R \Lambda_H\ [10\ \Lambda_R^2 + 4\ \Lambda_R \Lambda_H + \Lambda_H^2]\ E_{HR}. \tag{75}$$

The efficiency of hail for rain, E_{HR}, is assumed unity (e.g., Lin et al., 1983).

Collection by hail of snow

The production rate for hail due to snow particle collection is derived similar to PHS2 in Eq. (68); it is given as

$$PHS4 = \frac{3\pi}{7}\ N_{OH}\ \overline{W}_H\ Q_{SN}\ \Lambda_H [16\ \Lambda_S/3 + 16\ \Lambda_H \Lambda_S/5 + \Lambda_H^2]\ E_{HS}. \tag{76}$$

For hail dry growth the collection efficiency of hail for snow, E_{HS}, is assumed equal to 0.1 (Lin et al., 1983); for hail wet growth and temperatures greater than 273.16 K, E_{HS} is assumed unity.

Hail melting

The production rate for the melting of hail is developed similar to PSR1 in Eq. (55). The melting of hail results in the production of rain, and is computed when the temperature is greater than 273.16 K. Following Lin et al.

(1983), the rate at which hail melts is

$$P10 = -\frac{2\pi\ N_{OH}}{\rho_o\ L_f}\left[k_T(T-T_M) + L_v D_w \rho_o (Q_v - Q_{ssv})\right] \Lambda_H^2$$

$$\times\ [0.94 + 0.381\ S_M^{1/3} (\overline{W}_H \Lambda_H/\nu_m)^{0.5}]$$

$$-\frac{C_w(T-T_M)}{L_f}\ [PHCD1 + PHR3]; \qquad (77)$$

where in the derivation of Eq. (77) the ventilation factor for hail is assumed as (Mason and Thorpe, 1966)

$$F_H = 0.94 + 0.33\ S_M^{1/3}\ R_e^{1/2}, \qquad (78)$$

and where now the Reynolds number is defined as $R_e = W_H\ D_H/\nu_m$.

The rate of melting may not exceed the hail available and is only computed if melting occurs:

$$P10 = MAX\ [P10, -Q_H/\Delta t],$$

$$P10 = MIN\ [P10, 0].$$

The rate at which hailwater is transferred to rainwater is

$$PHR4 = P10 - PHCD1 - PHR3 \qquad (79)$$

The last two terms in Eq. (79) are due to the shedding of collected rain and cloud droplet water.

Hail wet growth

Hailstones grow by deposition and the accretion of liquid and solid hydrometeors. Growth by accretion of cloud droplets and rain drops is usually dominant and becomes more so as the hail diameter increases. Dry growth occurs when the surface of the hailstone is at subfreezing temperatures and the accreted liquid hydrometeors freeze quickly, leaving the surface essentially dry. During wet growth, only a portion of the collected liquid water freezes. Wet growth occurs because heat transfer to the surrounding air is insufficient to dissipate the excess heat that is released from the freezing of accreted water. Thus, the surface temperature of the hailstone rises to $0^{o}C$, and a portion of the accreted water is shed as rain. According to Musil (1970) this process is modified when the hailstone also accretes ice particles. Some of the excess heat contained by the hailstone can be absorbed by the cooler ice particles; hence, the hailstone's capacity to freeze accreted water is increased.

Parameterization of the wet growth process is similar to the formulation in Lin et al. (1983). First, a production term representing the maximum capacity for growth from the accreted hydrometeors is computed (PWET). If the rate of accreted liquid water exceeds PWET (the maximum growth rate), wet growth is assumed to occur. The growth rate for hail is then given by PWET; and the remaining portion of the accreted liquid water is shed as rain. However, if PWET exceeds the rate at which liquid water is accreted, then dry growth is assumed; and all of the accreted water is transferred into hail water. This test for wet growth is only computed when the air temperature is between 253.16 K and 273.16 K. Only hail particles are assumed to have the potential for wet growth; dry growth is always assumed for graupel particles (i.e., when $\overline{D}_G \leq 5 \times 10^{-3}$m).

The growth equation for wet growth was formulated by Musil (1970) and is similar to the production equation for melting. Assuming the ventilation factor given by Eq. (78) and integrating over all particle sizes yields,

$$PWET = -\frac{2\pi N_{OH}}{\rho_o L_f}\left[k_T(T-T_M) + L_v D_w \rho_o (Q_v - Q_{ssv})\right] \Lambda_H^2$$

$$x\ [0.94 + 0.381\ S_M^{1/3}(\bar{W}_H \Lambda_H/\nu_m)^{0.5}]$$

$$+ \left[1 - \frac{C_i(T-T_M)}{L_f}\right] (PHIC2/E_{HI} + PHS4/E_{HS}); \qquad (80)$$

which is only computed if $273.16 \geq T \geq 253.16$ K, and $\bar{D}_G > 5 \times 10^{-3}$.

Wet growth occurs if:

$$PWET < PHCD1 + PHR3;$$

in which case,

$$PHR5 = PWET - PHCD1 - PHR3,$$

where PHR5 represents the rate at which accreted water is shed as rain.

Dry growth occurs if:

$$PWET \geq PHCD1 + PHR3;$$

in which case

$$PHR5 = 0,$$

and all accreted water is consumed by the growing hail.

Condensation and evaporation of wet hail

The hailstone is assumed to be covered by a film of water whenever melting or wet growth occurs. The temperature of the liquid surface is assumed to be in equilibrium with the ice surface; thus, condensation on the hailstone occurs if vapor pressure of the air exceeds the saturation vapor pressure (for liquid water) at 273.16 K. In which case, water vapor condensed on the hailstone is transferred to rainwater. Evaporation, on the other hand, occurs if the vapor pressure at 273.16 K exceeds that of the air; in this case melt- and shed-water (which would otherwise become rain) are transferred to water vapor.

Similar to Eq. (60) the rate of condensation on wet hail is

$$\begin{aligned} P11 = {} & 2\pi N_{OH} D_w (Q_v - Q_{ssv}) \Lambda_H^2 \\ & \times [0.94 + 0.381 S_M^{1/3} (\bar{W}_H \Lambda_H / \nu_m)^{0.5}]; \end{aligned} \tag{81}$$

which is only computed when the hail or graupel particles are "wet"; i.e., when either PHR4 or PHR5 are less than zero; otherwise, P11 is set equal to zero.

Condensation on the hailstones occurs if $Q_v > Q_{ssv}$: the water condensed on the hail is tranferred to rainwater;

PRWV3 = P11.

Evaporation from the wet hail takes place if $Q_v < Q_{ssv}$;

$$PRWV3 = MAX\ [P11, -P12], \tag{82}$$

where the rate at which liquid water is available for evaporation is

$$P12 = -PHR4 - PHR5$$

By choosing the maximum of the two rates in Eq. (81), evaporation from the wet hail cannot exceed the rate at which excess liquid water is collected and/or melted. In other words, evaporation occurs as long as the hailstones are wet.

Growth of hail by deposition and sublimation

The production rate of hail due to deposition is formulated similar to Eq. (58); and is given by

$$PHWV1 = \frac{2\pi\ N_{OH}[Q_v - Q_{si}]\Lambda_H^2[0.94 + 0.381\ S_M^{1/3}(\bar{W}_H\Lambda_H/\nu_m)^{0.5}]}{\rho_o[Q_{si}\ A_1^* + B_1^*]}. \tag{83}$$

Deposition (or sublimation) is not computed if the hail surface is wet; i.e.,

$$PHWV1 = 0 \qquad \text{if } PRWV3 - PHR4 - PHR5 \leq 0.$$

Evaporation from wet ground

The rate of evaporation from the ground is computed as a source term in the water vapor and thermodynamic equations. The formulation is a crude approximation and assumes the ground surface, when it is wet, to be covered by a layer of liquid water.

The flux of vapor to the air from the wet ground is given by

$$A \frac{dM}{dt} = K_w \frac{d\rho_v}{dz} ,$$

where A is the surface area covered by water, M is the mass of water involved in the exchange, K_w is the eddy-diffusion coefficient for water vapor, and ρ_v is vapor density.

If $\rho_o Q_v \Delta x \Delta y \Delta z$ is substituted for M, and the gradient is approximated as $d\rho_v/dz \simeq [\rho_v(h) - \rho_{sv}(h)]/h$, then the production rate of Q_v due to surface evaporation is

$$PWVG = \frac{dQ_v}{dt} = \beta \frac{\langle K_M \rangle [Q_v(h) - Q_{sv}(h)]}{2 h^2} \qquad (84)$$

where β is an empirical constant and $h \equiv \Delta z/2$. In the absence of observations, the value of β is assumed unity.

The rate of ground evaporation is computed in the grid cells adjacent to the ground, and is only calculated if the ground is assumed wet. For a domain that is assumed stationary with respect to ground, the accumulated rainfall must locally exceed one millimeter before ground evaporation is computed. If the domain is moving (e.g., translating with a convective storm), then PWVG is computed locally, only when the rainfall rate exceeds 25 millimeters per hour.

Source Terms for the Thermodynamic and Moisture Substance Equation

The source terms for various microphysical interaction are formally listed below.[5]

[5]Actual computation is not as simple as summing all of the source terms for each prognostic equation. Details of the computational procedure are given in Section 6.

Thermodynamic equation

The source terms for the rate of diabatic heating which are used in Eq. (5) are:

$$S_v = PCDWV1 + PRWV1 + PRWV2 + PRWV3 - PWVG$$

$$S_f = PICCD1 + PICCD2 + PICCD3 + PSR1 + PSR2 + PSR3 + PSR4 + PHCD1 + PHR1 + PHR3 + PHR4 + PHR5$$

$$S_s = PICWV1 + PICWV2 + PSWV1 + PHWV1.$$

Moisture substance equations

The source terms in Eqs. (6) - (11) are as follows:

for water vapor

$$S_{vap} = - PCDWV1 - PICWV1 - PICWV2 - PRWV1 - PRWV2 - PRWV3 - PSWV1 - PHWV1 + PWVG;$$

for cloud droplet water

$$S_{CD} = PCDWV1 - PICCD1 - PICCD2 - PICCD3 - PRCD1 - PRCD2 - PRCD3 - PSCD1 - PHCD1;$$

for ice crystal water

$$S_{IC} = PICWV1 + PICWV2 + PICCD1 + PICCD2 + PICCD3 - PSIC1 - PSIC2 - PSIC3 - PSIC4 - PHIC1 - PHIC2;$$

for rain water

$$S_R = PRWV1 + PRWV2 + PRWV3 + PRCD1 + PRCD2 + PRCD3 - PSR1 - PSR2 - PSR3 - PSR4 - PHR1 - PHR2 - PHR3 - PHR4 - PHR5;$$

for snow water

$$S_S = PSWV1 + PSCD1 + PSIC1 + PSIC2 + PSIC3 + PSIC4 + PSR1 + PSR2 + PSR3 + PSR4 - PHS1 - PHS2 - PHS3 - PHS4;$$

and for hail water

$$S_H = PHWV1 + PHCD1 + PHIC1 + PHIC2 + PHR1 + PHR2 + PHR3 + PHR4 + PHR5 + PHS1 + PHS2 + PHS3.$$

Diagnostic Calculation of Radar Reflectivity

Radar reflectivity fields can be diagnosed from the simulated moisture substance fields, since specific size distributions have been assumed. The simulated radar-reflectivity fields are useful in the analysis of model results; and most important, they can be used to compare and validate the model results with actual radar observations.

The model radar reflectivity fields are diagnosed from the rain, snow, and hail fields. The cloud droplet and ice crystal fields, which are composed of relatively small particles, contribute very little to the radar reflectivity and can be neglected in most applications.

For rain the radar reflectivity factor is determined by assuming Rayleigh scattering:

$$Z_R = \int_0^\infty N(D_R)\, D_R^6\, dD_R. \tag{85}$$

Integration after substitution of Eq. (17) into (85), gives

$$Z_R = 7.2 \times 10^{20} N_{OR} \Lambda_R^7 \qquad [mm^6 m^{-3}]. \qquad (86)$$

For dry snow, the equivalent radar reflectivity factor must be assumed; i.e.,

$$Z_{SDRY} = \frac{|K_I|^2}{|K_W|^2} \frac{\delta_S^2}{\delta_w^2} \int_o^\infty N(D_S) D_S^6 \, dD_S;$$

substitution of Eq. (18) and integrating gives,

$$Z_{SDRY} = 7.2 \times 10^{20} \frac{|K_I|^2}{|K_W|^2} \frac{\delta_S^2}{\delta_w^2} N_{OS} \Lambda_S^7 \qquad [mm^6 m^{-3}] \qquad (87)$$

For wavelengths employed in weather radars, and for temperatures typical of meteorological problems, the dielectric factor for water, $|K_W|^2$, is 0.93, and the dielectric factor for ice, $|K_I|^2$, is 0.21 (Rogers, 1976). The specific density of snow is incorporated into Eq. (87) in order to adjust the snow particle diameter to its melted diameter (e.g., Battan, 1973).

For wet snow the radar reflectivity factor is simply

$$Z_{SWET} = 7.2 \times 10^{20} N_{OS} \Lambda_S^7 \qquad [mm^6 m^{-3}]. \qquad (88)$$

In the case of dry hail, the radar reflectivity factor is calculated in the same manner as dry snow; i.e.,

$$Z_{HDRY} = 7.2 \times 10^{20} \frac{|K_I|^2}{|K_W|^2} \frac{\delta_H^2}{\delta_w^2} N_{OH} \Lambda_H^7 \qquad [mm^6 m^{-3}]. \qquad (89)$$

An empirical formulation for the radar reflectivity of wet hail which includes the effects of Mie scattering has been determined by Smith et al.

(1975) as

$$Z_{HWET} = [7.2 \times 10^{20} N_{OH} \Lambda_H^7]^{0.95} \quad [mm^6 m^{-3}]. \quad (90)$$

The final radar reflectivity is computed from the sum of the radar reflectivity factors of rain, snow, and hail. The wet snow and hail radar reflectivity factors are assumed up to the 0^o C level. The wet hail radar reflectivity factor is also assumed in the updrafts up to the -8^o C level, if $\overline{D}_G > 5 \times 10^{-3}$ m.

Evaluation of Microphysical Constants

Several constants and variables need to be evaluated in order to solve for the cloud microphysics. Many of the physical constants vary only slowly with temperature and pressure; and thus, are defined in terms of variables from the reference environment (see Appendix C). For example, physical constants such as latent heat for vaporization of water (L_v), latent heat for fusion of water (L_f), latent heat of sublimation of water (L_s), specific heat of water (C_w), specific heat of ice, (C_I), dynamic viscosity of air (μ_D), and thermal conductivity (k_T) are evaluated as functions of the temperature of the reference atmosphere (T_o). Other physical constants such as the molecular viscosity of air (ν_m), the diffusivity of water vapor in air (D_w), and the Schmidt number (S_M) are defined in terms of temperature and pressure of the reference atmosphere.

Variables such as saturation vapor pressure are more sensitive to small changes and must be defined in terms of local variables. The expression for deducing the local values of the saturation vapor pressure with respect to

liquid water is obtained by integrating the Clausius-Clapeyron equation (e.g., Pruppacher and Klett, 1978) and expanding the exponent as

$$e_{sv}(T) = e_{svo}(T_o)\ [1 + x + x^2/2 + x^3/3];$$
$$x = L_v[T-T_o]/R_v T_o^2. \tag{91}$$

The saturation vapor pressure with respect to liquid water for the reference environment (e_{svo}) is accurately determined from an empirical relation (Appendix D). Similarly, the saturation vapor pressure with respect to ice is

$$e_{si}(T) = e_{sio}(T_o)\ [1 + x + x^2/2 + x^3/3];$$
$$x = L_s\ [T-T_o]/R_v\ T_o^2. \tag{92}$$

The solutions of the saturation vapor pressures from Eqs. (91) and (92) are accurate for most meteorological problems. The computations of the local values for the saturation vapor pressures are fast since no exponentials are involved.

The local temperature, T, which is needed in Eqs. (91) and (92) is not a working variable and must be diagnosed. Temperature may be evaluated from pressure and potential temperature with Poisson's equation; i.e.,

$$T = \theta\ (P/p_{oo})^{\kappa}, \tag{93}$$

where $p_{oo} = 101325$ pa and $\kappa \equiv R/C_p$. A computationally efficient formulation which avoids exponentiation can be obtained by a perturbation expansion of Eq. (93) as

$$T = T_o \left[\theta/\theta_o - \kappa\, p/P_o\right]. \tag{94}$$

The above approximation has reasonable accuracy for most meteorological problems.

5. INITIAL AND REFERENCE CONDITIONS

The reference environment is assumed unsaturated and steady state; its values are derived from a vertical profile sounding -- representing the hydrostatic environment to be modeled. Either an actual rawinsonde sounding, a composite of observed soundings, or a profile predicted by a regional hydrostatic model[6] may be used. All reference values are a function of height only.

The values for U_o, V_o, T_o, and Q_{vo} are determined from the input sounding, and are defined at each vertical level in the model by using a spline interpolation. Once these values are determined, then the remaining reference variables are computed; the reference pressure, P_o, is obtained by integrating the hydrostatic equation; the reference density, ρ_o, is solved from the equation of state; the reference potential temperature, θ_o, is determined from Poisson's equation; and the remaining thermodynamic variables are diagnosed using appropriate formulas (see Appendix E).

Basic Initial Field

The basic initial field is assumed to be horizontally homogeneous and is defined directly from the reference values; i.e., $u(x,y,z,t=o) = U_o(z)$, $v(x,y,z,t=o) = V_o(z)$, $w(x,y,z,t=o) = 0$, $p(x,y,z,t=o) = 0$, $(x,y,z,t=o) = {}_o(z)$ and $Q_v(x,y,z,t=o) = Q_{vo}(z)$. The remaining moisture substance fields (i.e., Q_{CD}, Q_{IC}, Q_R, Q_S, and Q_H) are specified as zero.

[6]Environmental soundings predicted by the Mesoscale Atmospheric Simulation System (Kaplan et al., 1982) may be used to initialize TASS. An advantage of a regional-scale model sounding is that it can be generated for almost any location and time.

The external forcing terms in Eqs. (2), (5) and (6) are defined such that the basic initial field remains steady-state. Thus, the fields cannot depart from their initial values unless a perturbation is added. The forcing terms are defined as:

$$(\partial u/\partial t)^* = [\partial \tau_{13}(t=o)/\partial z]/\rho_o; \tag{95}$$

$$(\partial v/\partial t)^* = [\partial \tau_{23}(t=o)/\partial z]/\rho_o; \tag{96}$$

$$(\partial \theta/\partial t)^* = [\partial S(\theta_o)/\partial z]/\rho_o; \text{ and} \tag{97}$$

$$(\partial Q_v/\partial t)^* = [\partial S(Q_v)/\partial z]/\rho_o. \tag{98}$$

Initial Perturbation Field

Numerical cloud modelers have devised various techniques in order to trigger convection in their simulations. The most common technique is to apply a moist or dry thermal perturbation. For example, Klemp and Wilhelmson (1978a, 1978b) have assumed a 21.6 km diameter initial thermal impulse. Although the scale is large and difficult to justify, its application did promote the development of a realistic appearing storm within a reasonable period of time. Other approaches for triggering the development of convective storms are: a superimposed velocity and temperature impulse (Schlesinger, 1984a), a meso-gamma scale vortex (Proctor, 1983), a heating function (Miller, 1978), a cooling function (Tripoli and Cotton, 1982), a mesoscale forcing function for velocity (Schlesinger, 1984b), random heating function (Hill, 1974; Yau and Michaud, 1982), and topographic uplift due to an isolated

mountain (Liu and Orville, 1969; Clark, 1979). Unfortunately all of the approaches suffer from some arbritrariness and a lack of understanding of how the mesoscale acts to force convection. Smolarkiewicz and Clark (1985) have simulated a cumulus field, by including surface energy and moisture balance equations, as well as nonhomogeneous terrain into their model. The simulated clouds were initiated by the flow over irregular terrain and the nonuniform ground heating. This approach for cumulus initiation is progressing in the right direction; but it is not yet practical in many applications. Also, mesoscale forcing may be more important than boundary layer forcing for certain types of storm development.

In the TASS model convection can be initiated by superimposing a velocity impulse and (or) a thermal impulse onto the basic initial field. The formulation of the velocity impulse is modified from Schlesinger (1984a). It assumes a cylindrical updraft of radius R_w and depth H_w, and is consistent with the anelastic equation for mass continuity; it is given by

$$u'(t=o) = - \frac{M}{2\rho_o} (x-x_o)\ \hat{G}\ dF/dz \tag{99}$$

$$v'(t=o) = - \frac{M}{2\rho_o} (y-y_o)\ \hat{G}\ dF/dz \tag{100}$$

$$w'(t=o) = \begin{cases} \frac{M}{\rho_o} \exp(-\hat{r}^2/R_w^2)\ [1 - (\hat{r}/R_w)^2] & \text{if} \quad r < R_w \\ 0 & \text{if} \quad r > R_w \end{cases} \tag{101}$$

where

$$\hat{G}\ (\hat{r}) = \begin{cases} \exp\ (-\hat{r}^2/R_w^2) & \text{if} \quad \hat{r} \leq R_w \\ R_w^2 \exp\ (-1)/\hat{r}^2 & \text{if} \quad \hat{r} > R_w, \end{cases}$$

$$F(z) = 6.75\ z\ (H_w - z)^2/H_w^3,$$

$$\hat{r}\ (x,y) = (x - x_o)^2 + (y - y_o)^2, \quad \text{and}$$

$$M = \rho_o\ W_{max}.$$

The maximum updraft speed, W_{max}, occurs at x_o, y_o, and $z = H_w/3$.

A thermal perturbation field may be added to the base state as

$$T = \Delta T\ \frac{\theta_o}{T_o}\ [1 - (\hat{r}/R_\theta)^2 - (2z-Z_\theta)^2/Z_\theta^2]; \tag{102}$$

$$\theta'(t=o) = \text{MAX}\ [0, T\ ].$$

The thermal perturbation field is an ellipsoid with a maximum horizontal radius R_θ and a depth Z_θ. The maximum temperature perturbation, ΔT, occurs at x_o, y_o and $z = Z_\theta/2$.

6. NUMERICAL PROCEDURE

Choice of Finite-Difference Approximations

Factors which influence the choice of finite-difference approximations are accuracy, economy, and long-term stability. Conservative schemes should be used, otherwise artificial generation of mass, momentum, vorticity, and energy would obviously invalidate the solutions. Especially desirable are schemes for space derivatives introduced by Arakawa (1966), which obey certain integral constraints on quadratic quanities, such as kinetic energy. These schemes are termed quadratic conservative or energy conservative, since when applied to advection they conserve both the first and second statistical moments of the dependent variable. These schemes are reasonably efficient and are especially popular in long-term integrations since they retard if not eliminate the development of nonlinear instability[7]. These numerical schemes, however, only possess their quadratic-conservative properties in the absence of time-differencing errors. An economical time differencing scheme which is complimentary to the quadratic-conservative space differencing is the second-order Adams-Bashforth method. Lilly (1965) has shown that the Adams-Bashforth method does not artifically generate kinetic energy when used with quadratic-conservative schemes; in addition, it has comparable accuracy, yet is more efficient when compared to certain second-order iterative methods. The Adams-Bashforth method also has comparable accuracy to the Leapfrog time-differencing scheme without the problems of time splitting instability; also

[7]Aliasing errors due to the finite differencing of nonlinear terms may lead to catostrophic rises in variances associated with the shortest resolvable wavelengths (e.g., Haltiner and Williams, 1980.) This so-called nonlinear instability cannot be eliminated by reducing the time step.

the method is not numerically diffusive, as in the case of the first-order upstream differencing scheme. Deardorff (1973), has found the Adams-Bashforth method to be more preferable in three-dimensional turbulent boundary layer simulations than the popular Leapfrog scheme.

A significant reduction in the run time of a compressible formulation can be achieved with the time-splitting integration procedure. This scheme has been developed for cloud models by Klemp and Wilhelmson (1978a) and Cotton and Tripoli (1978). The time-splitting procedure results in a substantial savings in computer time, yet results in little loss of accuracy, when compared to ordinary methods of compressible integration. In this scheme the higher frequency terms given by the LHS of Eqs. (2) and (4) are integrated with a time step compatible with the propagation of acoustic modes. The remaining terms in Eqs. (2) and (4) along with (5) - (11) are integrated with longer time steps which are appropriate for anelastic or incompressible flow.

In the TASS model the time-splitting integration procedure is used, and local time derivatives are approximated by the second-order Adams-Bashforth method. Space derivatives are approximated by second-order central differences in quadratic-conservative form. Details of the numerical formulation are given in the following sections.

Grid

The variables are arranged on a conventional staggered grid, often referred to as the Arakawa C mesh (Haltiner and Williams, 1980). All variables other than velocity are computed at a common point within the center of each grid cell. At the midpoints of the faces of the grid cells, the velocity component normal to the faces is computed. The grid arrangement

allows the use of quadratic conservative schemes and has improved accuracy over most other grid arrangements (e.g., Haltiner and Williams, 1980).

Vertical Stretching

A vertically stretched grid is obtained by continuously mapping the actual vertical coordinate z into the stretched vertical coordinate z'. The equations used for the transformation are the same as those used by Wilhelmson and Chen (1982).

The vertical coordinate z is mapped into z' as

$$z = (C_1 + C_2 z')z'. \tag{103}$$

A constant grid interval $\Delta z'$ in z' space is determined from Eq. (103) as

$$\Delta z' = [-\chi + ([\chi^2 + z_T]/C_2)^{0.5}]/(NL + 2); \tag{104}$$

where $\chi \equiv C_1/2C_2$, z_T is the height of the domain, and NL is the number of levels above the ground. The actual height of each grid point can be determined from Eq. (103), where:

$z' = (I-2)\,\Delta z'$ for w at I = 1, 2,...,NL + 2
$z' = (I-3/2)\,\Delta z'$ for all other variables at I = 1,2,...,NL + 2.

The mapping factor G is determined as

$$G = dz'/dz = [C_1 + 2\,C_2 z']^{-1}; \tag{105}$$

the vertical derivatives can be transformed into z' space as

$$d/dz = G\, d/dz', \qquad \text{and} \qquad d^2/dz^2 = G \frac{d}{dz'} \left(G \frac{d}{dz'}\right).$$

When grid stretching is applied the values typically assumed for constants C_1 and C_2 are 0.168 and 6.4×10^{-6} m, respectively. These values are taken from Wilhelmson and Chen except that the value for C_2 is an order of magnitude greater. This larger value for C_2 results in a more modest stretching; resulting in approximately a factor of 5 increase in vertical grid size from bottom to top. No stretching occurs (i.e., $z = z'$) with $C_1 = 1$ and $C_2 = 0$. Severe stretching (a large increase in grid size from top to bottom) is not recommended with the current turbulence closure scheme.

The vertical stretching of the grid mesh gives increased vertical resolution near the ground at the expense of resolution near the top of the domain. A primary reason for including vertical stretching in a cloud model is so that downdraft outflows and accompanying low-level features can be more adequately simulated.

Finite Difference Equations

Time derivatives

A generalized form of the Adams-Bashforth time differencing, which allows for a variable time step (Ochs, 1975) is employed in all large time-step calculations as

$$Q^{N+1} = Q^N + {}^N(Q)$$

where the operator $\phi(Q)$ is expressed as

$$\phi^N(Q) = \Delta t_N[(1 + \frac{\Delta t_N}{2\Delta t_{N-1}}) (\frac{\partial Q}{\partial t})_L^N - \frac{\Delta t_N}{2\Delta t_{N-1}} (\frac{\partial Q}{\partial t})_L^{N-1}], \quad (106)$$

where the subscript L refers to derivatives taken over the large time step. The time levels are defined according to the following notation:

$$Q^N \equiv Q(t),$$

$$Q^{N+1} \equiv Q(t + \Delta t_N),$$

and

$$Q^{N-1} \equiv Q(t - \Delta t_{N-1}).$$

The u component of velocity at small time level n+1 is approximated as

$$u^{n+1} = u^n + \frac{\Delta t_N}{2m} [3 (\frac{\partial u}{\partial t})_s^n - (\frac{\partial u}{\partial t})_s^{n-1}] + \frac{1}{m} \phi^N(u), \quad (107)$$

where there are m small time steps per large time step. Note that if $u^N = u^{n+\ell}$, then $u^{N+1} = u^{n+\ell+m}$. The subscript s signifies that the derivatives are taken over the small time step.

Both the v and w components of velocity, as well as the pressure deviation, are approximated in a similar fashion as u in Eq. (107).

Space derivatives

The finite-differencing for the space derivatives used in this study are expressed in the operator notation of Shuman (1962) and Lilly (1964) as

$$\delta_x Q \quad [Q(x + \frac{\Delta x}{2}) - Q(x - \frac{\Delta x}{2})]/\Delta x$$

and

$$\overline{Q}^{x} \equiv [Q(x + \tfrac{\Delta x}{2}) + Q(x - \tfrac{\Delta x}{2})]/2 \ ,$$

where x may represent y, z, z' or x.

In the notations described above the nonacoustical terms in Eq. (2) and (4) can be expressed as

$$\begin{aligned}\left(\frac{\partial u}{\partial t}\right)_L^N = & - \delta_x(\overline{u}^{x}\,\overline{u}^{x}) - \delta_y(\overline{u}^{y}\,\overline{v}^{x}) - G\delta_{z'}(\overline{u}^{z'}\,\overline{w}^{x}) \\ & + u\overline{\Phi}^{x} + f\overline{v}^{xy} - f_1\overline{w}^{xz'} \\ & + 2\,\delta_x(K_M\delta_x u) + \delta_y[\overline{K}_M^{xy}(\delta_y u + \delta_x v)] \\ & + G\delta_{z'}[\overline{K}_M^{*xz'}(G\delta_{z'}u + \delta_x w)]/\rho_o - \tfrac{2}{3}\,\delta_x(K_M\Phi) - \left(\frac{\partial u}{\partial t}\right)^{*} \\ & + \overline{\nu}^{x}[\delta_{xx}u + \delta_{yy}u + G\delta_{z'}(G\delta_{z'}u')], \end{aligned} \tag{108}$$

$$\begin{aligned}\left(\frac{\partial v}{\partial t}\right)_L^N = & - \delta_x(\overline{v}^{x}\,\overline{u}^{y}) - \delta_y(\overline{v}^{y}\,\overline{v}^{y}) - G\delta_{z'}(\overline{v}^{z'}\,\overline{w}^{y}) \\ & + v\overline{\Phi}^{y} - f\overline{u}^{xy} \\ & + \delta_x[\overline{K}_M^{xy}(\delta_y u + \delta_x v)] + 2\,\delta_y(K_M\delta_y v) \\ & + G\delta_{z'}[\overline{K}_M^{*xz'}(\delta_y w + G\delta_{z'}v)]/\rho_o - \tfrac{2}{3}\,\delta_y(K_M\Phi) - \left(\frac{\partial v}{\partial t}\right)^{*} \\ & + \overline{\nu}^{y}[\delta_{xx}v + \delta_{yy}v + G\delta_{z'}(G\delta_{z'}v')], \end{aligned} \tag{109}$$

$$\begin{aligned}\left(\frac{\partial w}{\partial t}\right)_L^N = & - \delta_x(\overline{w}^{x}\,\overline{u}^{z'}) - \delta_y(\overline{w}^{y}\,\overline{v}^{z'}) - G\delta_{z'}(\overline{w}^{z'}\,\overline{w}^{z'}) \\ & + w\overline{\Phi}^{z'} + f_1\overline{u}^{xz'} + g(\overline{H}^{z'} - 1) \\ & + \delta_x[\overline{K}_M^{xz'}(G\delta_{z'}u + \delta_x w)] + \delta_y[\overline{K}^{yz'}(\delta_y w + G\delta_{z'}v)] \\ & + 2G\delta_{z'}(K_M^{*}\,G\delta_{z'}w)/\rho_o - \frac{2G}{3}\,\delta_{z'}(K_M^{*}\Phi) \\ & + \overline{\nu}^{z}[\delta_{xx}w + \delta_{yy}w + G\delta_{z'}(G\delta_{z'}w)], \end{aligned} \tag{110}$$

$$\left(\frac{\partial p}{\partial t}\right)_L^N = -\delta_x(\bar{p}^x u) - \delta_y(\bar{p}^y v) - G\delta_{z'}(\bar{p}^z w) + p\Phi - \rho_o g\bar{w}^{z'} + \delta_x(\bar{K}_M^x \delta_x p) + \delta_y(\bar{K}_M^y \delta_y p) + G\delta_{z'}[\bar{K}_M^{*z'} G\delta_z p]/\rho_o, \quad (111)$$

where

$$\Phi = \delta_x u + \delta_y v + G\delta_{z'} w$$

$$f \equiv 2\,\Omega \sin \phi_\ell,$$

$$f_1 \equiv 2\,\Omega \cos \phi_\ell,$$

and

$$K^* = \rho_o K.$$

Any of the moisture substance equations can be expressed as

$$\left(\frac{\partial Q}{\partial t}\right)_L^N = -\delta_x(\bar{Q}^x u) - \delta_y(\bar{Q}^y v) - G\delta_{z'}(\bar{Q}^{z'} w) + Q\Phi - G\delta_{z'}(\bar{Q}^z W_Q \rho_o)/\rho_o + \delta_x(\bar{K}_T^x \delta_x Q) + \delta_y(\bar{K}_T^y \delta_y Q) + G\delta_{z'}(\bar{K}_T^{*z'} G\delta_z Q)/\rho_o + S, + \nu[\delta_{xx}Q + \delta_{yy}Q + G\delta_{z'}(G\delta_{z'}Q')] \quad (112)$$

where W_Q is the terminal velocity of any precipitating moisture substance variable Q. Obviously, the equations for water vapor, cloud droplets, and ice crystals will not have a term for the terminal velocity. The finite-difference equation for potential temperature has a form similar to Eq. (112).

To guarantee linear numerical stability for advection, an additional term has been added to Eqs. (108) - (110), and (112). In this term the numerical

diffusion coefficient, ν, is defined from criteria presented in the following section.

The local rate of deformation squared which is used in Eq. (12), is expressed as

$$|DEF|^2 = 2[(\delta_x u)^2 + (\delta_y v)^2 + (\delta_z w)^2]$$

$$+ (\delta_y \overline{u}^{xy} + \delta_x \overline{v}^{xy})^2 + (G\delta_{z'} \overline{v}^{yz'} + \delta_y \overline{w}^{yz'})^2$$

$$+ (\delta_x \overline{w}^{xz'} + G\delta_{z'} \overline{u}^{xz'})^2 - \frac{2}{3}\Phi^2.$$

The acoustically-active terms in Eq. (2) and (4) are computed at each small time step and are expressed in finite differences as

$$\left(\frac{\partial u}{\partial t}\right)_s^n = - \overline{H}^x (\delta_x p)/\rho_o,$$

$$\left(\frac{\partial v}{\partial t}\right)_s^n = - \overline{H}^y (\delta_y p)/\rho_o,$$

$$\left(\frac{\partial w}{\partial t}\right)_s^n = - \overline{H}^{z'} (G\delta_{z'} p)/\rho_o,$$

$$\left(\frac{\partial p}{\partial t}\right)_s^n = - \eta P \Phi,$$

where Φ is derived from the current values of u, v, and w; and P is approximated from values at the latest large time step; i.e., $P = p^N + P_o$.

Orlanski boundary condition

The Orlanski radiation boundary condition is expressed in a form

consistent with the Adams-Bashforth method and is applied to u, v and p at each small time step as

$$-\frac{(Q_b^{n+1}-Q_b^n)}{\Delta t_s}=\frac{3C^n}{2\Delta r}(Q_b^n-Q_{b-1}^n)-\frac{C^{n-1}}{2\Delta r}(Q_b^{n-1}-Q_{b-1}^{n-1});$$

where $\Delta t_s = \Delta t_{N+1}/m$; and Δr is the grid increment of the coordinate normal to the boundary. The phase velocity can be obtained from Eq. (16) as

$$C^n=\frac{C^{n-1}(Q_{b-1}^{n-2}-Q_{b-2}^{n-2})/2\Delta r-(Q_{b-1}^n-Q_{b-1}^{n-1})/\Delta t_s}{3\,(Q_{b-1}^{n-1}-Q_{b-2}^{n-1})/2\Delta r}.$$

which is limited by conditions on the south and west boundaries as

$$C^n=\begin{cases}0 & C^n>0\\ C^n & \text{if } 0\geq C^n\geq -0.5\,\Delta r/\Delta t_s\\ -0.5\,\Delta r/\Delta t_s & C^n<-0.5\,\Delta r/\Delta t_s,\end{cases}$$

and on the north and east boundaries as

$$C^n=\begin{cases}0.5\,\Delta r/\Delta t_s & C^n>0.5\,\Delta r/\Delta t_s\\ C^n & \text{if } 0\leq C^n\leq 0.5\,\Delta r/\Delta t_s\\ 0 & C^n\leq 0\ .\end{cases}$$

The Orlanski boundary condition for w need only to be applied at the large time steps. The procedure is similar to the above, with the large time step and time levels substituted instead.

Numerical Stability Criteria

Both the small and large time steps and numerical viscosity coefficient are chosen so as to enforce the linear stability of the numerical system. The critical short time step Δt_s^* guarantees linear stability for the acoustic modes. Linear stability of the lower frequency modes are enforced by the critical large time step Δt_L^* and the numerical viscosity coefficient ν. The linear stability analysis for the numerical scheme is found in Appendix F.

The critical large and small time steps are, respectively,

$$\Delta t_L^* = 0.5/\text{MAX}[|u|/\Delta x + |v|/\Delta y + |W|/\Delta z],$$

$$\Delta t_s^* = 0.5 \left\{\eta R \ \text{MAX}(T_o) \ (\Delta x^{-2} + \Delta y^{-2} + \text{MAX}[\Delta z^{-2}])\right\}^{-0.5},$$

where $|W| = \text{MAX}[|w|, \ |w-\bar{W}_H|, \ |w-\bar{W}_R|]$. The large time step is divided by $\sqrt{2}$ whenever it is exceeded by the critical time step Δt_L^*; i.e.,

$$\Delta t_{N+1} = \Delta t_N/\sqrt{2} \qquad \text{if} \qquad \Delta t_{N+1} > \Delta t_L^*.$$

The integer number of small time steps per large time step must be recomputed whenever the large time step is changed; it is given by

$$m = \text{Integer} \ [\Delta t_{N+1}/\Delta t_s^* + 0.999];$$

hence the small time step is

$$\Delta t_s = \Delta t_{N+1}/m,$$

which is always less than or equal to the critical small time step.

The numerical viscosity coefficient is determined such that a critical amount of diffusion exists in order to counter the small amplification of the Adams-Bashforth method; it is given as

$$\nu(x,y,z,t) = \Delta t^3 \left[\frac{|u|}{\Delta x} + \frac{|v|}{\Delta y} + \frac{|W|}{\Delta z}\right]^4 / 8[\Delta x^{-2} + \Delta y^{-2} + \Delta z^{-2}]$$

In cloud simulations ν is typically two to three orders of magnitude less than K_M; the numerical viscosity term is retained in the model formulation, but can probably be neglected with no significant impact in most integrations.

The maximum critical eddy viscosity is defined

$$K_{MAX} = [4\Delta t_L(\Delta x^{-2} + \Delta y^{-2} + \Delta z^{-2})]^{-1};$$

hence

$$K_M = \text{MIN}\ [K_M, K_{MAX}],$$

and

$$K_T = \text{MIN}\ [K_T, K_{MAX}].$$

This condition guarantees linear stability of the diffusion process. However, in typical cloud simulations K_T and K_M rarely, if ever, exceed K_{MAX}.

The numerical domain may be specified as being stationary with respect to the ground, or it may translate with a convective system. The latter offers advantages in that: 1) truncation error is reduced since the translation of fields relative to the domain is minimized; and 2) convective systems, especially fast moving storms, can be simulated with a detailed mesh for long periods of time.

The translation speed of the grid is variable and is computed as follows. The grid translation components U_G and V_G are computed every τ seconds according to:

$$U_G(t) = U_G(t-\tau) + \frac{\bar{x}(t) - \bar{x}(t-\tau)}{\tau} + 0.25\,\frac{\bar{x}(t) - x_o}{\tau},$$

$$V_G(t) = V_G(t-\tau) + \frac{\bar{y}(t) - \bar{y}(t-\tau)}{\tau} + 0.25\,\frac{\bar{y}(t) - y_o}{\tau},$$

where

$$\bar{x} = \frac{\iiint Qx\ dx\ dy\ dz}{\iiint Q\ dx\ dy\ dz} \quad \text{, and} \quad \bar{y} = \frac{\iiint Qy\ dx\ dy\ dz}{\iiint Q\ dx\ dy\ dz}.$$

By defining

$$Q = A^2 \rho_o w^2, \qquad \text{where} \qquad A = \begin{cases} 6 + \log_{10} & \zeta \geq 10^{-5}\ s^{-1} \\ 1.0 & \zeta \leq 10^{-5}\ s^{-1}, \end{cases}$$

and where $\zeta = \partial v/\partial x - \partial u/\partial y$; the grid will track the cyclonic rotating storm, attempting to keep it centered at location (x_o, y_o). Typically τ is set equal to 300 s and (x_o, y_o) is set to the center location of the grid.

Procedure

Computation of the cloud microphysics entails several steps per large time step:

Step 1. Tenative values for θ, Q_v, Q_{CD}, Q_{IC}, Q_R, Q_{SN}, and Q_H are computed from Eqs. (5) - (11) in the absence of source terms.

Step 2. T and Q_{vs} are diagnosed from θ, p, and e_{svo} using Eqs. (30), (91) and (94).

Step 3. Q_v, Q_{CD}, T, and Q_{sv} are adjusted for condensation of water vapor and the evaporation of cloud drops.[8]

Step 4. The production of hail from the riming of snow is computed and Q_H and Q_{SN} are adjusted accordingly.

Step 5. Production of hail or snow due to the collision of raindrops with ice crystals and the spontaneous freezing of raindrops are computed (see Appendix G); Q_R, T, Q_{sv}, Q_H and Q_{SN} are adjusted accordingly.

Step 6. Q_{svi} is computed from Eqs. (35) and (92).

[8]The saturation mixing ratios Q_{sv} and Q_{svi} are adjusted using formulas derived in Appendix D.

Step 7. Initiation of ice crystals, melting of ice crystals, freezing of cloud droplets, growth of ice crystals due to deposition and riming, and the conversion of ice crystals to snow are computed; Q_v, Q_{IC}, Q_{CD}, Q_{SN}, T, Q_{sv}, and Q_{svi} are adjusted accordingly.[8]

Step 8. The terminal velocities for rain and hail and the remaining microphysical interactions are computed.

Step 9. The potential temperature is adjusted for the latent heat released.

Numerical seeding

"Numerical seeding" in simulated clouds may occur due to the spurious presence of very small values of Q_R, Q_{SN}, or Q_H. In other words, very small values of rain, snow, or hail, artifically produced by truncation error or boundary reflection, may grow in areas where it should not occur.

In order to prevent numerical seeding the following procedure is used following step 1 in the microphysical procedure:

$$Q_{CD} = Q_{CD} + Q_R, \quad \text{and} \quad Q_R = 0 \quad \text{if} \quad 0 < Q_R \leq 10^{-7},$$
$$Q_{IC} = Q_{IC} + Q_{SN}, \quad \text{and} \quad Q_{SN} = 0 \quad \text{if} \quad 0 < Q_{SN} \leq 10^{-7},$$
$$Q_{IC} = Q_{IC} + Q_H, \quad \text{and} \quad Q_H = 0 \quad \text{if} \quad 0 < Q_H \leq 10^{-7}.$$

In other words, rain is converted to cloud droplets if the rain water content is positive and not less than 10^{-7} g g^{-1}; and etc.

This procedure also increases the computational efficiency of the model,

since some of the microphysical interactions need not be computed at grid points where small values of Q_R, Q_{SN}, or Q_H formerly existed.

Negative water

In nature Q_v, Q_{CD}, Q_{IC}, Q_R, Q_{SN}, and Q_H are positive definite quantities; but because of numerical approximations, may be negative at some locations in the computational domain. In this model's numerical framework, relatively small amounts of negative water are produced, and are treated periodically as described below. At the end of every 50 time steps the following procedure is applied to each of the moisture substance variables; i.e., $Q = Q_v$, Q_{CD}, Q_{IC}, Q_R, Q_{SN}, and Q_H:

1) The total integrated mass of Q in the domain is computed; i.e.,

$$TMQ = \iiint \rho_o \, Q \, dx \, dy \, dz;$$

2) next, negative values at each grid point are set equal to zero:

$$Q = 0 \qquad \text{if} \qquad Q < 0;$$

3) the total integrated mass of Q after eliminating the negative values is computed:

$$PTMQ = \iiint \rho_o \, Q \, dx \, dy \, dz;$$

4) the values of Q are multiplied by a factor, r_Q so that the integrated mass is the same as TMQ; i.e.,

$$Q = Qr_Q,$$

where[9]

$$r_Q = (TMQ + \alpha_w)/(PTMQ + \alpha_w).$$

Hence, the procedure eliminates the negative values of Q and approximately conserves the total integrated mass of Q.

Negative values of water substance are treated only periodically since retention of negative values may result in more accurate space differencing. In computing the microphysical production terms, negative values of Q are treated as zero.

Model Code

The model code is written in Cyber FORTRAN 200, using 64-bit word lengths. With the exception of much of the microphysics, the code is almost completely vectorized; vectorization is programmed explicitly, along each horizontal plane. Configuration of the model domain is made flexible; the grid sizes, the number of vertical levels, and the number of grid cells in either the x or y direction are input parameters. The model code has a restart capability, and simulated data from selected fields is transferred as

[9]The threshold constant α_w is given a value of 10^{-8} times the horizontal area of the domain.

output to disk at a selected time inverval.

The program runs in-core on the NASA Langley VPS-32 supercomputer. For a 63 x 63 grid with 32 vertically-stretched layers, the memory required is 5.5 million words, and the ratio of simulation time to computation time in cloud simulations is roughly 2:3. For a 43 x 43 grid with 27 vertically-stretched layers the memory required is 2.4 million words, and the ratio of simulation time to computation time is roughly 2:1. Actual run time depends on many factors such as grid size, number of grid points, speed of environmental winds, as well as the intensity and area of cumulus convection. Computations with vertically-stretched grids may be several times slower due to the time step constraint by the small mesh size near the ground.

A timing algorithm was run over several time steps during the mature phase of a simulated supercell storm. Table 2 shows that roughly half of the computational time is used in computing the microphysics. The actual percentages may vary with case, time, and the number of grid points assumed.

Table 2. BREAKDOWN OF COMPUTATIONAL TIME

ASSUMING A 63 x 63 x 33 GRID

Computation of	Percent of Time
Microphysics	52%
Velocity and Pressure (including boundary conditions)	26%
Remaining Prognostic Variables (including boundary conditions)	12%
Subgrid Eddy Viscosity	3%
Near Boundary Filters	2%
Other	5%
Total	100%

7. TEST CASES

Before attempting to evaluate the model against observed data sets, the model can be checked out against simplified atmospheric cases. These test cases are useful in uncovering any basic flaws in the model coding and formulation. Also, these test cases (and additional simulations with the two-dimensional axisymmetric version of TASS) are useful in evaluating the procedure used for the open lateral boundaries.

No Shear and Unidirectional Shear of the Environmental Winds

Two simulations are conducted using a composite sounding, representative of the atmosphere near Del City, Oklahoma, on 20 May 1977. However, in the first case, the environmental winds are removed; hence, convection is simulated in a calm environment. In the second case, only the V component of the environmental wind is removed (Fig. 2); thus convection is simulated with an environment having unidirectional windshear. In both of the cases the model domain is 40 km in both horizontal directions and 20 km in the vertical direction. The horizontal grid size is 1000 m and the vertical grid size is variable -- being defined by 31 vertically-stretched layers. Coriolis force is neglected. Convection is triggered by assuming a temperature perturbation defined by Eq. (102), with $\Delta T = 3^{o}C$, $z_{\theta} = 3000$ m, and $R_{\theta} = 10{,}000$ m. The perturbation is centered horizontally within the domain at $x = o$, $y = o$.

Simulation with no shear

The simplest test case is to assume an axisymmetric perturbation within an environment having no ambient wind. It is expected that the ensuing

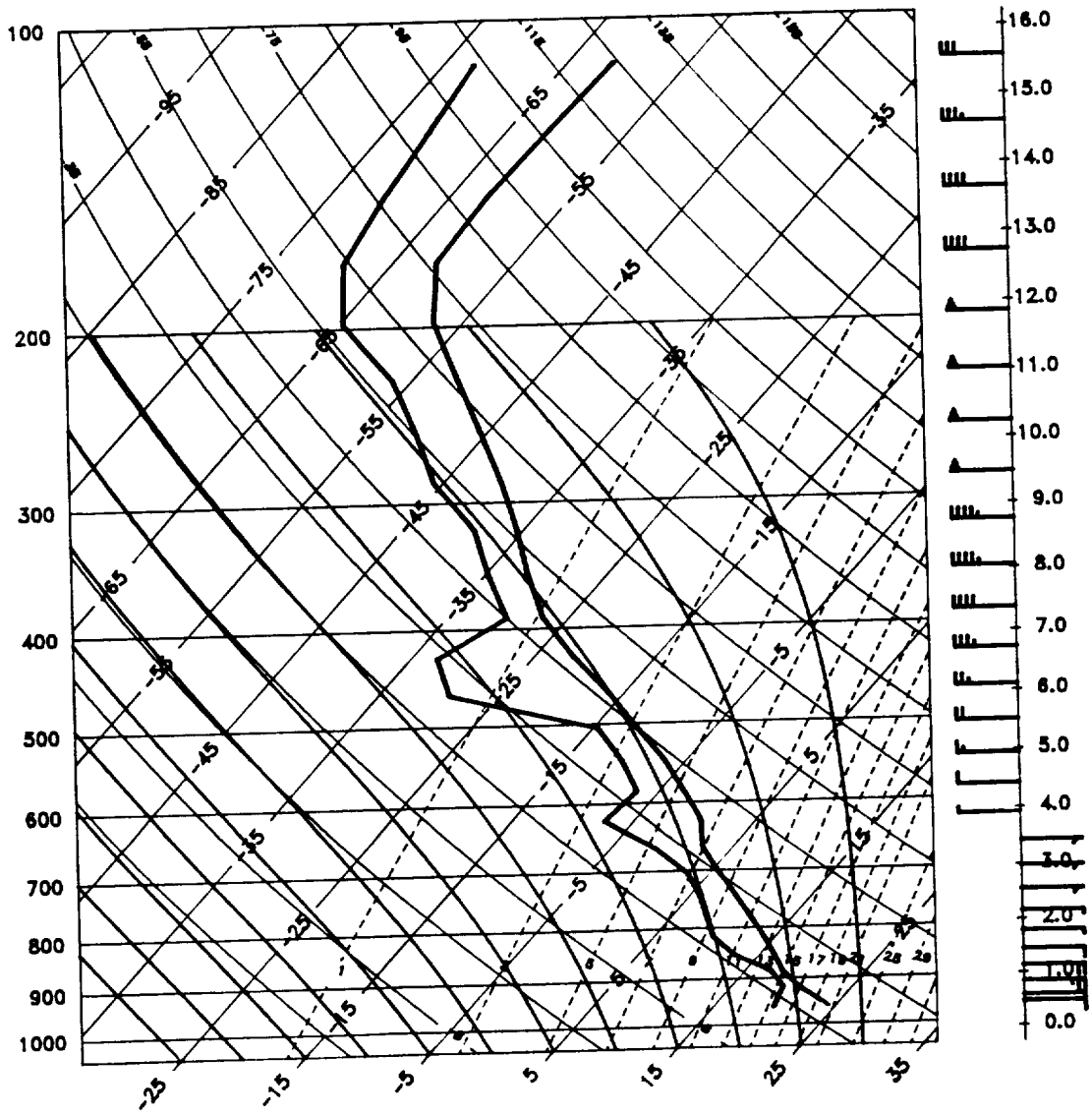

Fig. 2. Composite sounding for Del City, Oklahoma on 20 May 1977. The wind flags represent u component of winds only. Each full barb represents 5 m s^{-1}.

convection should be symmetric and stationary with respect to the vertical axis of the initial perturbation.

Figs. 3 and 4 portray y-z cross sections through the axis of the updraft at a time shortly after the maximum updraft speed is attained. Note that w, v, p, T' and radar reflectivity fields all show symmetry about y = o.

Simulation with unidirectional shear

In the case of unidirectional shear one expects to see the development of counter-rotating vortices which move obliquely from the direction of the wind shear. These diverging circulations are associated with the splitting of the updraft into two diverging parts (e.g., Wilhelmson and Klemp, 1978b). This case is useful in order to determine if the model is capable of simulating storm splitting, and is particularly useful in evaluating the storm tracking algorithm.

Results from this simulation are shown in Figs. 5-8. The horizontal coordinates along the grids are relative to the position in which convection was initiated (x = o, y = o), and change with time due to the translation of the domain.

Pronounced splitting of the updraft is evident by 60 min (Fig. 5b), and by 90 min, the northernmost updraft cell begins to exit through the north boundary. From Fig. 6b it is evident that the northernmost cell has anticyclonic rotation, while its cyclonic-rotating counterpart remains near the center of the grid. Each of the two cells are propagating in opposite directions normal to the mean tropospheric wind (which is from the west at 8 m s^{-1}). Hence, the cyclonic cell is propagating to the right of the mean wind, and the anticyclonic cell to the left of the mean wind. The cyclonic cell, however remains near the center of the grid, since the domain tracking

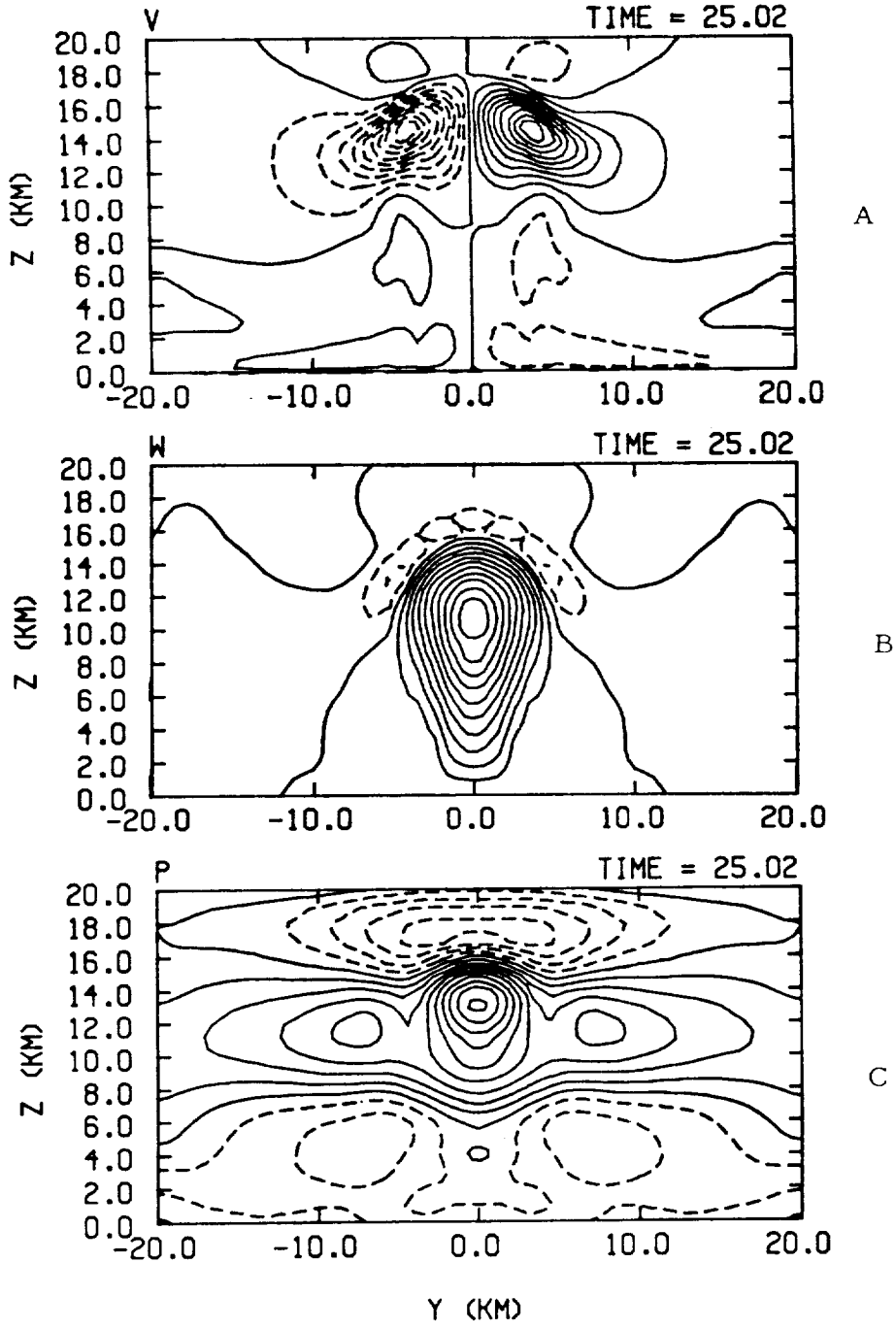

Fig. 3. Simulated field distributions in y-z plane for the no wind shear case. The fields are a) v component of velocity, b) w component of velocity, and c) pressure deviation from environment. The contour intervals are 3 m s^{-1} in a) 5 m s^{-1} in b) and 0.25 mb in c). Negative values are contoured with dashed line.

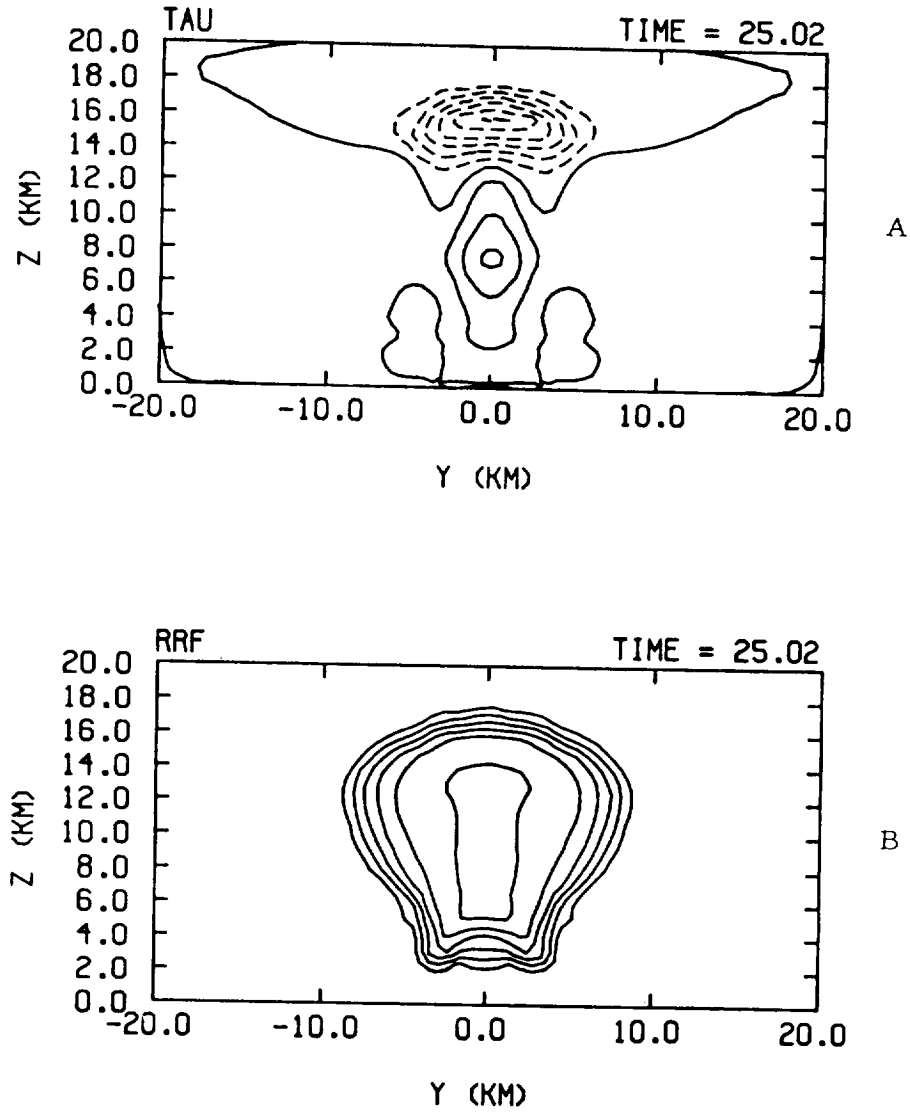

Fig. 4. Same as Fig. 3 except that the fields are a) temperature deviation from the environment and b) radar reflectivity. The contour intervals are 3°C in a) and 10 dBZ in b).

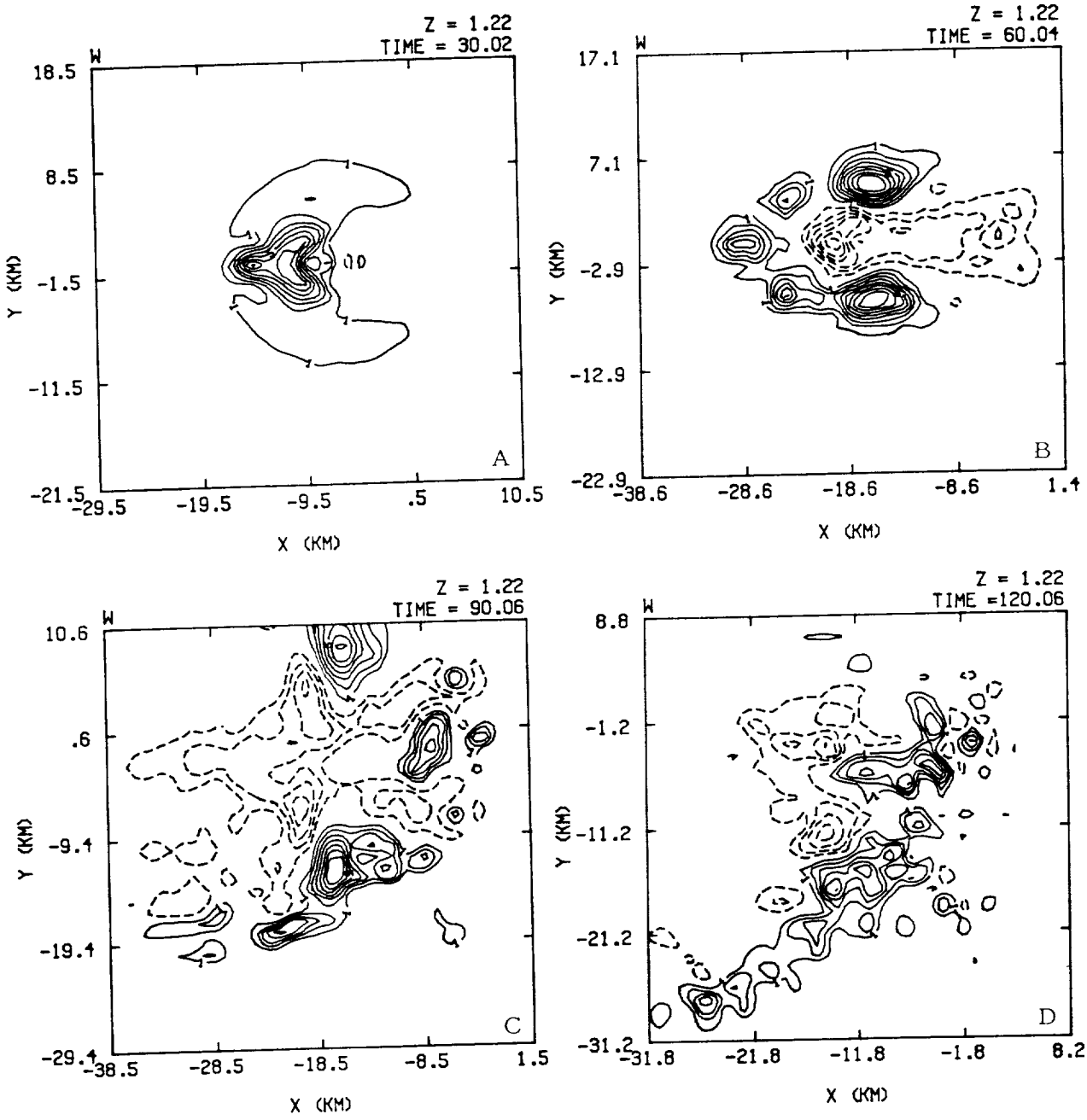

Fig. 5. Simulated field distribution for w in x-y plane at z = 1.22 km for unidirectional shear case. The fields are at a) 30 min, b) 60 min, c) 90 min and d) 120 min. The contour interval is 1 m s^{-1} (zero contour is suppressed). Negative values are contoured with dashed line.

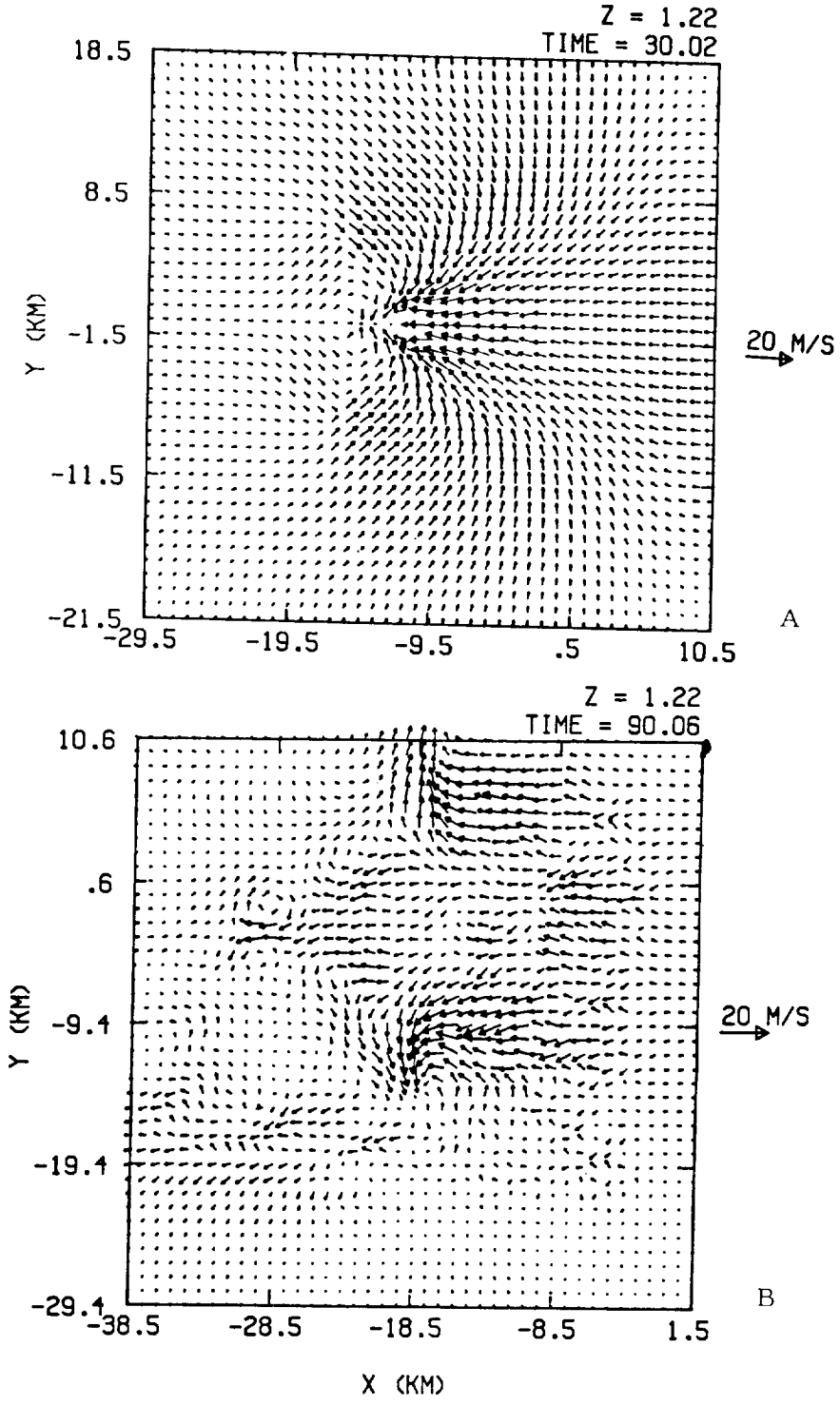

Fig. 6. Same as Fig. 5 except that plots represent wind vector fields at a) 30 min and b) 90 min. The wind vectors are determined from the horizontal velocity after the environmental winds have been removed.

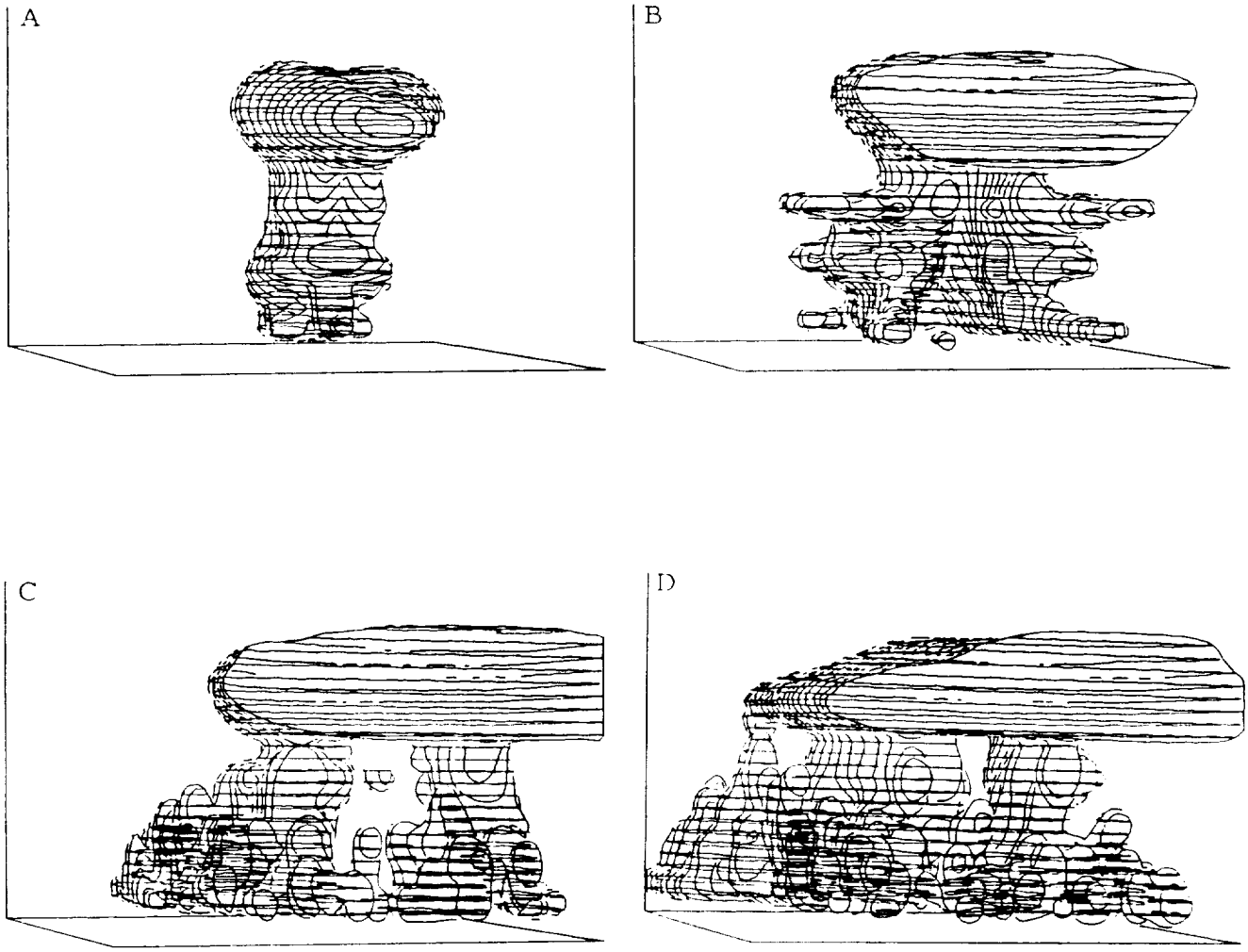

Fig. 7. Three-dimensional perspectives of simulated clouds for unidirectional wind shear case at a) 30 min, b) 60 min, c) 90 min and d) 120 min. Perspectives viewed from ESE (vertical coordinate in z´ space).

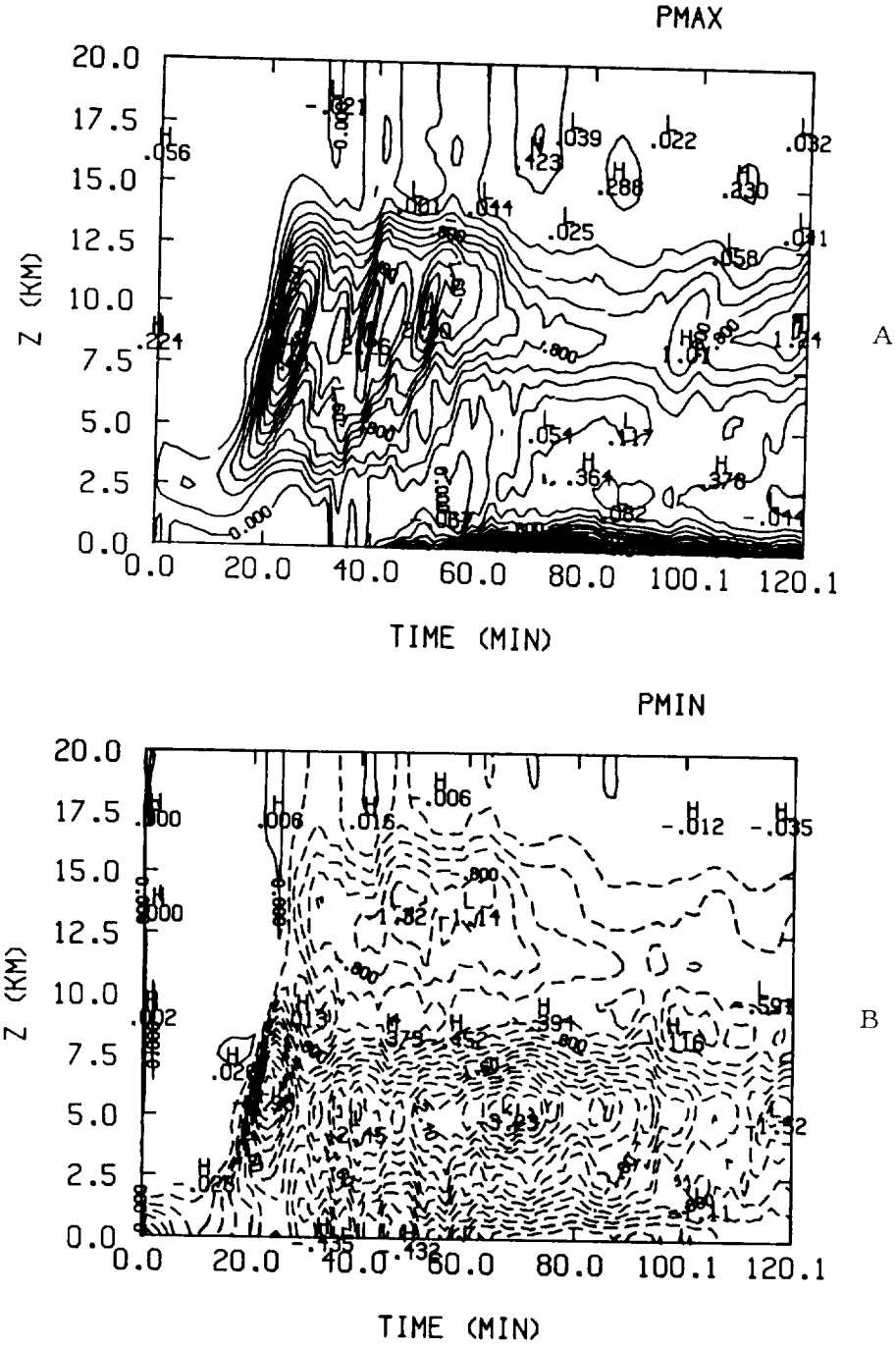

Fig. 8. Time - z plots of a) maximum pressure deviation and b) minimum pressure deviation for unidirectional wind shear case. The contour interval is 0.2 mb and values range from 3.8 mb in a) to -3.2 mb in b).

algorithm continually adjusts the translation speed of the domain. After 90 min, the anticyclonic rotating updraft exists through the north lateral boundary with no detrimental consequences to the numerical solution. New updraft cells form along the southwestern flank of the old cell (Fig. 5d) as rain cooled outflow undercuts the potentially unstable air. Three-dimensional perspectives of the simulated clouds (which are determined from the cloud droplet and ice crystal fields) are shown in Fig. 7 at 30, 60, 90 and 120 min.

The minimum and maximum pressure deviation in each horizontal level are plotted in Fig. 8 as a function of height and time. No obvious mass trends exist in the solution, even when the anticyclonic updraft exists through the north boundary after 90 min. The greatest values of maximum pressure deviation ($\tilde{<}$ 3.8 mb) occur at the surface after 40 min, and are associated with the onset of precipitation.

This case successfully demonstrates the models' capability of simulating storm splitting. Also demonstrated is the ability of the model domain to preferentially translate with the convective cell having cyclonic rotation. The lateral boundary conditions appear stable and allow the outward propagation of convective cells without detrimental effects.

Lateral Boundary Condition Test

Several experiments have been performed with both the axisymmetric version and 3-D version of TASS in order to evaluate the lateral boundary conditions. These experiments have been reported earlier in greater detail in Proctor (1985a).

Two-dimensional axisymmetric simulations

The lateral boundary condition procedure was tested in the two-dimensional model by simulating the outward propagation of a downburst gust front. Two model domain sizes were used: a 3 km radius x 5 km deep and a 5 km x 5 km domain. The grid resolution was 40 m in both the radial and vertical direction. The downburst circulation was initiated by specifying a distribution of hail along the top boundary (see Proctor, 1985b; and Chuang et al., 1984 for additional details). The melting of hail and the evaporation of rain cool the air and drive the circulation. A severe test to the lateral boundary conditions occurs as the gust front propagates through the lateral boundary.

Results from the two experiments are shown in Figs. 9 and 10. Two experiments were conducted with everything identical except the domain size. The results from the smaller 3 km x 5 km domain are in the left columns of Figs. 9 and 10, while results from the 5 km x 5 km domain are in the right columns. Comparison between the two experiments show little difference. The greatest error occurs in the pressure deviation field, with maximum pressure in the smaller domain being roughly 0.1 mb lower. These experiments demonstrate that the lateral boundary condition procedure allows the outward propagation of the gust front with only minimal reflections and almost no alteration of the interior solution.

Three-dimensional simulation

The boundary conditions were also tested in the three-dimensional simulation of convection for two different domain sizes. The large domain covered a horizontal area of 60 km x 60 km while the smaller domain covered 30 km x 30 km. Both experiments had equal horizontal grid lengths of 1 km and

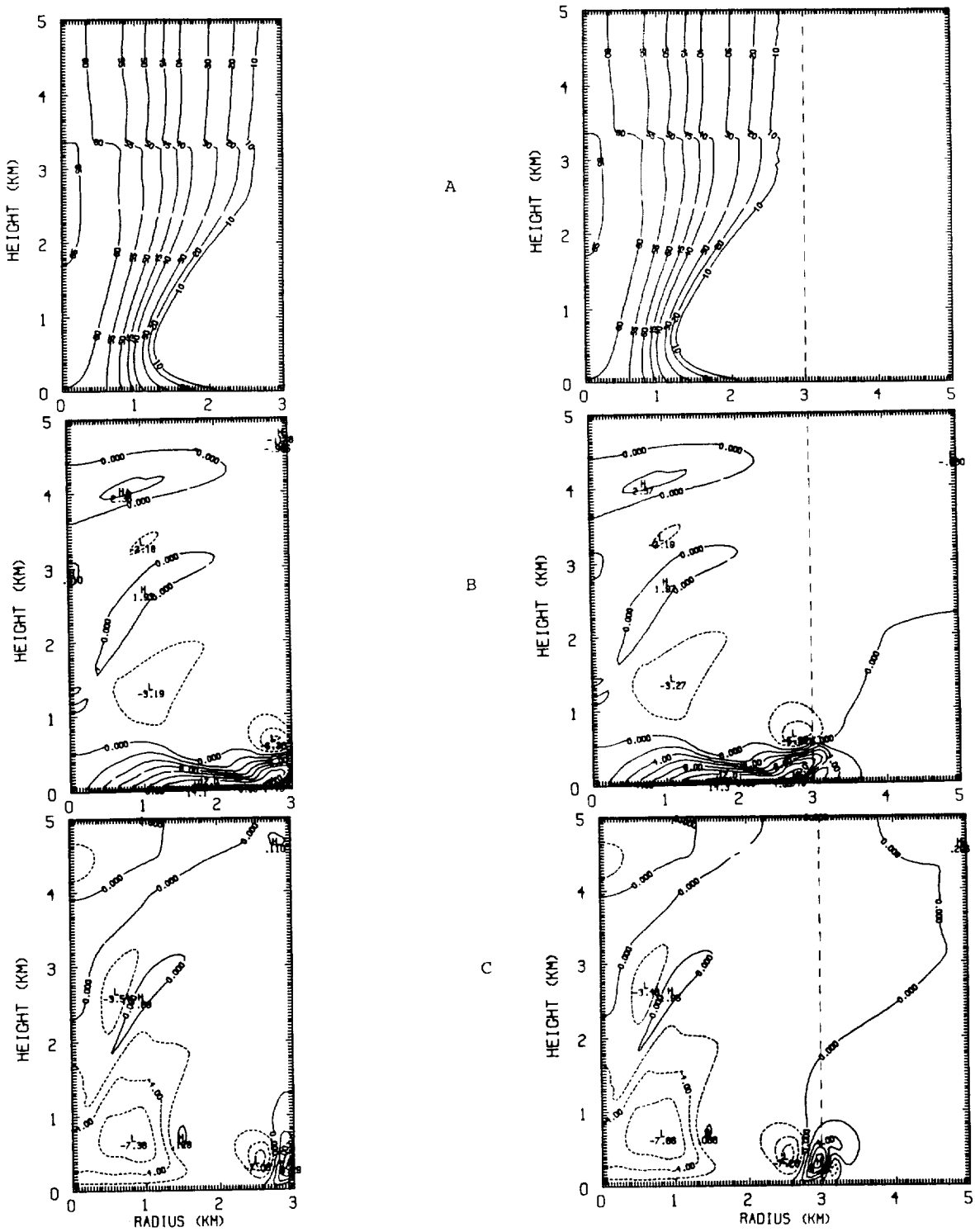

Fig. 9. Field distributions from 2-D axisymmetric model of a) simulated radar reflectivity, b) radial velocity, and c) vertical velocity. Plots in left column are from the 3 km x 5 km domain simulation, while plots in right column are from the 5 km x 5 km domain simulation. The contour interval is 10 dBZ in a) and 2 m s^{-1} in b) and c).

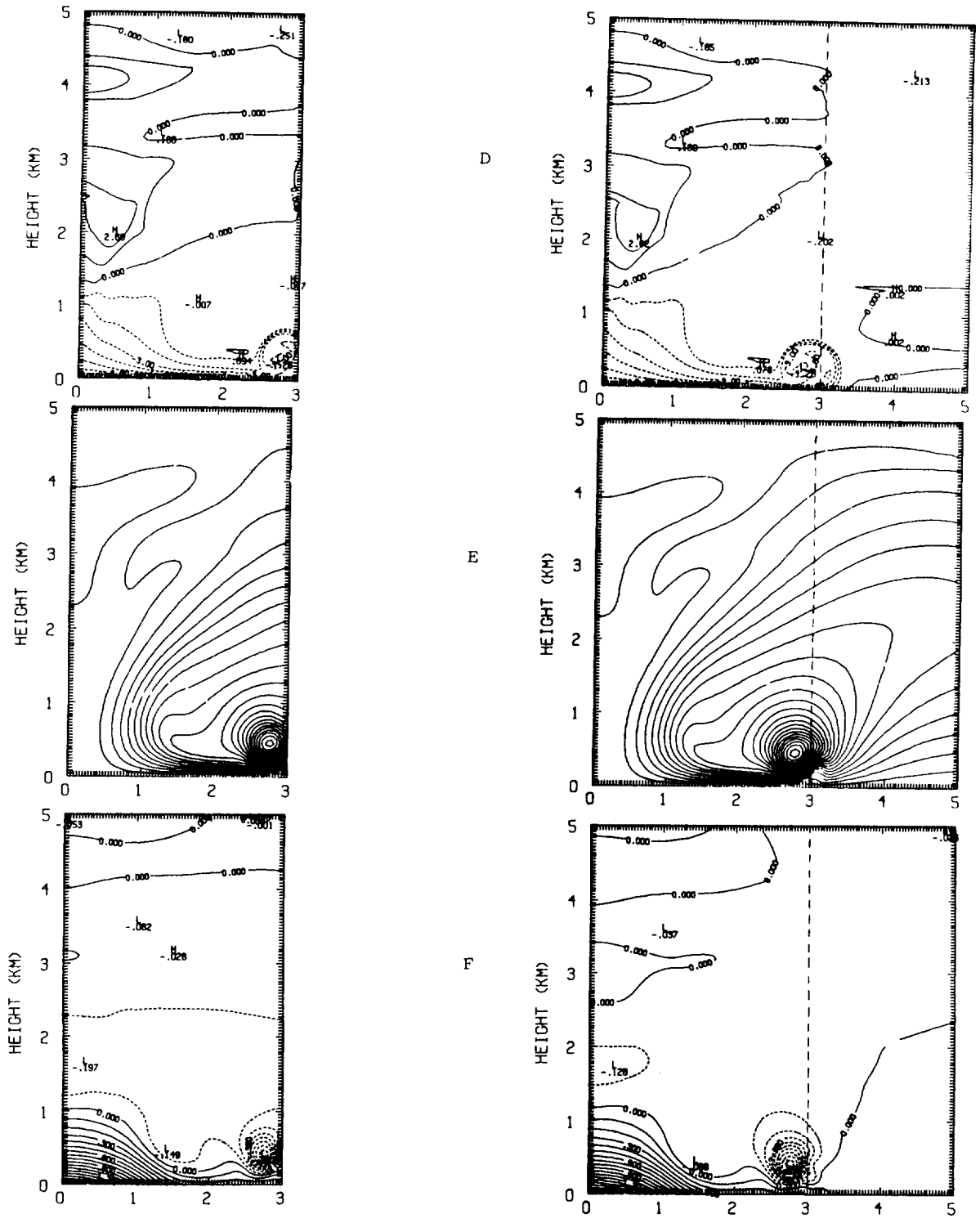

Fig. 10. Same as Fig. 9 except that the fields are d) temperature deviation from the environment, e) approximate stream function, and f) pressure deviation from the environment. The contour intervals are 1°C in d) and 0.1 mb in f).

the domain extended to a depth of 18.75 km with a constant vertical grid length of 750 m. No precipitation processes were included in these simulations.

A pair of convective cells were similarly initiated in both experiments, and remained near the corners of the 30 km x 30 km domain experiment throughout the 30 min simulation. The proximity of the convective cells to the corners should provide a good test for the lateral boundary conditions.

A horizontal cross section of the vector field and cloud boundary at $z = 8250$ m is shown in Fig. 11. The simulations agree very well as evidenced in Fig. 11.

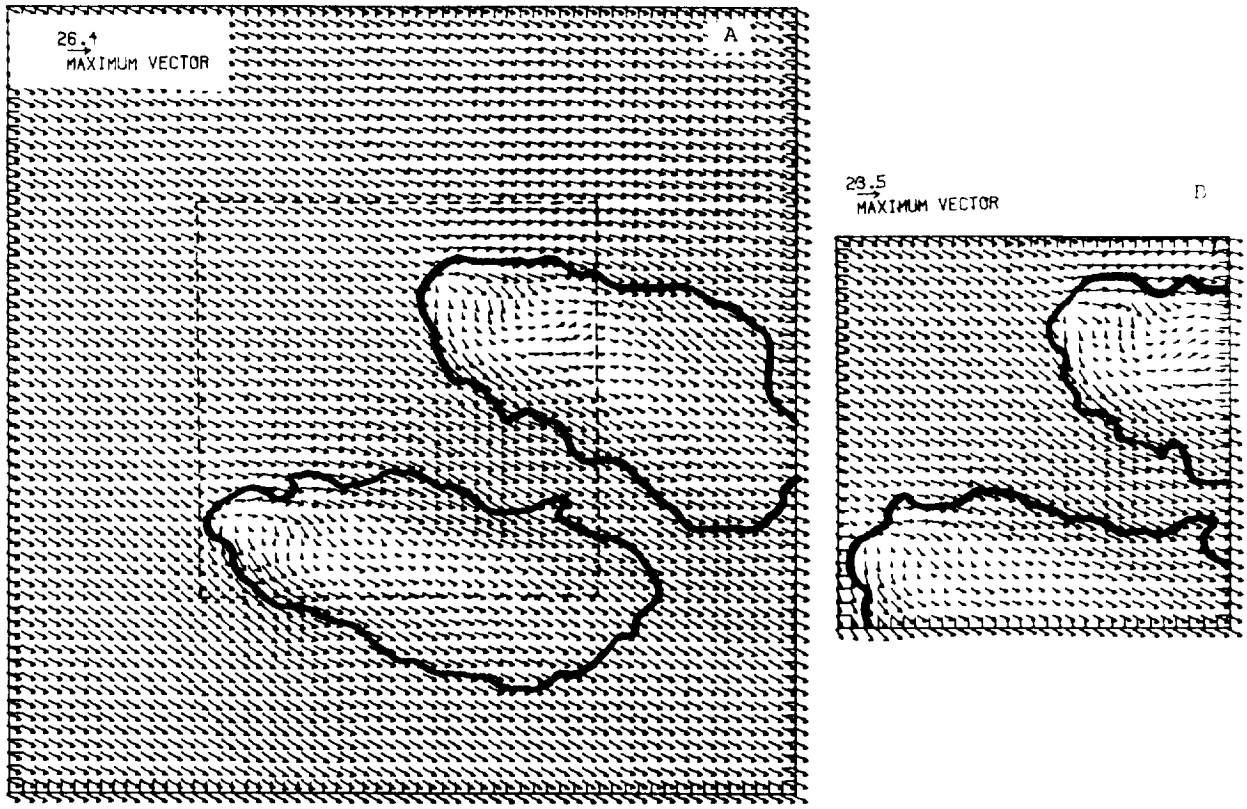

Fig. 11. Horizontal cross section of the cloud boundary and wind vector field at z = 8250 m for a) 60 km x 60 km domain, and b) 30 km x 30 km domain at t = 30 mins. Winds are relative to the translating grid.

8. SUMMARY AND CONCLUSIONS

In this report the theoretical formulation of the TASS model is described. The model contains a nonhydrostatic and compressible equation set and ice-phase microphysics, with prognostic equations for momentum, pressure, potential temperature, water vapor, cloud droplets, ice crystal, rain, snow, and hail. A new lateral boundary condition procedure is used which allows minimal distortion of the interior flow and the outward propagation of convective cells, without the mass trends which sometimes plague other boundary condition procedures. A diagnostic surface boundary layer formulation is introduced, which is based on similarity theory. The model utilizes the time splitting integration procedure with time derivatives approximated by the second-order Adams-Bashforth method. Space derivatives are approximated by second-order quadratic-conservative differences. The model includes an algorithm which allows the domain to translate along with a convective cell, even at variable speeds. In a storm splitting case it was shown that the algorithm allows the domain to translate with the convective cell having cyclonic rotation.

Two philosophical approaches are usually assumed in the parameterization of cloud microphysics with bulk models. The approach assumed by the Colorado State University modelers (e.g., Tripoli and Cotton, 1980; Cotton et al., 1982) is that the slope of the hydrometeor size distributions (i.e., Λ_R^{-1}, Λ_S^{-1}, and Λ_H^{-1}) remain constant and the intercepts (i.e., N_{OR}, N_{OS}, and N_{OH}) vary with water content. On the other hand, the approach assumed by the South Dakota School of Mines (e.g., Orville and Kopp, 1977; Lin et al., 1983) is that the intercepts remain constant and the slopes vary with water content. The parameterizations assumed in the TASS model follow the latter

approach, and thus differ from those used by the CSU group. It is felt that the approach developed by the North Dakota School of Mines Group is more simple and better substantiated by observations. Also included in the microphysics of the TASS model is an autoconversion of rainwater formulation developed by Berry and Reinhardt (1974b). This formulation, which was developed from data produced by a detailed stochastic growth model, has a threshold which is dependent upon both the total number of cloud droplets per unit volume and the dispersion of the droplet spectrum. In continental areas the autoconversion of rainwater may be completely suppressed, as is frequently observed.

The formulation of the TASS model is applicable to a wide range of meso-gamma scale and microscale phenomena. The TASS model has been applied to experiments ranging from the simulation of simple convective clouds to intense firestorms. Model verification, a comparison of TASS simulated results with detailed observed data sets, is to be given in a following report. One case study has been previously described in Proctor (1985c). In this study, a supercell hailstorm which passed through a meteorological data observing network is modeled. The quasi-steady structure of the storm was simulated throughout $4\frac{1}{2}$ hours of simulation time, and many of the observed features of the storm were successfully simulated.

REFERENCES

Arakawa, A., 1966: Computational design for long-term numerical integration of the equations of fluid motion: Two-dimensional incompressible flow, Part I. J. Comp. Phys., 1, 119-143.

Asai, T., 1965: A numerical study of the air-mass transformation over the Japan Sea in winter, J. Meteor. Soc. Japan, 43, 1-15.

Battan, L. J., 1973: Radar Observation of the Atmosphere, University of Chicago Press, 324 pp.

Berry, E. X., 1968: Modification of the warm rain process. Preprints First. Natl. Conf. Weather Modification, Albany, N. Y., Amer. Meteor. Soc., 81-88.

Berry, E. X., and R. L. Reinhardt, 1974a: An analysis of cloud drop growth by collection: Part I. Double distributions, J. Atmos. Sci., 31, 1814-1824.

Berry, E. X., and R. L. Reinhardt, 1974b: An analysis of cloud drop growth by collection: Part II. Single initial distributions, J. Atmos. Sci., 31, 1825-1831.

Berry, F. A., Jr., E. Bollay, and N. R. Beers, 1945: Handbook of Meteorology, McGraw-Hill, 354.

Bigg, E. K., 1953: The supercooling of water, Proc. Phys. Soc. London, B66, 688-694.

Businger, J. A., J. C. Wyngaard, Y. Izumi, and E. F. Bradley, 1971: Flux-profile relationships in the atmospheric surface layer, J. Atmos. Sci., 28, 181-189.

Byers, H. R., 1965: Elements of Cloud Physics, The University of Chicago Press, Chicago, 191 pp.

Cannon, T. W., J. E. Dye and V. Toutenhoofd, 1974: The mechanism of precipitation formation in northeastern Colorado cumulus. Part II: Sailplane measurements, J. Atmos. Sci., 31, 2148-2151.

Cho, H. R. and T. L. Clark, 1981: A numerical investigation of the structure of vorticity fields associated with a deep convective cloud, Mon. Wea. Rev., 109, 1654-1670.

Chuang, S., F. H. Proctor, J. W. Zack and M. L. Kaplan, 1984: A numerical weather prediction system designed to simulate atmospheric downburst phenomena, AIAA 22nd Aerospace Science Meeting, AIAA-84-0352, Reno, Nevada, 15 pp.

Clark, R. A., J. H. Ferziger and W. C. Reynolds, 1977: Evaluation of subgrid-scale turbulence models using a fully simulated turbulent flow. Report No. TF-9 Thermosciences Division, Department of Mechanical Engineering, Stanford University, Stanford, California, 119 pp.

Clark, R. A., J. H. Ferziger and W. C. Reynolds, 1979: Evaluation of subgrid-scale models using an accurately simulated turbulent flow, J. Fluid Mech., 91, 1-16.

Clark, T. L., 1979: Numerical simulations with a three-dimensional cloud model: Lateral boundary condition experiments and multicellular severe storm simulations, J. Atmos. Sci., 36, 2191-2215.

Cotton, W. R., M. A. Stephens, T. Nehrkorn, and G. J. Tripoli, 1982: The Colorado State University three-dimensional cloud/mesoscale model - 1982. Part II: An ice phase parameterization, J. de Rech. Atmos., 16, 295-320.

Cotton, W. R., and G. J. Tripoli, 1978: Cumulus convection in shear flow -- three-dimensional numerical experiments, J. Atmos. Sci., 35, 1503-1521.

Das, P., 1969: The thermodynamic equation in cumulus dynamics, J. Atmos. Sci., 26, 399-407.

Deardorff, J. W., 1970: A numerical study of three-dimensional turbulent channel flow at large Reynolds numbers, J. Fluid Mech., 41, 453-480.

Deardorff, J. W., 1972: Numerical investigation of neutral and unstable planetary boundary layers, J. Atmos. Sci., 29, 91-115.

Deardorff, J. W., 1973: Three-dimensional numerical modeling of the planetary boundary layer, Workshop on Micrometeorology, D. A. Haugen (ed.), Amer. Meteor. Soc., Boston, 271-311.

Durran, D. R., and J. B. Klemp, 1983: A compressible model for the simulation of moist mountain waves, Mon. Wea. Rev., 111, 2341-2361.

Dye, J. E., C. A. Knight, V. Toutenhootd and T. W. Cannon, 1974: The mechanism of precipitation formation in northeastern Colorado cumulus, III. Coordinated microphysical and radar observations and summary, J. Atmos. Sci., 8, 2152-2159.

Federer, B., and A. Waldvogel, 1975: Hail and raindrop size distributions from a Swiss multicell storm, J. Appl. Meteor., 14, 91-97.

Fitzgerald, J. W., and P. A. Spyers-Duran, 1973: Changes in cloud nucleus concentration and cloud droplet size distribution associated with pollution from St. Louis, J. Appl. Meteor., 12, 511-516.

Foote, G. B., and P. S. du Toit, 1969: Terminal velocity of raindrops aloft, J. Appl. Meteor., 8, 249-253.

Gunn, K. L. S., and J. S. Marshall, 1958: The distribution with size of aggregate snowflakes, J. Meteor., 15, 452-461.

Gunn, R., and G. D. Kinzer, 1949: The terminal velocity of fall for water drops in stagnant air, J. Meteor., 6, 243-248.

Hall, W. D., and H. R. Pruppacher, 1976: The survival of ice particles falling from cirrus clouds in subsaturated air, J. Atmos. Sci., 33, 1995-2005.

Haltiner, G. J. and R. T. Williams, 1980: Numerical Prediction and Dynamic Meteorology, John Wiley & Sons, 477 pp.

Herring, J. R., 1979: Subgrid scale modeling--An introduction and overview, Turb. Shear Flows, 1, 347-352.

Hess, S. L., 1959: Introduction To Theoretical Meteorology, Holt, Rinehart and Winston, 51-58.

Heymsfield, A. J., 1982: A comparative study of the rates of development of potential graupel and hail embryos in High Plains storms, J. Atmos. Sci., 39, 2867-2897.

Hill, G. E., 1974: Factors controlling the size and spacing of cumulus clouds as revealed by numerical experiments, J. Atmos. Sci., 31, 646-673.

Houze, R. A., Jr., P. V. Hobbs, P. H. Herzegh and D. B. Parsons, 1979: Size distributions of precipitation particles in frontal clouds, J. Atmos. Sci., 36, 156-162.

Jiusto, J. E., and G. E. Bosworth, 1971: Fall velocity of snowflakes, J. Appl. Meteor., 10, 1352-1354.

Kaplan, M. L., J. W. Zack, V. C. Wong, and J. J. Tuccillo, 1982: Initial results from a Mesoscale Atmospheric Simulation System and comparison with the AVE-SESAME I data set, Mon. Wea. Rev., 110, 1564-1590.

Kessler, E., 1969: On the distribution and continuity of water substance in atmospheric circulations, Meteor. Monogr., No. 32, Amer. Meteor. Soc., 84 pp.

Kinzer, G. D., and R. Gunn, 1951: The evaporation, temperature, and thermal relaxation-time of freely falling waterdrops, J. Meteor., 8, 71-83.

Klemp, J. B., and R. B. Wilhelmson, 1978a: The simulation of three-dimensional convective storm dynamics, J. Atmos. Sci., 35, 1070-1096.

Klemp, J. B., and R. B. Wilhelmson, 1978b: Simulations of right- and left-moving storms produced through storm splitting, J. Atmos. Sci., 35, 1097-1110.

Knight, C. A., N. C. Knight, J. E. Dye, and V. Toutenhoofd, 1974: The mechanism of precipitation formation in northeastern Colorado cumulus: I. Observations of the precipitation itself, J. Atmos. Sci., 31, 2142-2147.

Knight, C. A., W. A. Cooper, D. W. Breed, I. R. Paluch, P. L. Smith, and G. Vali, 1982: Microphysics, Hailstorms of the Central High Plains, Vol. 1, National Hail Research Experiment, C. A. Knight and P. Squires, Eds., Colorado Associated University Press, Boulder, 151-193 (Chapter 7).

Kopp, F. J., H. D. Orville, R. D. Farley, and J. H. Hirsh, 1983: Numerical simulation of dry ice cloud seeding experiments, J. Climate Appl. Meteor., 22, 1542-1556.

Langmuir, I., 1948: The production of rain by a chain-reaction in cumulus clouds at temperatures above freezing, J. Meteor., 5, 175-192.

Latham, J., and C. P. R. Saunders, 1970: Experimental measurements of the collection efficiencies of ice crystals in electric fields, Quart. J. Roy. Meteor. Soc., 96, 257-265.

Lilly, D. K., 1962: On the numerical simulation of buoyant convection, Tellus, 14, 148-172.

Lilly, D. K., 1964: Numerical solutions for the shape-preserving two-dimensional thermal convection element, J. Atmos. Sci., 21, 83-98.

Lilly, D. K., 1965: On the computational stability of numerical solutions of time-dependent non-linear geophysical fluid dynamics problems, Mon. Wea. Rev., 93, 11-26.

Lin, Y-L., R. D. Farley, and H. D. Orville, 1983: Bulk parameterization of the snow field in a cloud model, J. Climate Appl. Meteor., 22, 1065-1092.

Lipps, F. B., 1977: A study of turbulence parameterization in a cloud model, J. Atmos. Sci., 34, 1751-1772.

Liu, J. Y., and H. D. Orville, 1969: Numerical modeling of precipitation and cloud shadow effects on mountain-induced cumuli, J. Atmos. Sci., 26, 1283-1298.

Locatelli, J. D., and P. V. Hobbs, 1974: Fall speeds and masses of solid precipitation particles, J. Geophys. Res., 79, 2185-2197.

Lord, S. J., H. E. Willoughby, and M. M. Piotrowicz, 1984: Role of a parameterized ice-phase microphysics in an axisymmetric, nonhydrostatic tropical cyclone model, J. Atmos. Sci., 41, 2836-2848.

Love, M. D., and D. C. Leslie, 1977: Studies of subgrid modeling with classical closures and Burger's equation, Symp. on Turbulent Shear Flows, Pennsylvania State University, 14.1-14.10.

Macklin, W. C., and F. H. Ludlam, 1961: The fallspeeds of hailstones, Quart. J. Roy. Meteor. Soc., 87, 72-81.

Marshall, J. S., and W. M. Palmer, 1948: The distribution of raindrops with size, J. Meteor., 5, 165-166.

Mason, B. J., 1971: The Physics of Clouds, 2nd ed., Oxford University Press, 671 pp.

Mason, B. J., and A. D. Thorpe, 1966: The evaporation of ice spheres and ice crystals, Brit. J. Appl. Phys., 17, 541-548.

McDonald, J. E., 1960: An aid to computation of terminal fall velocities of spheres, J. Meteor., 17, 463-465.

Mesinger, F., and A. Arakawa, 1976: Numerical Methods Used in Atmospheric Models, 1, GARP Publication Series No. 17, World Meteor. Organization, 64 pp.

Miller, M. J., 1978: The Hampstead storm: A numerical simulation of a quasi-stationary cumulonimbus system, Quart. J. Roy. Meteor. Soc., 104, 413-427.

Miller, M. J., and R. Pearce, 1974: A three-dimensional primitive equation model of cumulonimbus convection, Quart. J. Roy. Meteor. Soc., 100, 133-154.

Musil, D. J., 1970: Computer modeling of hailstone growth in feeder clouds, J. Atmos. Sci., 27, 474-482.

Ochs, H. T. III, 1975: Modeling of cumulus initiation in METROMEX, J. Appl. Meteor., 14, 873-882.

Ogura, Y., and T. Takahashi, 1971: Numerical simulation of the life cycle of a thunderstorm cell, Mon. Wea. Rev., 99, 895-911.

Orlanski, I., 1976: A simple boundary condition for unbounded hyperbolic flows, J. Comp. Phys., 21, 251-269.

Orville, H. D., and F. J. Kopp, 1977: Numerical simulation of the history of a hailstorm, J. Atmos. Sci., 34, 1596-1618.

Pastushkov, R. S., 1975: The effects of vertical wind shear on the evolution of convective clouds, Quart. J. Roy. Meteor. Soc., 101, 281-291.

Perkey, D. J., and C. W. Kreitzberg, 1976: A time-dependent lateral boundary scheme for limited-area primitive equation models, Mon. Wea. Rev., 104, 744-755.

Pitter, R. L., 1977: A reexamination of riming on thin ice plates, J. Atmos. Sci., 34, 684-685.

Price, P. E., 1985: Microphysical model comparisons of seeded and non-seeded North Dakota clouds, M.S. Thesis, Dept. of Meteor., SD School of Mines and Technology, Rapid City, SD, 70 pp.

Price, P. E., R. D. Farley, J. H. Hirsch, and H. D. Orville, 1986: Microphysical model comparisons of seeded and non-seeded North Dakota clouds, Preprints, Tenth Conf. on Wea. Modification, Arlington, VA, Amer. Meteor. Soc., 159-164.

Proctor, F. H., 1982: A numerical study on the evolution of tornadoes, PhD dissertation, Texas A & M University, College Station, 267 pp. (Available from University Microfilms Internationa, Ann Arbor Michigan, No. 83-09-693).

Proctor, F. H., 1983: Numerical simulation of a bell-shaped cumulonimbus, Preprints, 13th Conf. on Severe Local Storms, Tulsa, Oklahoma, Amer. Meteor. Soc., 235-240.

Proctor, F. H., 1985a: Application of radiative boundary conditions to nonhydrostatic primitive equation models, Seventh Conf. on Numerical Wea. Pred., Montreal, Canada, Amer. Meteor. Soc., 291-298.

Proctor, F. H., 1985b: Numerical simulation of precipitation induced downbursts, Second Int. Conf. on the Aviation Weather System, Montreal, Canada, Amer. Meteor. Soc., 257-264.

Proctor, F. H., 1985c: Three-dimensional simulation of the 2 August CCOPE hailstorm with the Terminal Area Simulation System, Int. Cloud Modelling Workshop/Conf., Irsee, FRG, World Meteor. Soc., 14 pp.

Pruppacher, H. R., and J. D. Klett, 1978, Microphysics of Clouds and Precipitation, D. Reidel, 714 pp.

Ranz, W. E., and W. R. Marshall, 1952: Evaporation from drops. Part II, Chem. Engng. Prog., 48, 173-180.

Rogers, R. R., 1976: A Short Course in Cloud Physics, Pergamon Press, 227 pp.

Rutledge, S. A., and P. V. Hobbs, 1983: The mesoscale and microscale structure and organization of clouds and precipitation in midlatitude cyclones. VIII: A model for the "seederfeeder" process in warm-frontal rainbands, J. Atmos. Sci., 40, 1185-1206.

Rutledge, S. A., and P. V. Hobbs, 1984: The mesoscale and microscale structure and organization of clouds and precipitation in midlatitude cyclones. XII: A diagnostic modelling study of precipitation development in narrow cold-frontal rainbands, J. Atmos. Sci., 41, 2949-2972.

Schlesinger, R. E., 1975: A three-dimensional numerical model of an isolated deep convective cloud: Preliminary results, J. Atmos. Sci., 32, 934-957.

Schlesinger, R. E., 1978: A three-dimensional numerical model of an isolated thunderstorm. Part I: Comparative experiments for variable ambient wind shear, J. Atmos. Sci., 35, 690-713.

Schlesinger, R. E., 1982: Effects of mesoscale lifting, precipitation and boundary layer shear on severe storm dynamics in a three-dimensional numerical modeling study, Preprints 12th Conf. on Severe Local Storms, San Antonio, Amer. Meteor. Soc., 536-541.

Schlesinger, R. E., 1984a: Mature thunderstorm cloud-top structure and dynamics: A three-dimensional numerical simulation study, J. Atmos. Sci., 41, 1551-1570.

Schlesinger, R. E., 1984b: Effects of the pressure perturbation field in numerical models of unidirectionally sheared thunderstorm convection: Two versus three dimensions, J. Atmos. Sci., 41, 1571-1587.

Schultz, P., 1979: Estimation of surface stress from wind, Boundary-Layer Meteor., 17, 265-267.

Sekhon, R. S., and R. C. Srivastava, 1970: Snow size spectra and radar reflectivity, J. Atmos. Sci., 27, 299-307.

Shuman, F. G., 1962: Numerical experiments with the primitive equations, Proc. Int. Symp. on Numerical Weather Prediction, Tokyo, Meteor. Soc. of Japan, 85-107.

Simpson, J., and V. Wiggert, 1969: Models of precipitating cumulus towers, Mon. Wea. Rev., 97, 471-489.

Smith, P. L., Jr., C. G. Myers, and H. D. Orville, 1975: Radar reflectivity factor calculations in numerical cloud models using bulk parameterization of precipitation, J. Appl. Meteor., 14, 1156-1165.

Smolarkiewicz, P. K., and T. L. Clark, 1985: Numerical simulation of the evolution of a three-dimensional field of cumulus clouds. Part I: Model description, comparison with observations and sensitivity studies, J. Atmos. Sci., 42, 502-522.

Sommeria, G., 1976: Three-dimensional simulation of turbulent processes in an undisturbed trade wind boundary layer, J. Atmos. Sci., 33, 216-241.

Steiner, J. T., 1973: A three-dimensional model of cumulus cloud development, J. Atmos. Sci., 30, 414-435.

Tripoli, G. J., and W. R. Cotton, 1980: A numerical investigation of several factors contributing to the observed variable intensity of deep convection over South Florida, J. Appl. Meteor., 19, 1037-1063.

Tripoli, G. J., and W. R. Cotton, 1982: Colorado State University three-dimensional cloud/mesoscale model, 1982: Pt. 1, General theoretical framework and sensitivity experiments, J. de Rech. Atmos., 16, 185-219.

Vittori, O., and G. di Caporiacco, 1959: The density of hailstones, Nubila, 2, 51-57.

Wexler, A., 1976: Vapor pressure formulation for water in the range 0^{o} to 100^{o}C -- A Revision, J. Res. Natl. Bur. Stand., 80A, p. 775 ff.

Wexler, A., 1977: Vapor pressure formulation for ice, J. Res. Natl. Bur. Stand., 81A, 5-20.

Wilhelmson, R. B., 1977: On the thermodynamic equation for deep convection, Mon. Wea. Rev., 105, 545-547.

Wilhelmson, R. B., and C. S. Chen, 1982: A simulation of the development of successive cells along a cold outflow boundary, J. Atmos. Sci., 39, 1466-1483.

Willoughby, H. E., H.-L. Jin, s. J. Lord, and J. M. Piotrowicz, 1984: Hurricane structure and evolution as simulated by an axisymmetric, nonhydrostatic numerical model, J. Atmos. Sci., 41, 1169-1186.

APPENDIX A

List of Symbols

A_1^*, A_2^*, A_3^*	Thermodynamic terms
a	Microphysical threshold parameter
B_1^*	Thermodynamic term
C	Capacitance of ice particles or wave phase speed
C_D	Drag coefficient for hailstones (= 0.45)
C_I	Specific heat of ice
C_p	Specific heat of air at constant pressure (1004.6 J kg^{-1} k^{-1})
C_v	Specific heat of air at constant volume (717.57 J kg^{-1} k^{-1})
C_w	Specific heat of water
C_1	Constant in grid stretching function
C_2	Constant in grid stretching function
D_{IC}	Diameter of hexagonal plate-like ice crystal
D_H	Hailstone diameter
D_o	Critical snow diameter in hail conversion process (5 x 10^{-3} m)
D_R	Raindrop diameter
D_S	Snow-particle diameter
D_w	Diffusivity of water vapor in air
$\overline{D}_G$	Mean mass-weighted graupel particle diameter
$\overline{D}_H$	Mean mass-weighted hailstone diameter
$\overline{D}_{IC}$	Mean diameter of ice crystal
DEF	Rate of deformation
E_{HIC}	Collection efficiency of hail for ice crystals
E_{HR}	Collection efficiency of hail for rain (=1)
E_{HS}	Collection efficiency of hail for snow

E_{ICCD}	Collection efficiency of ice crystals for cloud droplets
E_{RIC}	Collection efficiency of rain for ice crystals (=1)
E_{RS}	Collection efficiency of rain for snow (=1)
E_{SCD}	Collection efficiency of snow for cloud droplets
E_{SIC}	Collection efficiency of snow for ice crystals
$\overline{E}_{RCD}$	Mean collection efficiency of rain for cloud droplets
e_i	Vapor pressure for ice
e_{si}	Saturation vapor pressure for ice
e_{sio}	Saturation vapor pressure for ice at temperature of reference environment
e_{sv}	Saturation vapor pressure for liquid water
e_{svo}	Saturation vapor pressure for liquid water at temperature of reference environment
e_v	Saturation vapor pressure for liquid water
F	Initial velocity impulse function
F_H	Ventilation factor for hail
F_I	Ventilation factor for ice particles
F_R	Ventilation factor for rain
F_S	Ventilation factor for snow
f, f_1	Coriolis terms
G	Mapping factor for vertical grid stretching
G_F	Function in Bigg's freezing equation
G_H	Universal wind shear function for heat
G_M	Universal wind shear function for momentum
g	The acceleration due to gravity (9.8 m s^{-2})
H	Density ratio term
H_w	Depth of initial velocity impulse
h	Height of lowest level of grid points above ground ($\Delta z/2$)

K_M	Subgrid eddy viscosity for momentum
K_{MAX}	Critical subgrid eddy viscosity for numerical linear stability
K_s	Stokes number
K_T	Subgrid eddy viscosity for heat and moisture substances
$\overline{K}_s$	Mean Stokes number
$\|K_I\|^2$	Dielectric factor for ice (0.21)
$\|K_w\|^2$	Dielectric factor for water (0.93)
$\langle K_M \rangle$	Mean eddy viscosity within surface layer
k	Von Karman constant (0.4)
k_T	Thermal conductivity of air
L	Monin-Obukhov length
L_f	Latent heat of fusion for water
L_s	Latent heat of sublimation for water
L_v	Latent heat of vaporization for water
L_2	Parameter in autoconversion formula
M	Mass
M_s	Mass of snow per mass of dry air
$\overline{M}_{CD}$	Average mass of cloud droplet
m	Number of small time steps per large time step
N	Time level for large time step
$N(D_H)$	Number of hail particles per unit diameter D_H per unit volume
$N(D_R)$	Number of raindrops per unit diameter D_R per unit volume
$N(D_S)$	Number of snow particles per unit diameter D_S per unit volume
NL	Number of vertical grid levels above the ground
N_{OH}	Intercept value in hail size distribution
N_{OR}	Intercept value in raindrop size distribution (2.5×10^7 m^{-4})
N_{OS}	Intercept value in snow particle size distribution

n	Time level for small time step
n_{CD}	Number concentration of cloud droplets
n_{IC}	Number concentration of ice crystals
P	Atmospheric pressure
PCDWV1	Production of cloud droplet water due to condensation
PICCD1	Production of ice crystal water due to riming
PICCD2	Melting of ice crystal water into cloud droplet water
PICCD3	Production of ice crystal water due to freezing of cloud droplets
PICWV1	Rate of ice crystal initiation
PICWV2	Production of ice crystal water due to deposition
PF	Probability of spontaneous drop freezing
PHCD1	Production of hail due to the accretion of cloud droplet water
PHIC1	Production of hail from ice crystal water due to rain collecting ice crystals
PHIC2	Production of hail due to collection of ice crystal water
PHR1	Production of hail due to the spontaneous freezing of raindrops
PHR2	Production of hail from rainwater due to rain collecting ice crystals
PHR3	Production of hail due to accretion of rainwater
PHR4	Melting of hail into rainwater
PHR5	Rate at which accreted water is shed as rain during hail wet growth
PHS1	Production of hail due to rain collecting snow
PHS2	Production of hail due to rain collecting snow
PHS3	Autoconversion of snow into hail due to riming
PHS4	Production of hail due to collection of snow
PHWV1	Production of hail due to deposition
PRCD1	Autoconversion of cloud droplet water into rain

PRCD2	Production of rain due to collection of cloud droplets
PRCD3	Production of rain due to collection of cloud droplets by melting snow
PRWV1	Evaporation of rainwater
PRWV2	Production of rain due to condensation on melting snow
PRWV3	Production of rain due to condensation on wet hail
PSCD1	Production of snow due to accretion of cloud droplet water
PSIC1	Conversion of ice crystal water into snow
PSIC2	Production of snow due to collection of ice crystal water
PSIC3	Autoconversion of ice crystal water into snow
PSIC4	Production of snow from ice crystal water due to rain collecting ice crystals
PSR1	Production of snow due to collection of rainwater
PSR2	Melting of snow into rainwater
PSR3	Production of snow due to the spontaneous freezing of rainwater
PSR4	Production of snow from rain due to rain collecting ice crystals
PSWV1	Production of snow due to deposition
PWET	Maximum rate at which hail water can be produced from accreted liquid water (used in wet growth calculation)
PWVG	Rate at which moisture is evaporated from wet ground
P1	Depositional growth of ice crystals
P2	Collection of cloud droplets by snow
P3	Collection of rain by snow
P4	Depositional growth of snow
P5	Condensation on wet snow
P6	Accretion of liquid water by melting snow
P7	Spontaneous freezing of raindrops
P8	Collection of ice crystals by raindrops

P9	Collection of raindrops by ice crystals
P10	Rate of hail melting
P11	Condensation on wet hail
P12	Production of liquid water available for shedding
P_o	Pressure of reference environment
P_{oo}	Constant in Poisson's equation (10^5 pascals)
p	Pressure deviation from reference environment
Q	Dummy variable
Q_{CD}	Mixing ratio of cloud droplet water
Q_H	Mixing ratio of hail water
Q_{IC}	Mixing ratio of ice crystal water
Q_R	Mixing ratio of rain water
Q_{SN}	Mixing ratio of snow water
Q_T	Sum of mixing ratios of hydrometeor water (e.g., rain, snow, hail, cloud droplets, ice crystals)
Q_{b-1}	The value of Q at its first interior grid point from boundary
Q_{si}	Saturation mixing ratio with respect to ice
Q_{sio}	Saturation mixing ratio with respect to ice of reference environment
Q_{ssv}	Saturation mixing ratio with respect to liquid water on surface of ice particle
Q_{sv}	Saturation mixing ratio with respect to liquid water
Q_{svo}	Saturation mixing ratio with respect to liquid water of reference environment
Q_v	Water vapor mixing ratio
Q_{vo}	Water vapor mixing ratio of reference environment
q	Dummy variable
R	Gas contant for dry air (287.04 J kg^{-1} K^{-1})
R_e	Reynolds number

R_f	Richardson flux number
R_i	Richardson number
R_v	Gas constant for water vapor (461.5 J kg^{-1} K^{-1})
R_w	Radius of initial velocity impulse
R_θ	Radius of initial thermal impulse
r	Space coordinate normal to boundary
r'	Droplet radius parameter
$\hat{r}$	Radial distance from center of initial impulse
S(q)	Subgrid eddy flux of q
S_{CD}	Source term in prognostic equation for cloud droplet water
S_{IC}	Source term in prognostic equation for ice crystal water
S_H	Source term in prognostic equation for hail water
S_M	Schmidt number
S_R	Source term in prognostic equation for rainwater
S_S	Source term in prognostic equation for snow water
S_f	Production of ice from liquid water
S_s	Production of ice from water vapor
S_v	Production of liquid water from water vapor
S_{vap}	Source term in prognostic equation for water vapor
T	Atmospheric temperature
T_M	Melting temperature (273.16 K)
T_o	Temperature in reference environment
T_2	Time parameter in autoconversion formula
t	Time
U_G	Component of grid translation in x direction
U_o	Westward wind component in reference environment
u	Westward wind component

u'	$= u - U_o$
V	Horizontal wind component
V_G	Component of grid translation in y direction
V_o	Southward wind component in reference environment
v	Southward wind component
v'	$= v - V_o$
W_B	Weighting coefficient for sponge boundary
W_H	Terminal velocity of hailstones
W_{MAX}	Maximum updraft speed of initial velocity impulse
W_R	Terminal velocity of raindrops
W_S	Terminal velocity of snow particles
$\overline{W}_H$	Mean mass-weighted terminal velocity for hailstones
$\overline{W}_R$	Mean mass-weighted terminal velocity for raindrops
$\|W\|$	Maximum magnitude of vertical component of either air velocity or mean hydrometeor velocity
w	Vertical component of velocity
x	West-east coordinate
x_o	Reference point for initial perturbation
y	South-north coordinate
y_o	Reference point for initial perturbation
Z_{HDRY}	Radar reflectivity factor for dry hail
Z_{HWET}	Radar reflectivity factor for wet hail
Z_R	Radar reflectivity factor for rain
Z_{SDRY}	Radar reflectivity factor for dry snow
Z_{SWET}	Radar reflectivity factor for melting snow
Z_θ	Depth of thermal impulse
z	Vertical coordinate
z_o	Aerodynamic roughness height

z'	Stretched vertical coordinate
α	Constant in subgrid-turbulence formulation (0.35)
α_1	Constant in Bigg's freezing equation (10^{-2} m^3 s^{-1})
α_2	Constant in Bigg's freezing equation (0.66 K^{-1})
$\Gamma(4.8)$	17.83786198....
β_{IC}	Constant in Fletcher's equation (10^{-2} m^{-3})
Δ	Subgrid turbulence length scale
ΔT	Maximum value of initial temperature impulse
ΔV	Difference between fall velocities of cloud droplets and ice crystals (0.4 ms^{-1})
Δt	Large time step
Δt_N	Large time step at level N
Δt_L	Large time step
Δt_s	Small time step
Δt_L^*	Critical large time step for linear stability
Δt_s^*	Critical small time step for linear stability
Δx	Grid increment in x direction
Δy	Grid increment in y direction
Δz	Vertical grid increment
$\Delta z'$	Constant vertical grid increment in z' space
δ_H	Density of hail (900 kg m^{-3})
δ_S	Density of snow (100 kg m^{-3})
δ_w	Density of water (10^3 kg m^{-3})
ε	Ratio of gas constants (R/R_v = 0.62197...)
ζ	Ratio of z/L or vertical component of vorticity
η	Ratio of specific heats (C_p/C_v = 1.4)
θ	Potential temperature
θ_o	Potential temperature of reference environment

θ'	Deviation of potential temperature from environment
κ	R/C_p (0.28571...)
Λ_H	Inverse slope of hailstone size distribution
Λ_R	Inverse slope of raindrop size distribution
λ_s	Amount of vapor available for deposition
λ_v	Amount of vapor available for condensation
Λ_S	Inverse slope of snow particle size distribution
μ_D	Dynamic viscosity of air
ν	Numerical viscosity
ν_m	Molecular viscosity of air
π	PI (3.1415926...)
ρ	Density of (wet) air
ρ'	Deviation of air density from the environment
ρ_{CD}	Partial density of cloud droplet water
ρ_{IC}	Partial density of ice crystal water
ρ_H	Partial density of hail water
ρ_R	Partial density of rain water
ρ_S	Partial density of snow water
ρ_d	Density of dry air
ρ_{do}	Density of dry air in the environment
ρ_o	Density of (moist) air in the environment
ρ_v	Partial density of water vapor
ρ_{vo}	Partial density of water vapor in the environment
ρ_{vs}	Partial density of water vapor at saturation with respect to liquid water
σ	Dispersion coefficient for cloud-droplet spectrum
τ	Turbulence stress or parameter in grid tracking algorithm
Φ	Three-dimensional mass divergence

Φ_H	The nondimensional temperature gradient in the surface layer
Φ_M	The nondimensional wind shear in the surface layer
ϕ	Operator in Adams-Bashforth time difference approximation
ϕ_ℓ	Latitude
ψ_H	Universal function for heat in surface layer parameterization
ψ_M	Universal function for momentum in surface layer
Ω	Angular velocity of Earth's rotation (7.292×10^{-5} s^{-1})

APPENDIX B

Derivation of Equation of State and Equation for Pressure

Given a volume of air, τ, in which the precipitation contained by the volume is falling at its terminal velocity, the total mass in τ is

$$M = M_d + M_v + M_w, \tag{B-1}$$

where M_d is the mass of the dry air in τ, M_v is the mass of the water vapor, and M_w is the mass of the liquid and frozen water in τ. [For precipitation falling at its terminal velocity, the drag force exerted by the precipitation is in exact balance with its gravitational force; thus the precipitation imparts its mass to the air.]

Dividing (B-1) by the volume of τ gives

$$\rho = \rho_d + \rho_v + \rho_w, \tag{B-2}$$

where ρ_d is the density of dry air, ρ_v is the partial density of water vapor, and ρ_w is the partial density of the liquid and frozen water, and ρ is the effective air density; i.e., $\rho_d = M_d/\tau$, $\rho_v = M_v/\tau$, and $\rho_w = M_w/\tau$. Eq. (B-2) can be rewritten as

$$\rho = P_d\,[1 + Q_v + Q_w]/RT, \text{ or}$$
$$\rho = (P - e_v)\,[1 + Q_v + Q_w]/RT \tag{B-3}$$

where $Q_v \equiv \rho_v/\rho_d$, $Q_w = \rho_w/\rho_d$, P is atmospheric pressure, e_v is vapor pressure, R is the gas constant for dry air, and T is temperature. Since in atmospheric problems

$$e_v \approx Q_v \, P/\varepsilon,$$

where ε is the ratio of gas constants for dry air and water vapor, Eq. (B-3) becomes

$$\rho = \frac{P}{RT} [1 - 0.608 \, Q_v + Q_w], \tag{B-4}$$

which is the equation of state modified for the effects of water substance.

The elastic mass continuity equation expressed in cartesian tensors is

$$\frac{d\rho}{dt} + \rho \frac{\partial u_i}{\partial x_i} = 0. \tag{B-5}$$

Taking d/dt of (B-4) and substituting into (B-5) gives

$$\frac{dP}{dt} = \frac{P}{T} \frac{dT}{dt} - \frac{P}{G} \frac{dG}{dt} - P \frac{\partial u_i}{\partial x_i}, \tag{B-6}$$

where $G \equiv 1 + 0.608 \, Q_v + Q_w$.

Taking the log-derivative of Poisson's equation as

$$\frac{1}{T} \frac{dT}{dt} = \frac{1}{\theta} \frac{d\theta}{dt} + \frac{R}{C_p} \frac{1}{P} \frac{dP}{dt},$$

where θ is the potential temperature and C_p the gas constant for air at

constant pressure. Substituting the above equation into (B-6) and rearranging terms gives

$$\frac{1}{\eta}\frac{dP}{dt} = - P \frac{\partial u_i}{\partial x_i} + \frac{P}{\theta}\frac{d\theta}{dt} - \frac{P}{G}\frac{dG}{dt} , \qquad \text{(B-7)}$$

where $\eta = 1 - \frac{R}{C_p} = C_v/C_p$.

If we assume $P(x,y,z,t) = P_o(z) + p(x,y,z,t)$, where $\partial P_o/\partial z = - \rho_o g$, then (B-7) can be expressed as,

$$\frac{\partial p}{\partial t} = - u_i \frac{\partial p}{\partial x_i} + u_i \rho_o g \delta_{i3} = \eta P \frac{\partial u_i}{\partial x_i} + \eta \frac{P}{\theta}\frac{d\theta}{dt} - \eta \frac{P}{G}\frac{dG}{dt} , \qquad \text{(B-8)}$$

where

$$\frac{\eta P}{G}\frac{dG}{dt} = \eta P \left[0.608 \frac{dQ_v}{dt} + \frac{dQ_w}{dt} \right] / (1 + 0.608\, Q_v + Q_w),$$

or since Q_v and Q_w are much less than one,

$$\frac{\eta P}{G}\frac{dG}{dt} \cong \eta P \left[0.608 \frac{dQ_v}{dt} + \frac{dQ_v}{dt}\right] (1 - 0.608\, Q_v - Q_w).$$

APPENDIX C

Constant Stress Layer Approximations for Unsaturated Atmosphere

The wind shear and temperature gradient in the constant stress layer (e.g., Haltiner and Martin, 1980) are respectively

$$\frac{\partial V}{\partial z} = \frac{V_*}{kz}\,\phi_M, \qquad \text{(C-1)}$$

$$\frac{\partial \theta}{\partial z} = \frac{T_*}{kz}\,\phi_H, \qquad \text{(C-2)}$$

where V is the horizontal wind speed $[V = (u^2 + v^2)^{0.5}]$, V_* is the frictional velocity, T_* is the nondimensional temperature, θ is potential temperature, k is von Karman's constant, ϕ_M is the nondimensional wind shear, and ϕ_H is the nondimensional temperature gradient. Both ϕ_M and ϕ_H are a function of z/L where L is the Monin-Obukhov length; both ϕ_M and ϕ_H are assumed to be universal from which the values can be determined from field data. Integration of (C-1) and (C-2) from the ground to height h (assuming that the surface roughness, z_o is much less than h) is

$$V = V_* G_M/k, \qquad \text{(C-3)}$$

and

$$\theta(h) - \theta(z=o) = T_* G_H/k, \qquad \text{(C-4)}$$

where

$$G_M \equiv \ell n\ (h/z_o) - \psi_M\ (\tfrac{h}{L}); \tag{C-5}$$

$$\psi_M \equiv \int_{z_o/L}^{h/L} [1 - \phi_M(\zeta)]\, d\ell n\ \zeta, \quad \zeta \equiv h/L;$$

$$G_H \equiv 0.74\ [\ell n\ (h/z_o) - \psi_H\ (\tfrac{h}{L})]; \tag{C-6}$$

$$\psi_H \equiv \int_{z_o/L}^{h/L} [1 - \phi_H\ (\zeta)]\ d\ell n\ \zeta, \ \zeta \equiv h/L.$$

From (C-1) the mean wind shear in the constant stress layer (assuming $z_o \ll h$) is

$$\left\langle \frac{\partial V}{\partial z} \right\rangle = \frac{\int_{z_o}^{h} V_* \phi_M/kz\ dz}{\int_{z_o}^{h} dz} = V_*\ G_M/hk. \tag{C-7}$$

With the aid of (C-3) the above result reduces to

$$\left\langle \frac{\partial V}{\partial z} \right\rangle = V\ (h)/h. \tag{C-8}$$

Similarly, by integrating (C-2), the mean temperature gradient is

$$\left\langle \frac{\partial \theta}{\partial z} \right\rangle = \frac{\int_{z_o}^{h} T_* \phi_H/kz\ dz}{\int_{z_o}^{h} dz} = \frac{T_* G_H}{kh}\ . \tag{C-9}$$

Since,

$$T_* = \overline{T}_v\ V_*^{\,2}/g\ k\ L,$$

where $\overline{T}_v$ is the average virtual temperature, and g is the acceleration due to gravity; (C-9) with the aid of (C-3) can be expressed as

$$\left\langle \frac{\partial \theta}{\partial z} \right\rangle = \frac{\overline{T}_v \, V(h)^2}{g \, h^2} \frac{G_H}{G_M^2} \left(\frac{h}{L}\right). \qquad \text{(C-10)}$$

The stress due to the vertical wind shear in the surface layer is

$$\tau_z = K_M \frac{\partial V}{\partial z} ,$$

where K_M is the eddy viscosity for momentum. With the aid of (C-1), τ_z at $z = h$ can be expressed as

$$\tau_z = K_M(h) \, V_* \, \phi_m\left(\frac{h}{L}\right)/kh. \qquad \text{(C-11)}$$

Since τ_z is independent of height in the surface stress layer, the mean stress-layer eddy viscosity, $\langle K_M \rangle$, can be defined such that

$$\tau_z = \langle K_M \rangle \left\langle \frac{\partial V}{\partial z} \right\rangle ;$$

thus from (C-7) and (C-11),

$$\langle K_M \rangle = \tau_z \, / \left\langle \frac{\partial V}{\partial z} \right\rangle = K_M(h) \, \phi_M / G_M . \qquad \text{(C-12)}$$

APPENDIX D

Formulation of the Microphysical Adjustment Scheme

The development for several formulas which are used in microphysical adjustment processes are below. Most of the derivation for the condensation adjustment is excerpted from Proctor (1982).

The methodology for condensation and evaporation follows Asai (1965). The condensation adjustment scheme maintains saturation by either the condensation of water vapor into cloud droplets, or by the evaporation of cloud droplets. However, if during evaporation there is an insufficient quanity of cloud-droplet water to maintain saturation, then all of the available cloud droplet water is evaporated. The derivation for the condensation adjustment is as follows.

Assuming a pseudoadiabatic and isobaric process, the saturation mixing ratio Q_{vs}, is (e.g. Hess, 1959)

$$dQ_{sv} = L_v Q_{sv} dT/T^2 R_v. \qquad \text{(D-1)}$$

Since $d\theta/\theta = dT/T$ in an isobaric process, Eq. (D-1) may also be expressed as

$$dQ_{sv} = L_v Q_{sv} d\theta/R_v T\theta. \qquad \text{(D-2)}$$

Now if the saturation surplus is defined as

$$\Delta Q \equiv Q_v - Q_{vs} = \Delta Q_1 + \Delta Q_2, \qquad \text{(D-3)}$$

where, if the air is supersaturated ($\Delta Q > 0$), the amount of water vapor to be condensed is represented by ΔQ_1. The condensation of ΔQ_1 then releases latent heat which increases the air's capacity to store additional water vapor by ΔQ_2. For the case of cloud droplet water in the presence of subsaturated air $\Delta Q < 0$, the maximum amount of cloud droplet water that can be evaporated is ΔQ_1, which is less than ΔQ since the evaporation of ΔQ_1 reduces the air's temperature and capacity to store water. The warming (cooling) due to condensation (evaporation) is then

$$\Delta\theta_1 = L_v\theta\ \Delta Q_1/C_pT. \tag{D-4}$$

The increased (decreased) storage ΔQ_2, as a result of condensational warming (evaporative cooling) is obtained by combining (D-2), (D-3) and (D-4), hence giving

$$\Delta Q_2 = \frac{Q_{sv}L_v\Delta\theta_1}{R_vT\theta} = \frac{L_v^2Q_{sv}\Delta Q_1}{C_pR_vT^2}\ . \tag{D-5}$$

Since only a fraction r, of the saturation surplus (deficiency) can be used in the condensation (evaporation) process, we may define $\Delta Q_1 \equiv r\Delta Q$. Then by use of (D-5), we may solve for r as

$$r = \frac{\Delta Q_1}{\Delta Q} = \frac{\Delta Q_1}{\Delta Q_1 + \Delta Q_2} = \Delta Q_1[\Delta Q_1 + L_v^2\ \Delta Q_1\ Q_{sv}/C_pR_vT^2]^{-1},$$

or

$$r = [1 + L_v^2\ Q_{sv}/C_pR_vT^2]^{-1}\ . \tag{D-6}$$

Thus the amount of water vapor to be condensed or the maximum amount of cloud droplet water that can be evaporated, is given by

$$\lambda_v \equiv r\Delta Q. \tag{D-7}$$

A similar formulation follows for deposition and sublimation if saturation with respect to ice is maintained; i.e.,

$$dQ_{si} = L_s Q_{si} dT/T^2 R_v, \tag{D-8}$$

and

$$\lambda_s = (Q_v - Q_{si}) \left[1 + L_s^2 Q_{si}/C_p R_v T^2\right]^{-1}. \tag{D-9}$$

Several useful formulas that are derived from (D-1), and (D-8), which can be used to compute adjustments to the saturation mixing ratios are as follows:

1) the change in Q_{sv} due to ice deposition

$$dQ_{sv} = - L_v L_s Q_{sv} dQ_v/T^2 R_v C_p; \tag{D-10}$$

2) the change in Q_{sv} due to the production of frozen water Q_I, from liquid water

$$dQ_{sv} = L_v L_f Q_{sv} dQ_I/T^2 R_v C_p; \tag{D-11}$$

3) the change in Q_{si} due to deposition

$$dQ_{si} = - L_s^2 Q_{si} dQ_v / T^2 R_v C_p; \qquad \text{(D-12)}$$

and 4) the change in Q_{si} due to the production of frozen water Q_I, from liquid water

$$dQ_{si} = L_s L_f Q_{si} dQ_I / T^2 R_v C_p. \qquad \text{(D-13)}$$

APPENDIX E

Evaluation of Physical Constants

Many of the physical constants vary only slowly with temperature and pressure. So, in order to simplify the model computations and reduce run time, the physical constants are defined in terms of the temperature and pressure of the reference environment (T_o, P_o), rather than local values. The expressions below are very accurate empirical curve fits deduced from experimental data. All expressions below are defined in terms of the MKS unit system.

The latent heat for vaporization of water (Pruppacher and Klett, 1978) is

$$L_v(T_o) = 2.50078 \times 10^6 \, (273.16/T_o)^y,$$

where $y = 0.167 + 3.67 \times 10^{-4} \, T_o$.

The latent heat for fusion of water (Pruppacher and Klett, 1978) for $T_o \leq 273.16$ K is

$$L_f(T_o) = 3.3369 \times 10^5 + 2030.6 \, (T_o - 273.16) - 10.467 \, (T_o - 273.16)^2.$$

At elevations where $T_o > 273.16$ K, the value for the melting point of the latent heat of fusion is assumed; i.e.,

$$L_f = 3.3369 \times 10^5 \qquad \text{for } T_o > 273.16.$$

From the first law of thermodynamics (the conservation of energy) the

latent heat of sublimation for water is

$$L_s(T_o) = L_v(T_o) + L_f(T_o).$$

The specific heat of ice (Pruppacher and Klett, 1978) for $T_o \leq 273.16$ K is

$$C_I(T_o) = 2106.1 + 7.327\,(T_o - 273.16)$$

[Otherwise, for $T_o > 273.16$ K the specific heat of ice is assumed as: $C_I = 2106.1$.]

The specific heat of water (Pruppacher and Klett, 1978) is

$$C_w(T_o) = \begin{cases} 5400 & \text{for } T_o < 223.16, \\ 4217.8 + 0.3471\,(T_o - 273.16)^2 & \text{for } 273.16 \geq T_o > 223.16, \\ 4178 + 0.01298\,(T_o - 308.16)^2 + 1.591 \times 10^{-5}\,(T_o - 308.16)^4 & \text{for } T_o > 273.16. \end{cases}$$

The dynamic viscosity of air (List, 1971) is

$$\mu_D(T_o) = 1.8325 \times 10^{-5}\ \frac{416.16}{T_o + 120}\left(\frac{T_o}{296.16}\right)^{1.5}.$$

The molecular viscosity of air is simply

$$\nu_m(P_o, T_o) = \mu_D/\rho_o.$$

The diffusivity of water vapor in air (Hall and Pruppacher, 1976) is

$$D_w (P_o,T_o) = 2.11 \times 10^{-5}(101325/P_o) (T_o/273.16)^{1.94}.$$

The Schmidt number is defined as the ratio of molecular viscosity to the diffusivity of water vapor; i.e.,

$$S_M (P_o,T_o) = \nu_m/D_w.$$

The thermal conductivity (Wisner et al., 1972) is

$$k_T (T_o) = 1414 \mu_D.$$

Local values of the saturation vapor pressures are determined from functions of the saturation vapor pressure of the reference atmosphere. The saturation vapor pressure with respect to liquid water of the reference atmosphere (e_{svo}), and the saturation vapor pressure with respect to ice of the reference atmosphere (e_{sio}) (Wexler, 1976, 1977) are respectively

$$\begin{aligned} e_{svo}(T_o) = \exp[&- 2991.2729\, T_o^{-2} \\ &- 6017.0128\, T_o^{-1} + 18.87643854 \\ &- 0.028354721\, T_o + 0.17838301 \times 10^{-4}\, T_o^{2} \\ &- 0.84150417 \times 10^{-9}\, T_o^{3} + 0.44412543 \times 10^{-12}\, T_o^{4} \\ &+ 2.858487 \ln T_o], \end{aligned}$$

$$\begin{aligned} e_{sio}(T_o) = \exp[&- 5865.3696\, T_o^{-1} \\ &+ 22.241033 + 0.013749042\, T_o \\ &- 0.34031775 \times 10^{-4}\, T_o^{2} + 0.26967687 \times 10^{-7}\, T_o^{3} \\ &+ 0.6918651 \ln T_o]. \end{aligned}$$

APPENDIX F

Linear Stability Analysis of Numerical Scheme

Large time step

Any of the prognostic equations, excluding acoustical terms, may be linearized as

$$\frac{\partial q}{\partial t} = - u \frac{\partial q}{\partial x} - v \frac{\partial q}{\partial y} - w \frac{\partial q}{\partial z} + K \left[\frac{\partial^2 q}{\partial x^2} + \frac{\partial^2 q}{\partial y^2} + \frac{\partial^2 q}{\partial z^2}\right] \qquad \text{(F-1)}$$

where $q = q(x,y,z,t)$, and u,v,w, and K are constants. The stability analysis of the finite difference analogue of Eq. (F-1) can be found if we assume a general solution as

$$q(x,y,z,t) = Q(t) \exp[i(\ell x + my + kz)] \qquad \text{(F-2)}$$

where ℓ, m, and k represent wave numbers, and i is the square-root of minus one.

Following Mesinger and Arakawa (1976), the amplitude factor, λ, is defined such that

$$Q^{N+1} = \lambda Q^N \qquad \text{(F-3)}$$

where the superscript refers to the time level.

$$\text{The solution is } \begin{cases} \text{amplifying} \\ \text{neutral} \\ \text{decaying} \end{cases} \quad \text{if} \quad \begin{matrix} |\lambda| > 1 \\ |\lambda| = 1 \\ |\lambda| < 1 \end{matrix}$$

A numerical scheme is considered stable if $|\lambda| \leq 1$.

Approximating space derivatives in Eq. (F-1) by second-order central differences and the time derivative by the Adams-Bashforth method; and then substituting (F-2) gives,

$$\lambda^2 = \lambda[1 + 1.5\ (i\xi - \mu)] + 0.5\ (i\xi - \mu), \qquad \text{(F-4)}$$

where

$$\xi \equiv \Delta t_L(|u|/\Delta x + |v|/\Delta y + |w|/\Delta z),$$

assuming a critical wavelength for advection of $4\Delta x$; and

$$\mu \equiv 4\Delta t_L K\ (\Delta x^{-2} + \Delta y^{-2} + \Delta z^{-2}),$$

assuming a critical wavelength for diffusion of $2\Delta x$. Solutions for the physical mode, λ_1, and the computational mode, λ_2, can be obtained from (F-4) by using a Taylor-series expansion. The physical mode is

$$|\lambda_1| = 1 + \xi^4/4 + \xi^6/2 - \mu - 5\xi^2\mu/4 + \mu^2/2 + \ldots.\text{H.O.T.} \qquad \text{(F-5)}$$

As $\mu \to 0$ (advection only) the numerical scheme has a weak instability of order $\xi^4/4$. As $\xi \to 0$ (diffusion only) the numerical scheme is conditionally stable if $\mu \leq 1$.

In order to counter the slight instability of advection, which is maximum for $4\Delta x$ waves, a numerical diffusion coefficient, ν, is defined such that $|\lambda_1| \tilde{\leq} 1$. Assuming a wavelength of $4\Delta x$ for <u>both</u> advection and diffusion, then

$$1 \leq |\lambda_1| = 1 + \xi^4/4 - \mu/2 + \ldots.H.O.T.,$$

and solving for μ,

$$\mu = \xi^4/2 + \ldots.H.O.T. .$$

Thus,

$$4\Delta t_L \nu \ (\Delta x^{-2} + \Delta y^{-2} + \Delta z^{-2}) \simeq 0.5 \ [\Delta t_L(|u|/\Delta x + |v|/\Delta y + |w|/\Delta z)]^4,$$

or

$$\nu = \Delta t_L^3 \ [|u|/\Delta x + |v|/\Delta y + |w|/\Delta z)]^4/[8(\Delta x^{-2} + \Delta y^{-2} + \Delta z^{-2})]. \quad (F-6)$$

Hence, by defining a numerical diffusion coefficient according to (F-6) and setting the following criteria:

$$\Delta t_L \leq = 0.5 \ [|u|/\Delta x + |v|/\Delta y + |w|/\Delta z]^{-1},$$

and

$$K_{MAX} = [4\Delta t_L \ (\Delta x^{-2} + \Delta y^{-2} + \Delta z^{-2})];$$

then the linear stability of the numerical system is enforced over the large time step.

Small time step

Numerical stability of the acoustically active terms can be determined by linearizing the high frequency terms in Eqs. (2) and (4); i.e.,

$$\frac{\partial u_j}{\partial t} + \alpha_o \frac{\partial p}{\partial x_j} = 0, \tag{F-7}$$

and

$$\frac{\partial p}{\partial t} + \eta P_o \frac{\partial u_j}{\partial x_j}, \tag{F-8}$$

where P_o and $\alpha_o \equiv \rho_o^{-1}$ are both assumed constant. Approximating (F-7) and (F-8) by the Adams-Bashforth time difference and central space differences, and then elimating u gives (where now i, j, and k represent the grid indices respectively in the x, y, and z direction)

$$p_{ijk}^{n+1} - 2\, p_{ijk}^{n} + p_{ijk}^{n-1} = r_c[9\, \phi_{ijk}^{n} - 6\, \phi_{ijk}^{n-1} + \phi_{ijk}^{n-2}], \tag{F-9}$$

where

$$r_c \equiv \Delta t \eta \alpha_o P_o / 4 = \Delta t \eta R T_o / 4,$$

and

$$\phi_{ijk}^{n} = (p_{i+1jk}^{n} + p_{i-1jk}^{n} - 2\, p_{ijk}^{n})/\Delta x^2 + (p_{ij+1k}^{n} + p_{ij-1k}^{n} - 2\, p_{ijk}^{n})/\Delta y^2 + (p_{ijk+1}^{n} + p_{ijk-1}^{n} - 2\, p_{ijk}^{n})/\Delta z^2.$$

Assuming a general solution as

$$p = \Omega(t) \exp[i\ (\ell x + my + kz)],$$

and substituting into (F-9) gives,

$$\lambda^3 + (54\ r_c - 2)\lambda^2 + (1-36\ r_c)\lambda + 6\ r_c = 0. \qquad \text{(F-10)}$$

Eq. (F-10) has 3 solutions which are real. The critical small time step is chosen such that $|\lambda_1| \leq 1$, $|\lambda_2| \leq 1$, and $|\lambda_3| \leq 1$; it is given as

$$\Delta t_s \leq 0.5\ [\eta RT_o\ (\Delta x^{-2} + \Delta y^{-2} + \Delta z^{-2})]^{-0.5}. \qquad \text{(F-11)}$$

Hence, approximation of the high frequency terms in Eqs. (2) and (4) by the Adams-Bashforth method and central differences has a conditional numerical stability.

APPENDIX G

Raindrop Freezing

Special treatment is required in computing raindrop freezing, especially since the production rates for this process may acquire large magnitudes.

From Eq. (63) and (64) the rate of depletion of rain due to spontaneous freezing is

$$DR1A = - Q_R \; P7', \qquad \text{(G-1)}$$

where $P7' = MAX[20\pi \; \alpha_1 \; \Lambda_R^3 \; G_F, \; 0.25/\Delta t]$, and where Δt is the size of the large time step. From Eq. (67) the depletion of rain due to contact freezing with ice crystals is

$$DR1B = - Q_R \; P9', \qquad \text{(G-2)}$$

where $P9' = 6.96 \; \pi \; \eta_{IC} \; \Lambda_R^2 \; \overline{W}_R \; E_{RIC}$.

Hence, the depletion of rain due to spontaneous freezing and contact freezing is

$$(dQ_R/dt)_F = - Q_R(P7' + P9').$$

By treating P7' and P9' as constant during the time interval Δt, the depletion of rain during the large time step interval is

$$\Delta Q_R = Q_R[1 - \exp[-\Delta t(P7' + P9')]]. \qquad \text{(G-3)}$$

If $\beta \tilde{<} 0.5$, where $\beta \equiv \Delta t(P7' + P9')$, Eq. (G-3) can be approximated as

$$\Delta Q_R \simeq Q_R \beta (1 - 0.5 \beta).$$

The mixing ratios may then be adjusted as follows:

$$Q_H = Q_H + \Delta Q_R \quad \text{if} \quad Q_R > 10^{-4} \text{ g g}^{-1},$$
$$Q_{SN} = Q_{SN} + \Delta Q_R \quad \text{if} \quad Q_R \leq 10^{-4} \text{ g g}^{-1},$$

and

$$Q_R = Q_R - \Delta Q_R.$$

This procedure prevents the over depletion of rain when the production rates for drop freezing are of large magnitude.

Standard Bibliographic Page

1. Report No. DOT/FAA/PM-86/50, I NASA CR-4046	2. Government Accession No.	3. Recipient's Catalog No.
4. Title and Subtitle The Terminal Area Simulation System Volume I: Theoretical Formulation		5. Report Date April 1987 6. Performing Organization Code
7. Author(s) F. H. Proctor		8. Performing Organization Report No.
9. Performing Organization Name and Address ST Systems Corporation (STX) 17 Research Drive Hampton, VA 23666		10. Work Unit No. 11. Contract or Grant No. NAS1-17409
12. Sponsoring Agency Name and Address National Aeronautics and Space Administration, Washington, DC 20546 U.S. Dept. of Transportation and Federal Aviation Admin., Washington, DC 20591		13. Type of Report and Period Covered Contractor Report 14. Sponsoring Agency Code 505-67-41

15. Supplementary Notes ST Systems Corporation (STX) formerly SASC Technologies, Inc.
Langley Technical Monitor: Roland L. Bowles
F. H. Proctor: MESO, Inc., Hampton, Virginia.
Prepared under subcontract 85-6000-A1603
Volume II: NASA CR-4047

16. Abstract
A new three-dimensional numerical cloud model has been developed for the general purpose of studying convective phenomena. The model utilizes a time splitting integration procedure in the numerical solution of the compressible nonhydrostatic primitive equations. Turbulence closure is achieved by a conventional first-order diagnostic approximation. Open lateral boundaries are incorporated which minimize wave reflection and which do not induce domain-wide mass trends. Microphysical processes are governed by prognostic equations for potential temperature water vapor, cloud droplets, ice crystals, rain, snow, and hail. Microphysical interactions are computed by numerous Orville-type parameterizations. A diagnostic surface boundary layer is parameterized assuming Monin-Obukhov similarity theory. The governing equation set is approximated on a staggered three-dimensional grid with quadratic-conservative central space differencing. Time differencing is approximated by the second-order Adams-Bashforth method. The vertical grid spacing may be either linear or stretched. The model domain may translate along with a convective cell, even at variable speeds. In storm splitting cases, the domain translates with the convective cell having cyclonic rotation and allows the other cell(s) to pass through the lateral boundary without detrimental consequences. Potential applications of the model range from the simulation of shallow cumulus to supercell cumulonimbus, including such convective phenomena as downbursts, tornadoes, gust fronts, and hailstorms.

17. Key Words (Suggested by Authors(s))		18. Distribution Statement
Numerical model	Boundary layer	Unclassified - Unlimited
Cloud model	Severe local storms	
Convection	Numerical boundary conditions	Subject Category 03
Microphysics		
Wind shear	Hail model	

19. Security Classif.(of this report)	20. Security Classif.(of this page)	21. No. of Pages	22. Price
Unclassified	Unclassified	176	A09

For sale by the National Technical Information Service, Springfield, Virginia 22161

NASA-Langley, 1987